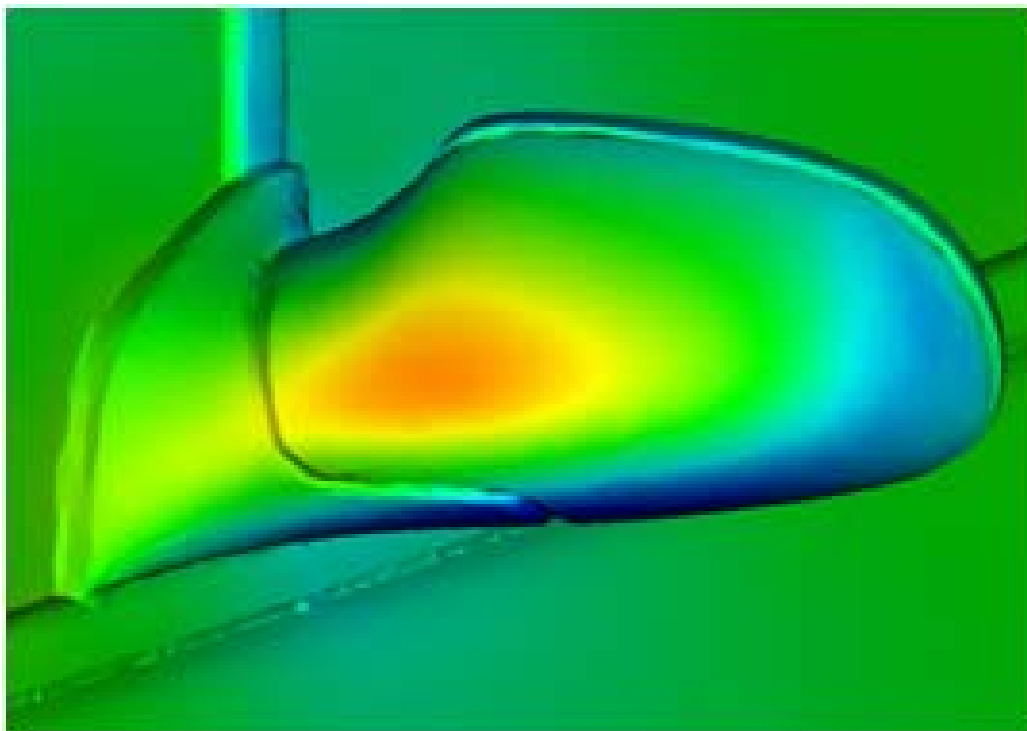


# CHALMERS



## Designing and Optimizing Side-View Mirrors

*Master's Thesis in Automotive Engineering*

MARTIN OLSSON

Department of Applied Mechanics  
*Division of Vehicle Engineering and Autonomous Systems*  
CHALMERS UNIVERSITY OF TECHNOLOGY  
Göteborg, Sweden 2011  
Master's Thesis 2011:27



MASTER'S THESIS 2011:27

# Designing and Optimizing Side-View Mirrors

Master's Thesis in Automotive Engineering  
MARTIN OLSSON

Department of Applied Mechanics  
*Division of Vehicle Engineering and Autonomous Systems*  
CHALMERS UNIVERSITY OF TECHNOLOGY

Göteborg, Sweden 2011

Designing and Optimizing Side-View Mirrors  
MARTIN OLSSON

©MARTIN OLSSON, 2011

Master's Thesis 2011:27  
ISSN 1652-8557  
Department of Applied Mechanics  
Division of Vehicle Engineering and Autonomous Systems  
Chalmers University of Technology  
SE-412 96 Göteborg  
Sweden  
Telephone: + 46 (0)31-772 1000

Cover:  
A picture, from PowerViz, of the standard mirror of a Mercedes-Benz A-class (W168), which shows the velocity magnitude.

Chalmers Reproservice  
Göteborg, Sweden 2011

Designing and Optimizing Side-View Mirrors  
Master's Thesis in Automotive Engineering  
MARTIN OLSSON  
Department of Applied Mechanics  
Division of Vehicle Engineering and Autonomous Systems  
Chalmers University of Technology

### Abstract

Today, reducing the carbon dioxide emissions is vital. The car industry has a responsibility to reduce the fuel consumption and will thereby reduce carbon dioxide emissions. One of the main questions in the automotive industry how to go about this. One possibility is to change the propulsion system. Another option is to reduce the aerodynamic drag of the car; the topic of this thesis. The drag is of great importance when it comes to velocities over 60 kph.

There are many parts of the car that contribute to drag. One such part is the (side-view) mirrors. The mirrors increase the total amount of drag by 2-7 percent. There numerous regulations and legal demands when it comes to mirrors due to the aspects of safety. Moreover, the mirrors affect the soiling of the windows which creates yet another safety issue. Dirty windows reduce the visibility for the driver.

Many different mirror designs and parameters have been investigated. To get the amount of drag, computer simulations (CFD) have been done. The car which the mirrors have been attached to is a Mercedes-Benz A-class (W168) quarter scale model. Wind tunnel testing (at FKFS, Stuttgart) in quarter scale has been done for correlation. (The correlation did not match the CFD well, however, the trends were the same.)

After various tests, one can observe that small changes to the mirror, such as change edges radius, inclinations, adding gutters, and edges, affect the flow both around the mirror and in the rear of the car. The best drag reduction was achieved when the housing curvature of the mirror was changed from rather bulky to flatter model which produced the same drag reduction as having no mirrors at all.

The mirror plays a major role in drag contribution for the entire car and therefore mirror optimization is considered very important. Mirror optimization is not an easy task due to uncertainties in the CFD simulations of a few drag counts which makes it impossible to trust all findings. In order to find a good mirror design, a combination of wind tunnel testing in full scale, and CFD simulations is necessary. Mirror design optimization shows great potential.

Keywords: Drag reduction, CFD, Wind Tunnel, Side-View Mirrors



# Contents

<b>Abstract</b>	<b>i</b>
<b>Contents</b>	<b>iii</b>
<b>Preface</b>	<b>v</b>
<b>1 Introduction</b>	<b>1</b>
1.1 Objective	1
1.2 Background	1
1.3 Method	1
1.4 Limitations	2
1.5 Universität Stuttgart and IVK/FKFS	2
<b>2 Theory</b>	<b>3</b>
2.1 Side-View Mirrors	3
2.1.1 Design	3
2.1.2 Flow	3
2.1.3 Soiling	4
2.1.4 Regulations and Legal Demands [1]	4
2.2 Fluid Mechanics	6
2.3 Computational Fluid Dynamics (CFD)	7
2.4 Wind Tunnel	8
<b>3 The Subject - Mercedes-Benz A-Class</b>	<b>13</b>
3.1 Car	13
3.2 Scale Model	13
3.3 Computer Model	14
<b>4 Cases</b>	<b>15</b>
4.1 Standard Mirror	15
4.2 Without Mirror	15
4.3 Reference Mirror	16
4.4 Varying the Gap	16
4.5 Varying the Height of the Foot	17
4.6 Varying the Inclination	17
4.7 Varying the Inner Radius	18
4.8 Different Housing Curvatures	18
4.9 Single Changes	19
4.10 Combined Changes	20
<b>5 Case Setup (CFD)</b>	<b>21</b>
5.1 Variable Resolution (VR) Regions	21
5.2 gence and Averaging	22
<b>6 Wind Tunnel Setup</b>	<b>25</b>
6.1 Information	25
6.2 Setup	25
6.3 Rapid Prototyping	26

6.4	Selection of Mirrors for Wind Tunnel Testing . . . . .	27
<b>7</b>	<b>Results</b>	<b>28</b>
7.1	CFD . . . . .	28
7.2	Wind Tunnel . . . . .	32
7.3	Comparison . . . . .	34
7.4	Reynolds Sweep . . . . .	36
<b>8</b>	<b>Flow Analysis and Comparison</b>	<b>37</b>
8.1	Standard Mirror (Half Car) . . . . .	37
8.2	Standard Mirror (Whole Car) . . . . .	41
8.3	Without Mirror . . . . .	45
8.4	Reference Mirror . . . . .	47
8.5	Varying the Gap . . . . .	50
8.6	Varying the Height of the Foot . . . . .	52
8.7	Varying the Inner Radius . . . . .	53
8.8	Varying the Inclination . . . . .	55
8.9	Different Housing Curvatures . . . . .	58
8.10	Single Changes . . . . .	59
8.11	Combined Changes . . . . .	63
<b>9</b>	<b>Discussion</b>	<b>64</b>
<b>10</b>	<b>Conclusion</b>	<b>66</b>
10.1	Future Work . . . . .	66
	<b>Reference</b>	<b>67</b>
	<b>Appendices</b>	
<b>A</b>	<b>PowerCASE Parameters</b>	<b>I</b>
<b>B</b>	<b>Mirror Glass Investigation</b>	<b>V</b>
<b>C</b>	<b>Detailed Results</b>	<b>IX</b>
<b>D</b>	<b>PowerCASE Case Summary (Example)</b>	<b>XIII</b>

# Preface

This study focuses on designing and optimizing side-view mirrors for a Mercedes-Benz A-klasse (W168), by using both Computational Fluid Dynamics (CFD) and wind tunnel testing. The work has been carried out in Institut für Verbrennungsmotoren und Kraftfahrwesen (IVK), Querschnittsprojekte und High Performance Computing, in Universität Stuttgart, Germany with Dr.-Ing. Timo Kuthada as supervisor and Professor Lennart Löfdahl as examiner. Finally, a special thanks to Kuthada, who has made this study possible.

Göteborg April 2011  
Martin Olsson



# 1 Introduction

## 1.1 Objective

The objective is to construct side-view mirrors that are aerodynamically optimized as well satisfy today's regulations and legal demands. Finally, the mirrors will be attached to a model scale car and be tested in a wind tunnel for correlation.

## 1.2 Background

Reducing fuel consumption, and therefore reducing the carbon dioxide emissions, is one of the most important goals in today's car industry. One way this can be achieved by reducing the engine size, using an electric motor with a combustion engine, and reducing the weight of the car or the aerodynamic drag of the car. The latter is of great importance when it comes to velocities over 60 kph. Above this velocity, the aerodynamic resistance is higher than the rolling resistance [2]. The drag equation for an object moving through a fluid is as followed

$$F_D = \frac{1}{2}\rho v^2 C_d A \quad (1.1)$$

where  $F_D$  is the force of the drag,  $\rho$  is the density,  $v$  is the velocity,  $C_d$  is the drag coefficient and  $A$  is the reference area. The most important variables are the reference area (frontal area of the car) and the drag coefficient. By reducing these the aerodynamic drag will be reduced, which will then lead to lower fuel consumption rate.

## 1.3 Method

The method for this Master thesis is as follows:

- Literature study about mirrors
- CAD Clean-up (fixing the mesh) of a scanned model
- CFD simulations on the original mirror
- Coming up with ideas for new mirrors
- Designing mirrors in CAD
- Optimizations and more CFD simulations
- Creating sets of mirrors by using Rapid prototyping
- Check correlation for the CFD simulations in a wind tunnel

This method involves a number of different computer programs:

- ANSA from BETA CAE Systems S.A. is used for CAD Clean-up.
- PowerDELTA and PowerCASE both from EXA Corporation are used for simulation preparation.
- PowerFlow from EXA Corporation is used for simulations.
- PowerVIZ, also from Exa Corporation is used for result analysis.

- CATIA V5 from Dassault Systèmes is used for drawings and design, as a CAD program.

## 1.4 Limitations

In this thesis the following limitations have been applied:

- Simplification of regulations and legal demands
- Omission of acoustical factors
- Simplified design of the mirrors, i.e.; no interior components. N.B. fold of the mirror used only as point of reference.

## 1.5 Universität Stuttgart and IVK/FKFS

This thesis has been carried out at Universität Stuttgart in Germany at the Institut für Verbrennungsmotoren und Kraftfahrwesen (IVK) in the division of Querschnittsprojekte und High Performance Computing. Universität Stuttgart and IVK are situated just outside of Stuttgart, in the suburb of Vaihingen. The University has about 19,000 students [3]. IVK has an agreement with Forschungsinstitut für Kraftfahrwesen und Fahrzeugmotoren Stuttgart (FKFS), a research institute. FKFS is an independent institute and provides research and development services for the international automotive industry.[4]

## 2 Theory

This section covers a brief look at the theory behind the different sections of this thesis. For a deeper understanding and more detailed information, books such as *Low-Speed Wind Tunnel Testing* by Barlow, Rae and Pope, and *Aerodynamik des Automobils* by Hucho are recommended. In this thesis the word mirrors refers to side-view mirrors.

### 2.1 Side-View Mirrors

The automobile side-view mirror is a device for indirect vision that facilitates observance the traffic area adjacent to the vehicle which cannot be observed by direct vision. Being able to see what is behind the car is vital when reversing or changing lanes. The mirrors are often situated on, just in front of, the driver's and front passenger's doors. Due to legislation, today's cars have two mirrors. There are many regulations and laws when it comes to mirrors, mainly due to safety factors. Today's mirrors are made up of more than a reflective glass. The mirror housing often holds the indicators, illumination features and a blind spot alarm.

#### 2.1.1 Design

Mirrors have gone through many changes when it comes to appearance. In figure 2.1 designs over the years are shown. Often the esthetic design is more important than a good aerodynamic design. As time progresses aerodynamic aspects have become more important and influential.

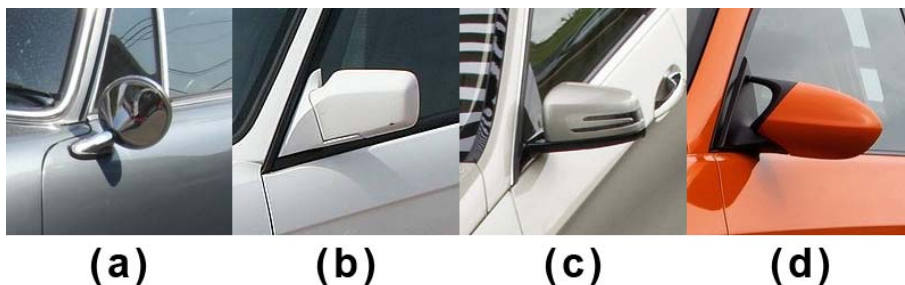


Figure 2.1: Different mirror designs over the years. (a) is a Porsche 911T from 1972, (b) is a BMW M3 (E30) from 1988, (c) is a Mercedes-Benz E-class (W212) from 2010 and (d) is a BMW M3 GTS (E92) from 2011. Picture sources: Netcarshow.com, Asian-winds.com and Carbodykits.com

#### 2.1.2 Flow

The flow around the mirror is of great importance. Vibration of the mirror should be minimal in order to prevent a consequent mirror glass vibration. Vibration leads to a blurry outlook from the mirror. This flow also affects the aeroacoustics of the mirror. Many noises has there origin from the mirror. The area where the mirror is located is a complicated area from an aerodynamical point of view. This complications comes from the a-pillar which often creates an unsteady flow and vorticities. According to Heico,

the mirrors increase the total amount of drag by 2-7 percent [5]. This means the mirrors contribute more to drag than they should in comparison to their size and the frontal area.

### 2.1.3 Soiling

Driving in wet conditions often results in dirty windows and mirror glasses. Having dirty windows reduces the visibility for the driver, which then affects the safety. There are two main types of soiling; dirty water drops from surrounding vehicles or rain, and soiling from dirt kick up and dirty water from ones own wheels. In this thesis, only the soiling on the side windows, directly after the a-pillar, is of interest. The a-pillar controls most of the soiling of the side windows, however, the mirrors also have some influence.

### 2.1.4 Regulations and Legal Demands [1]

There are many different legal demands and regulations for mirrors. Only a short summary of the relevant factors will be dealt with. In this thesis, Class III mirrors for the vehicle type M1 is the focus. Class III stands for a main mirror (small), which is the only compulsory mirror type for M1 besides the interior mirror (Class I). M1 stands for a vehicle used for the carriage of passengers and comprises not more than eight seats in addition to the driver's seat.

The name of the current directive is 2003/97/EC. The following bulleted list is an extraction of some of the most important "design" demands.

- There must be two mirrors, one driver side and one on the passenger side.
- Mirror must be adjustable.
- The edge of the reflecting surface must be enclosed in a protective housing.
- The dimensions of the mirror glass must be such that it is possible to inscribe; a rectangle 40 mm high with a base length depending on the average of the radii of curvature measured over the mirror glass and a segment which is parallel to the height of the rectangle. The height of the rectangle is 70 mm long.
- The mirror glass must be either flat or spherically convex.
- Mirrors must be placed so that the driver, when sitting in the driver's seat, in a normal driving position, has a clear view of the road to the rear, side(s) or front of the vehicle.
- Where the lower edge of an exterior mirror is less than 2 m above the ground when the vehicle is loaded to its technically permissible maximum laden mass, this mirror must not project more than 250 mm beyond the overall width of the vehicle measured without mirrors.
- The field of vision must be such that the driver can see the marked areas in figure 2.2.

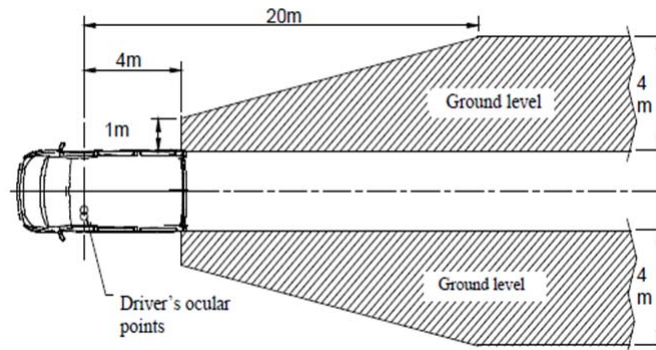


Figure 2.2: Field of vision of class III mirrors. [1]

It is easy to see if a mirror on a production car fulfills the legal demands by simply looking at the EC component type-approval mark. This mark tells the class number where the mirror has been approved and along with the "case" number. This mark must be inscribed on an integral part of the mirror so it can be clearly seen. An example of this mark can be seen in figure 2.3. The numerals written in Roman is the class type, the number that comes after the letter 'e' shows from which member state the mirror has been type-approved. The two digit number in the last line indicates the sequence number of the latest amendment to the directive on the date the type-approval was granted. In this case the number would be 03. The final number is the component type-approval number.

II  
e 4  
03\*1870

Figure 2.3: Seen here is an example of the EC component type-approval mark, which shows that it is a Class II mirror that has been approved in the Netherlands (e4) under the number 03\*1870. [1]

There are many different demands for the mirror and its location and its glass size. In order to simplify the design process an investigation of the average mirror glass size has been done. Different car mirror glass area's have been measured and then the average has been calculated. This calculated value has then been used as a minimum value for the mirror glasses of the different cases in this thesis. More information about this investigation can be found in appendix B.

## 2.2 Fluid Mechanics

Fluid mechanics is the study of fluids either in motion or at rest. The two different types of fluid in motion are laminar and turbulent flow. Laminar flow is smooth and the adjacent layers of fluid slide past each other in an orderly fashion. Meanwhile, turbulent flow is unsteady, dissipative, 3-dimensional, and flow properties vary in a random and chaotic way. The structures in turbulence varies in size between large eddies that take their energy from the main flow, to the smallest structures that are small enough so molecular diffusion becomes important. The Reynolds number (discussed later) tells us if the flow is turbulent or laminar. Next to a surface is a thin layer of air flow that is slowed down by the presence of the surface. This layer is called boundary layer. The thickness of this layer grows with the distance from the front of the surface. Boundary layers are laminar in the beginning, and change into turbulent at a transition point. Flow separation occurs when the outer layers no longer can pull the inner layers along. This happens when the gradual increase in pressure is too great, resulting in slowing the mixing process to a level no longer adequate to keep the lower part of the layer moving. The two expressions used for separation are adverse pressure gradient and favourable pressure gradient. With an adverse pressure gradient, the air flows from a low pressure to a high one and the favourable pressure gradient means the opposite. A favourable pressure gradient inhibits separation.

The flow can be described with the Navier-Stokes (N-S) equations (non-linear system of partial differential equations), see equation 2.1.

$$\frac{\partial \mathbf{u}_i}{\partial t} + \mathbf{u}_j \frac{\partial \mathbf{u}_i}{\partial \mathbf{x}_j} = -\frac{1}{\rho} \frac{\partial \mathbf{p}}{\partial \mathbf{x}_i} + \frac{\partial}{\partial \mathbf{x}_j} \left[ \nu \left( \frac{\partial \mathbf{u}_i}{\partial \mathbf{x}_j} + \frac{\partial \mathbf{u}_j}{\partial \mathbf{x}_i} \right) \right] \quad (2.1)$$

where  $\mathbf{u}$  is the velocity,  $t$  is time,  $\mathbf{x}$  is the position,  $\mathbf{p}$  is pressure and  $\rho$  is density.

### Full scale vs Model Scale

The Reynolds number is an important parameter for describing the flow, if it is laminar or turbulent for example. The Reynolds number can be expressed in the following terms; velocity  $v$ , density  $\rho$ , viscosity  $\mu$  and length  $l$ . Which gives the following expression:

$$Re = \frac{\rho v l}{\mu} \quad (2.2)$$

The Reynolds number is of great importance when it comes to scale testing. If the Reynolds number increases as the velocity increases, then the transition position moves forward. With an adverse pressure gradient, this results in the boundary layer becoming thinner and enabling the turbulent boundary layer to keep the flow attached longer before it separates. Moving the separation point backwards will give a narrower wake, which leads to decreased drag. An example of the influence of the Reynolds number is shown in figure 2.4, with a circular rod. A clear dip in the drag curve at a certain Reynolds number can be noticed. Bluff bodies, with sharp edges are not

affected by this phenomenon. A car today has both sharp edges and smooth circular areas. Every car has a different Reynolds number dependency and can have drag value drops at different Reynolds numbers. Usually the drag value decreases for a scale model until it reaches the value of the full scale car. So when doing wind tunnel testing with scaled model cars, a Reynolds sweep is often performed to see if there is Reynolds number dependency. [2]

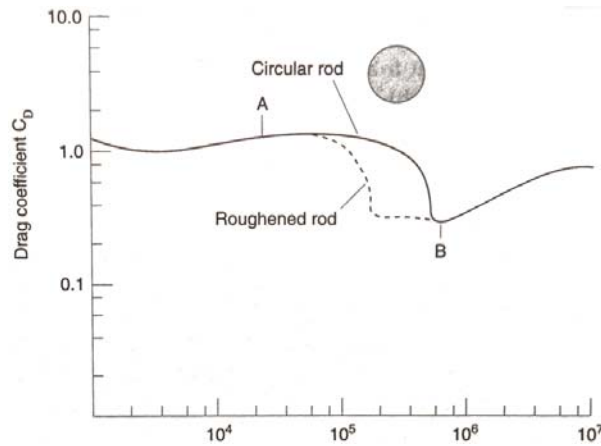


Figure 2.4: Reynolds number dependence on  $C_d$ . [2]

### 2.3 Computational Fluid Dynamics (CFD)

Computational fluid dynamics (CFD), using computer simulation, analyzes systems of fluid flows, heat transfer, and associated phenomena such as chemical reactions. Examples of areas CFD can be applied to are; design of internal combustion engines, aerodynamics of aircrafts and vehicles, meteorology (weather prediction), and external environment of buildings (wind loads and ventilation). CFD has many advantages over experiment-based approaches, such as reduction of lead times and costs of new designs, study systems under hazardous conditions, systems that are impossible to study with controlled experiments and, the unlimited level of detail of results. There are also problems with CFD. The physics are complex and the result from CFD is only as good as the operator and the physics embedded. With today's computer power, there is a limitation of grid fineness and the choice of solving approach (DNS, LES and turbulence model). This can result in errors, such as numerical diffusion, false diffusion and wrongly predicted flow separations. The operator must then decide if the result is significant. While presently, CFD is no substitute for experimentation, it is a very helpful and powerful tool for problem solving. [6]

When working with CFD a number of different steps are followed. These steps are illustrated in figure 2.5.



Figure 2.5: The CFD process.

The first step is to create a geometry (with CAD). This is often already done by other departments or done by scanning a model. The geometry cannot have any holes, it has to be airtight, and unnecessary things in the CAD model that do not affect the flow has to be removed to save computer power. This is called CAD clean-up. The next step is to generate a mesh and this is often done automatically by a meshing program. Then the flow is simulated by a solver. After the simulation is ready, it is time for post processing. Post processing involves getting drag and lift data, and analyzing the flow.

There are different approaches for solving the flow. Here are the most common approaches:

- Direct Numerical Simulations (DNS), which solve the Navier-Stokes equation numerically. This will resolve all the different turbulent scales. The solution will be transient and requires a very fine mesh with sufficiently small time steps. Due to the extreme grid size and number of time steps required for a simulation at high Reynolds number, this approach is not today possible (lack of computer power).
- Reynolds-Averaged Navier-Stokes (RANS), which gives an approximate time-averaged solution to the Navier-Stokes equation and focuses on the mean flow properties. The fluctuating velocity field, also called Reynolds stress, has to be modeled. But this turbulence model cannot solve all turbulence scales.
- Large Eddy Simulations (LES), which computes the larger eddies in a time-dependent simulation while the universal behavior of the smaller eddies can be captured with a model. LES uses a spatial filtering operation to separate the larger and the smaller eddies.
- Lattice Boltzmann Method (LBM), which is the one that the solver uses in this thesis. The solver uses Very Large Eddy Simulations (VLES), a variant of LES, coupled to the LBM for the large eddies, and the smaller are resolved by a turbulence model.

## 2.4 Wind Tunnel

To be able to confirm the results from the CFD simulations the aerodynamic forces have to be measured in the real world. The easiest way today is to use a wind tunnel. A wind tunnel, simplified, is a big fan that blows air onto a test subject, which is located in a test section. The test subject is connected to a balance that measures forces. There are a lot of things that can be tested in a wind tunnel; aerodynamic forces and moments, yaw conditions, engine cooling performance, local flow field measurements, climate effect and aeroacoustic. There are many ways to design a wind tunnel, but there are two basic types of wind tunnels and "two" basic test sections. From these basic configurations there are an enormous number of different configurations.

## Wind Tunnel Types

The two basic wind tunnel types are open circuit and closed circuit. An outline of an open circuit wind tunnel can be seen in figure 2.6. In this type of wind tunnel the flow has a straight path from the entrance to the exit. There is contraction to the test section, which is then followed by the test section (which can be of different types), then a diffuser and a fan. The inlet and exhaust are open to the atmosphere. The advantages with this type of wind tunnel are that the construction costs are less and that extensive flow visualizations (smoke) is possible, due to no contamination of the incoming air. The disadvantages are wind and weather can affect the measurements, so screening is required. Other disadvantages are that it requires a lot of energy to run and it is also really noisy. [7]

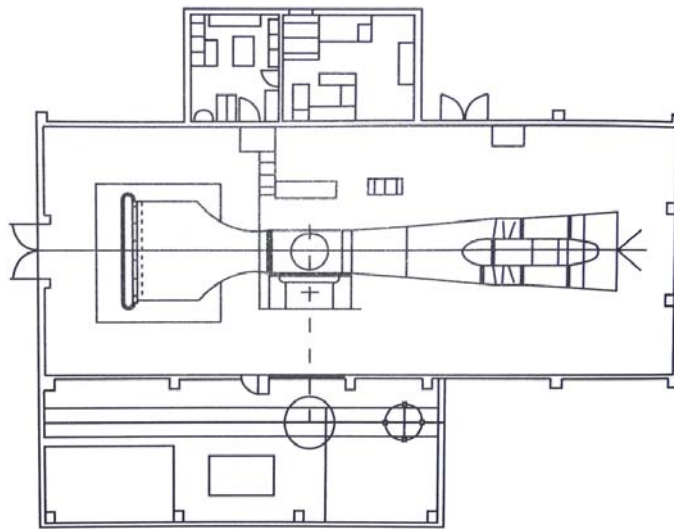


Figure 2.6: Outline of an open circuit wind tunnel (Diamler-Benz Aerospace Airbus, Bremen, Germany). [7]

The closed circuit wind tunnel has a recirculation of the air. Turning vanes and screens are used to control the quality of the flow. The test section can be of different types. An outline can be found in figure 2.7. The advantages with this type of wind tunnel are that the flow can be controlled (by using the turning vanes and screens) and it is independent of the weather conditions. Other advantages are that it requires less energy to run and is producing less noise to the environment. The disadvantages are that the construction costs are higher, extensive flow visualization (smoke etc.) will contaminate the flow and the wind tunnel if there is no way of cleaning the flow and if the utilization of the wind tunnel is high the flow temperature rises and there has to be some sort of cooling. This type is the one that is most common for automotive tunnels. [7]

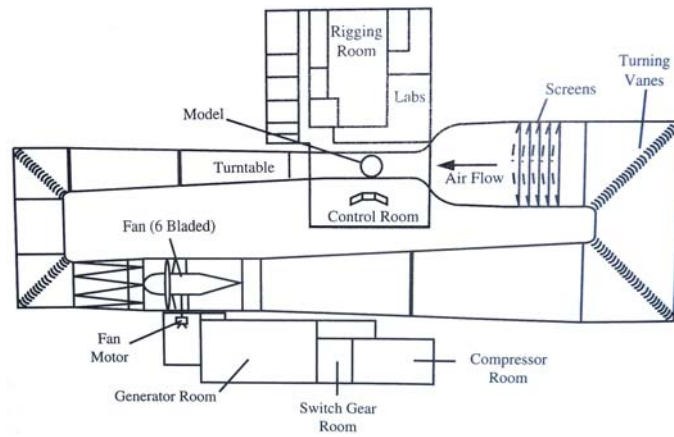


Figure 2.7: Outline of a closed circuit wind tunnel (DERA, Bedford, England). [7]

### Test Section

The test section is where measurements take place. The varying designs of the test sections creates varying results. The most common are; open (open jet), closed, and closed with slotted walls (figure 2.8).

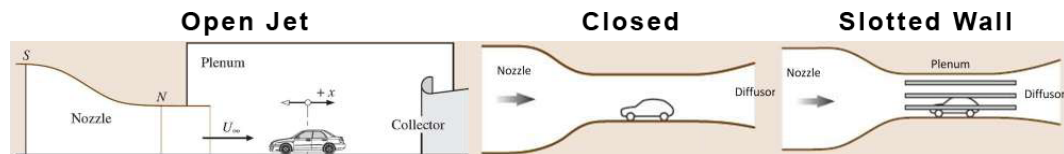


Figure 2.8: Outline of three different types of test sections. [8]

In an open jet test section the flow enters through a nozzle into a volume that is much larger in the cross-sectional area than the nozzle. This volume is called plenum. The flow then passes by the car and ends in the collector. This type of test section was created to resemble the conditions in the real world, however, the still air in the plenum affects the jet and thus the result. The large volume of the plenum makes the test section easy to access and enables that different measuring equipment can easily be fitted inside the wind tunnel. The disadvantage is that the length of the test section is limited, and due to the jet, is affected by the still standing air in the plenum. This reduces the jet's core velocity. [8]

The closed test section also uses a nozzle to accelerate the air, this time into a "tunnel". In this tunnel the car is placed. Within the tunnel the boundary layer is growing. In order to minimize the effect of a growing boundary layer the tunnel also grows in size to maintain a constant core velocity and static pressure. This means that the test section can be longer than it could with the open test section. Contrastingly, the closed test section suffers from high level of blockage. The flow is compressed, which leads to an accelerated flow around the car and it's rear wake. [8] The slotted wall test section is a mixture of an open and closed test section. A ambient pressure area (plenum) surrounds the test section and this allows the ambient air to

access it. By using just slots to separate the test section from the plenum, the turbulence mixing is reduced in comparison to the open test section. [8]

### **Blockage Effects**

As previously mentioned, there is a blockage in the test section, which affects the results. Blockage is allowed to a certain limit, yet after this limit is reached the measurements do not represent the 'real world' any more. For an open test section 10-15%, closed test section 5-7% and for a slotted wall test section 7-10% (the percentage value is defined as car cross-sectional area divided by the test section cross-sectional area). With an open test section a larger amount of blockage can be accepted, than with the other two alternatives. For the different blockage correction methods, see lecture notes in [8]. For the open test section there is both nozzle and collector blockage. The nozzle blockage is due to the stagnation pressure at the front of the car, which affects the flow upstream in the nozzle. This will lead to a uniform outflow from the nozzle as well as a higher velocity, which increases the drag. The collector blockage is due to the wake of the car. For the closed test section the blockage results in accelerated flow around the car and its wake. This will lead to higher forces and a false higher drag. There has not been more than a very few publications blockage correction for a slotted wall. [8]

### **Wind Tunnels vs The Real World**

The largest difference between the wind tunnel tests and the actual road conditions can be seen in the observations; in a wind tunnel the air flows past the car opposed to in the real world where the car goes through the air. Luckily, the result is the same. There is, however, a complication; the relative motion between the car and the road. In a wind tunnel both the car and the "road" are standing still. In the real world the car does not stand still. This affects the aerodynamic forces due to a boundary layer which builds up in front of the test section. This issue can be handled in a variety of ways. One option is to have a different belt configuration under the car that moves at the same speed as the air. To reduce the boundary layer, suction through holes can be used. An additional difference can be found in the fact that the real world can be affected by different types of wind. The direction and magnitude of these change constantly. Local atmospheric wind is notable as it gives a turbulent boundary layer with a thickness of about 100-500 m, meaning cars drive in the bottom of this layer [2].

### **Force Measurements**

Measuring the aerodynamic forces is done by using a strain-gaged balance. There are two main approaches. The first one is to connect the car to a rigid sting. The balance can then be connected directly to the sting or to the car. The sting can be placed on top of the car or behind the car. It will interfere with the flow in one way or another. The car has to be modified to be able to connect to the sting. Setting up a sting configuration takes a considerable amount of time. The advantage of using a sting is that a full width moving ground system can be used, rather than just belts. The other

approach is to connect the car to the balance by using small struts close to the wheels. These struts also affect the flow, but only locally. This type of force measurement allows fast changes between cars/models. [8]

### **Wind Tunnel Errors**

There could be a number of different errors when doing wind tunnel tests. The main errors are; scale or Reynolds number effects (discussed in subsection 2.2), the influence road movement relative to the car (this error can almost be reduced to zero when using moving ground) and the errors due to blockage. When doing model scale testing an additional error can occur; failure to model fine detail accurately. With models there are often no interior components (e.g. engine etc.) or cooling device as compared to a full scale car, which also has an affect on the results.

### 3 The Subject - Mercedes-Benz A-Class

The car that has been the base subject for the mirror modifications is a Mercedes-Benz A-Class.

#### 3.1 Car

This car is of the first generation of the Mercedes-Benz A-class, with the internal name of W168. It is a 5-door hatchback. It is equipped with 205/55 R16 wheels and the mirrors are located slightly behind the a-pillar. What characterizes the A-class from others is the short engine hood and the detruncated rear part, which give the car a narrow and high appearance. Figure 3.1 shows the front and rear of the car.



Figure 3.1: The front and rear of a full scale Mercedes-Benz A-Class (W168).

#### 3.2 Scale Model

A simplified scale model of the original car has been made, with the scale 1:4. The model has no interior components or engine compartment. All gaps have been sealed and the underside is completely plain. The model is equipped with windscreen wipers back and front, but the one at the front windscreen is missing one of the wiper arms. Figure 3.2 shows the model. (Note: the wheels in the picture have not been used during wind tunnel measurements.)



Figure 3.2: The front and rear of the model.

The wheels are made of aluminum and have a five spoke design, which can be seen in figure 3.3. The tires have no thread. The model has three different ride heights; the middle one has been chosen for its likeness to the real car's ride height. It should be noted that the car itself is slightly slanted or crooked.



Figure 3.3: The aluminum wheel for the scale model.

### 3.3 Computer Model

The computer model, which is in the file format stl, is a scan of the model car. The scan consisted of about 4.3 million triangles and was reduced to about 1.3 million triangles, by using PowerDELTA, in order to quicken simulation time, and for general manageability. The computer model had some gaps and overlapping surfaces after the scan. These problems were fixed in ANSA. To simplify the simulations, the wipers, both for the front and rear windscreen, have been removed. The lower air-intake grid has been removed due to too damaged data from the scanning. Another simplification is that the wheels have no wheel nuts. It can also be noted here as with the model car, the computer model is similarly crooked. Figure 3.4 shows the computer model.

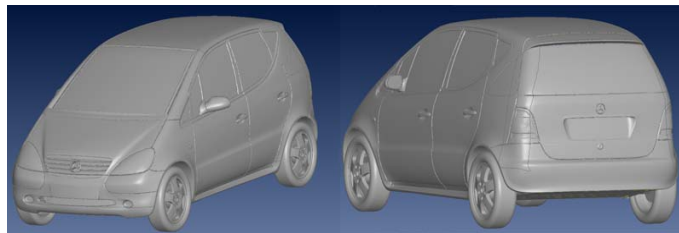


Figure 3.4: The front and rear of the computer model.

## 4 Cases

During work on this thesis a large amount of different cases have been simulated. A selection of these cases will be investigated. The main cases are the standard mirror, without mirror, and a reference mirror. The case with the standard mirror has been done with both whole and half car. All other cases are just simulated with a half car. This has been done to decrease the simulation time. The reference mirror has been chosen after testing different mirror shapes. All additional cases to the original three, are modifications of the reference mirror and satisfy the simplified legal and regulation requirements. To make it easier with the wind tunnel tests, the position of the mirror attachment to the car is the same for all cases, and comes from the standard mirror. The design of all mirrors have been simplified (i.e. no gaps, no folding mechanics etc.).

### 4.1 Standard Mirror

The standard mirror (figure 4.1) is the mirror that is mounted on the car, when it comes from the factory. This mirror is rather bulky especially around the foot (the attachment of the mirror housing to the car). The standard mirror involves two cases, one simulation with the half car, and one with the whole car.

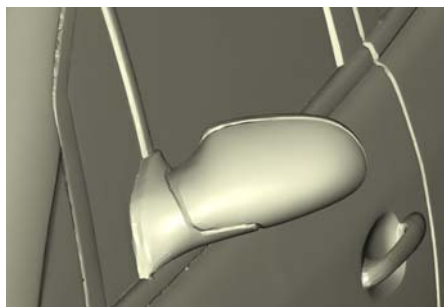


Figure 4.1: Case: The standard mirror.

### 4.2 Without Mirror

In this case, the mirror has just been removed (figure 4.2). On the window, over the position of the standard mirror, there is a beam. This beam has been extended to give this case a believable appearance. To do simulations without a mirror is to see how big the mirror's influence is.



Figure 4.2: Case: Without mirror.

### 4.3 Reference Mirror

As afore mentioned, an number of different designed mirrors were tested until a reference mirror (figure 4.3) was selected. This mirror was selected for showing the most promise and having the least drag value. This mirror is the base for comparison when it comes to the modifications of this reference mirror. The reference mirror has a much smaller foot than the standard mirror in order to allow for flow between the mirror housing and the body of the car. The foot has been connected to the car body through an attachment plate. The attachment angle has been chosen to be parallel to the window.

Some important measurements (when it comes to the modifications)

- The distance between the attachment plate and the foot is 10 mm.
- The height of the foot is 3 mm.
- The depth of the glass is 1.8 mm.
- The outer point of the mirror is situated 48 mm from the window.
- The radius of the inner front edge is 7 mm.

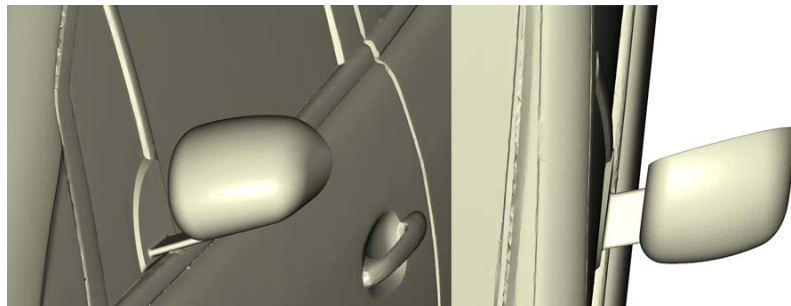


Figure 4.3: Case: The reference mirror.

### 4.4 Varying the Gap

The gap (the distance between the attachment plate and the mirror housing) has been varied (figure 4.4). Seven different gap distances have been simulated; 4 mm, 7 mm, 10 mm (reference mirror) 13 mm, 16 mm and 19 mm. Changing this distance also moves the mirror away from the car's body. The regulations allow the mirror to protrude no more than (both sides included) 62.5 mm (250 mm in full scale) from the widest part of the car body. The 19

mm gap just fulfills this requirement. The intention with this modification is to allow a greater flow between the mirror housing and the car body.

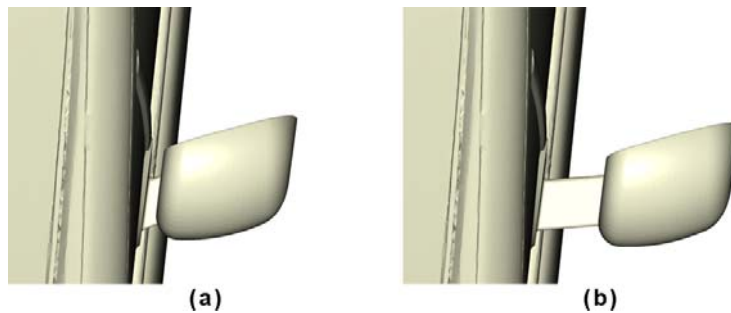


Figure 4.4: Case: Varying the gap, where (a) is 4 mm and (b) 19 mm.

#### 4.5 Varying the Height of the Foot

The height and thickness of the foot is mostly important for stability of the mirror. With a foot that is too weak the mirror may start to vibrate. Four different heights of the foot have been simulated; 3 mm (reference mirror), 5 mm, 7 mm and 9 mm (figure 4.5). The profile of the foot has been kept as similar as possible for all the thicknesses.

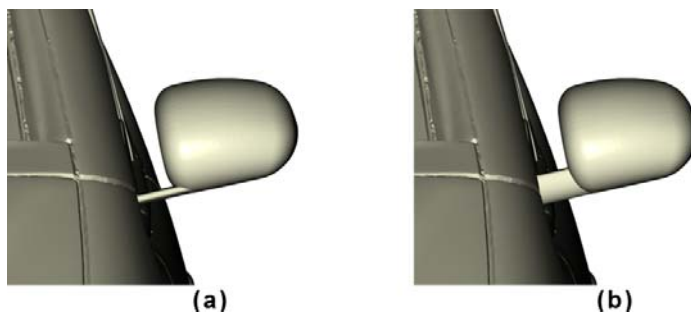


Figure 4.5: Case: Varying the height of the foot, where (a) is 3 mm and (b) 9 mm.

#### 4.6 Varying the Inclination

The angle between the attachment plate/window and the inner side of the mirror housing will be referenced in this thesis as the inclination angle. This inclination can be both positive and negative. Seven different inclination angles have been simulated; -15 deg, -10 deg, -5 deg, 0 deg (reference mirror), 5 deg, 10 deg and 15 deg (figure 4.6). The distance between the attachment plate and the rear inner edge of the mirror housing has been kept the same throughout the varying of the inclination angle. The reason for this change is to see if there is any diffuser effect or influence of moving the front inner edge of the mirror housing on the flow. A smaller inner radius (next case) of 4 mm has been used for all inclination cases to get a more distinct edge.

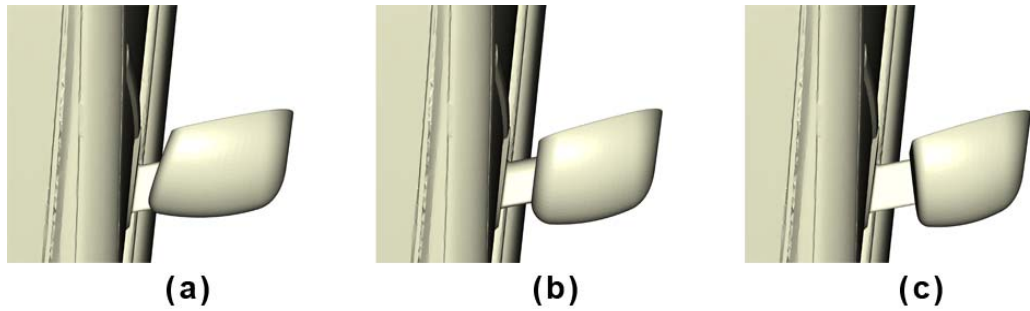


Figure 4.6: Case: Varying the Inclination, where (a) is 15 deg, (b) is 0 deg and (c) is -15 deg.

#### 4.7 Varying the Inner Radius

The front edge of the inner side of the mirror housing has been named inner radius. Four different inner radii have been simulated; 1 mm, 4 mm, 7 mm (reference mirror) and 10 mm. The inner radius influences the flow between the mirror housing and the car body.

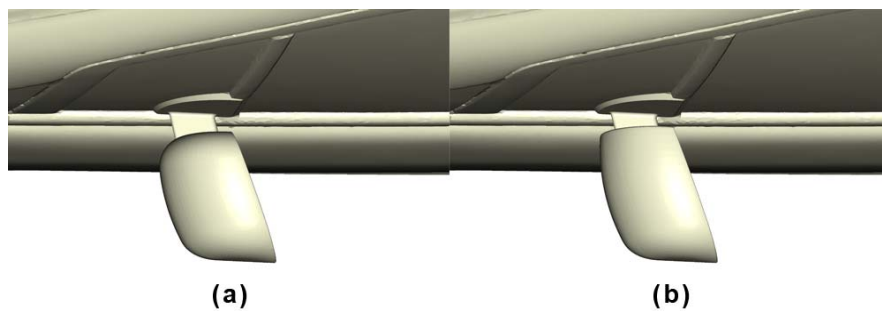


Figure 4.7: Case: Varying the Inner Radius, where (a) is 10 mm and (b) is 1 mm.

#### 4.8 Different Housing Curvatures

The curvature of the mirror housing affects the flow to a great extent and is therefore of interest. Three different mirror housing curvatures have been simulated; one that is flat, the reference mirror, and one that is somewhere in between the two afore mentioned (figure 4.8).

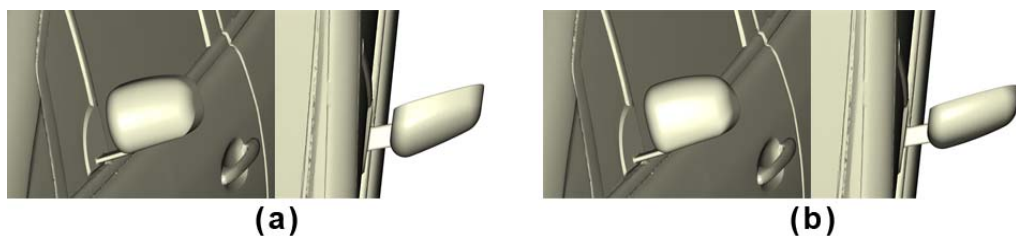


Figure 4.8: Case: Different Housing Curvatures, where (a) is medium and (b) is flat.

## 4.9 Single Changes

The following singular modifications have been done.

### Gutter

A gutter (figure 4.9) has been created on the upper side of the mirror. This feature is common on commercial vehicle mirrors, mainly due to acoustic and soiling reasons. The gutter is 0.5 mm deep and 0.7 mm wide. Gaps (gutters) often provoke flow separations.

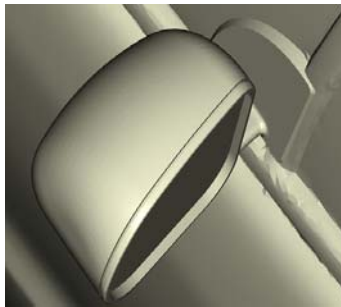


Figure 4.9: Case: Gutter on the upper side.

### Edge

An edge (figure 4.10) has been made on the underside of the mirror. This feature is also common on commercial vehicle mirrors for the same reason as the gutter on the upper side. The gutter is 0.5 mm high and 0.5 mm wide.

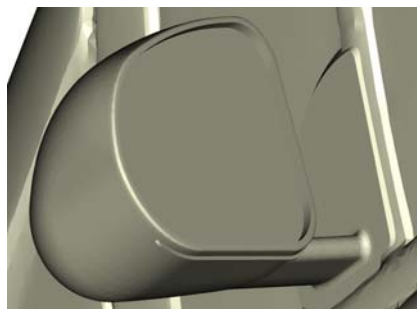


Figure 4.10: Case: Edge on the under side.

### Deeper Glass

The depth of the mirror glass (figure 4.11) can be varied to an extent that it is not covered by the edges of the mirror housing from the view of the driver. The mirror glass has been put 5 mm deeper than the reference to a depth of 6.8 mm.

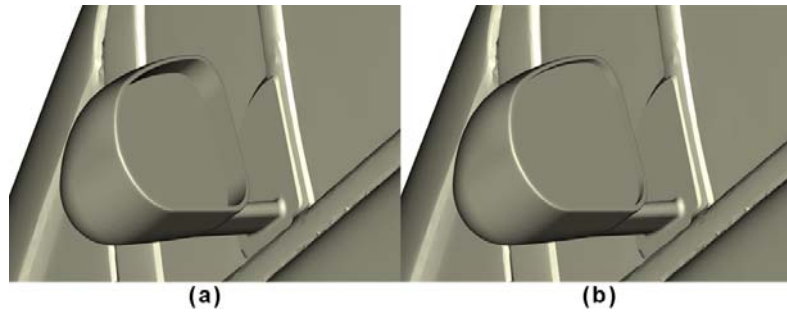


Figure 4.11: Case: Deeper glass, where (a) is 5 mm deeper and (b) is the reference depth.

### **Straight Angle**

The reference mirrors housing is parallel to the window, but the window is not vertical. In this case, the angle of the mirror housing is changed so it is vertical (figure 4.12).

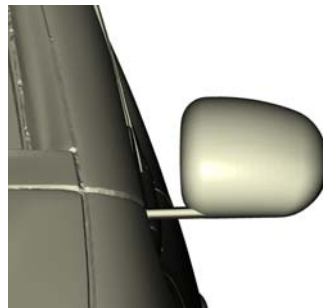


Figure 4.12: Case: Straight angle.

## **4.10 Combined Changes**

To see the result of combining changes, two cases were made:

- Housing Curvature medium, Deeper Glass, Gutter on the Upper Side and Gap 16 mm
- Housing Curvature medium and Gap 16 mm

## 5 Case Setup (CFD)

A template called Aero Wind Tunnel, in PowerCASE was used. This template facilitates work with wind tunnel simulations. The dimension of the wind tunnel is set by the template itself. An option for moving ground has been used, which includes both a center belt and wheel belts. The sizes of the belts are the same as the scale model wind tunnel. To simulate the rotation for each individual rim, four Rotating Reference Frames regions (MRF) were created. Additionally, the wheels were lowered into the belts, with 2 mm, to better resemble the wind tunnel conditions. All cases use the same setup. An inlet velocity of 50 m/s has been used, due to praxis at FKFS and the conditions in the scale model wind tunnel. The simulation volume consists of around 17 million Voxels (half car). For parameters see appendix A.

### 5.1 Variable Resolution (VR) Regions

In total 9 different levels of VR regions have been utilized. The coarsest grid, level 0, is furthest away from the car. The finest grid, level 9, is just exactly 4 cells from the car's body. The sizes for the different VR regions is in accordance with the praxis from the PowerFLOW Best Practice guide. Figure 5.1 and 5.2 shows the different VR regions around the car.

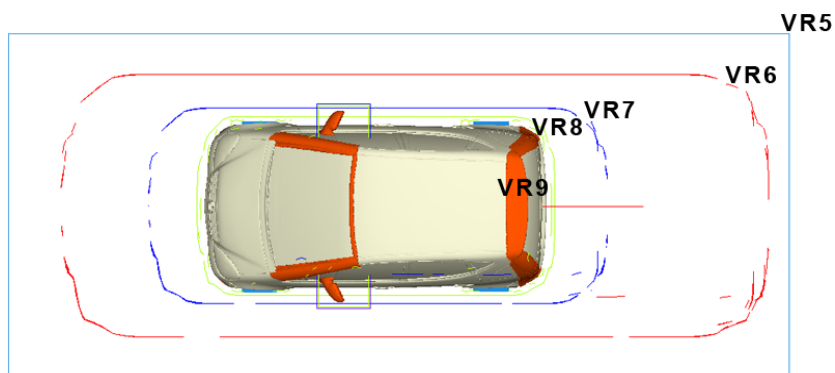


Figure 5.1: Different VR regions around the car, top view.

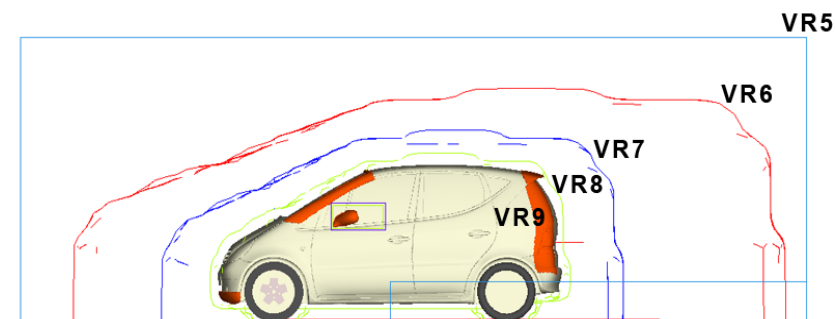


Figure 5.2: Different VR regions around the car, side view.

The different VR regions have different colors. The orange regions have the highest level, which are offsets of the c-pillar, a-pillar, the transition between the windshield and the roof, the mirrors, the rear spoiler and the

lower part of the bumper. This to cover the flow separation in these areas. Level 8, which is demonstrated with yellow, is situated around the mirrors (as a box) and around the car body. The later uses a construction mesh which can be seen in Figure 5.3. The construction mesh is made from the car body and simplified. Level 7 is also around the mirrors (as a box) and the car body, and is presented as blue. Level 6, which only exists around the car, can be identified with red. Both level 7 and 6 are created by a construction mesh (figure 5.3). This mesh differs from the VR8 construction mesh in that it does not follow the underside or wheels of the car. This creates better coverage of the flow under the car. The exact offset for the VR regions in PowerCase can be found in appendix A.

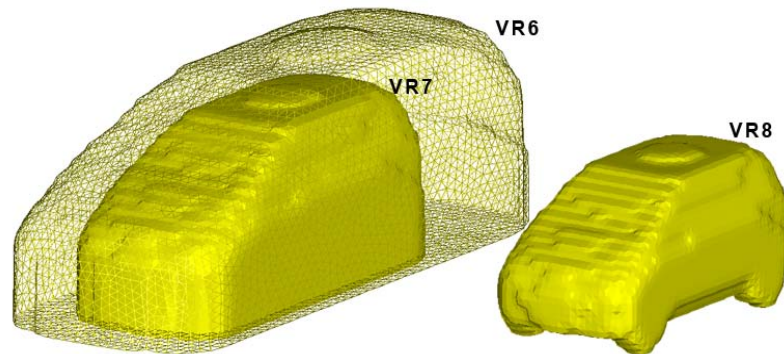


Figure 5.3: VR6, 7 and 8 construction model.

The VR regions for level 5 to level 0 (simulation volume) are created by the template itself. These can be seen in Figure 5.4. In this figure the inlet and outlet can also be seen.

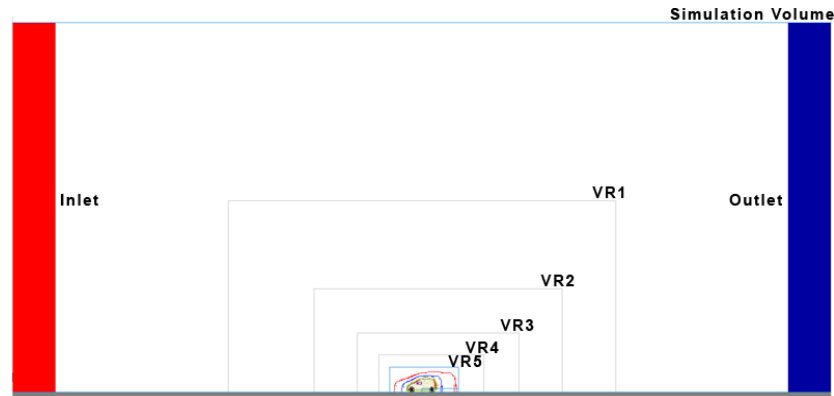


Figure 5.4: VR regions for the wind tunnel.

## 5.2 gence and Averaging

Most of the simulations have run for 400,000 time steps before they have been averaged. The average interval for the majority of cases has been from 240,000 to 400,000 time steps. Some cases have run less then 400,000 time steps, so they have been averaged over a shorter interval. To hasten simulation time, data from an old run has been used as a constant for all cases. Figure 5.5 shows an example of how the forces ( $F_x$  and  $F_z$ ) changed during

a simulation. The red area indicates the interval where the averaging has taken place. As can be seen, the forces vary noticeably, even in the end. This variation is due to the fact that the drag oscillates in a sinus-shaped curve and with the standard mirror case, the oscillation repeats every 4 Hz.

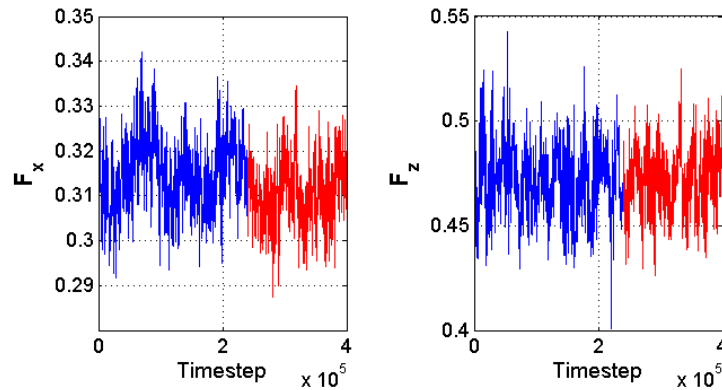


Figure 5.5: Convergence example.

The choice of averaging the interval will affect the outcome. Figure 5.6 displays how the averaging interval affects the averaged drag value. The graph is made as follows; an interval that corresponds to 4 Hz (length of one time step is 2.228e-06 seconds) has been moved from time step 0 to the end. The averaged value that has been used in this case is marked with an 'x'. As seen in the figure, having the interval too early gives a considerably unsteady result. When the drag value (averaged value) becomes somewhat stable an uncertainty remains in the result. In this case it is around 1.5 drag counts. Note: the force presented in these graphs cannot be compared to those of the upcoming result section due to a variation in calculating force methods.

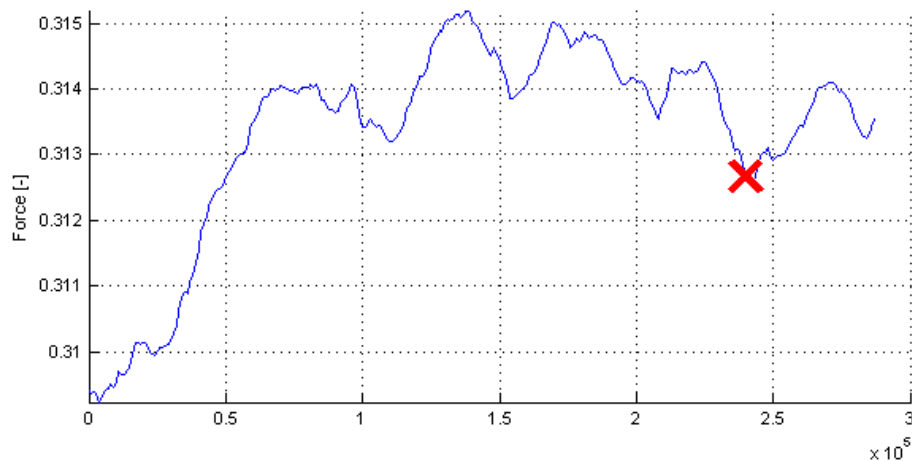


Figure 5.6: Averaging example, where the 'x' shows the used averaged value.

It is important to bear in mind that the "averaging curve" changes appearance from case to case. Figure 5.7 exhibits the averaging for another case and the appearance is not the same. This case has an uncertainty of around 2 drag counts. When comparing different cases' drag values, the uncertainties in the simulations may also sum up (underestimation and overestimation

of the drag), so the uncertainty can be worse than 2 drag counts. Having the same averaging interval for all cases is not the best solution, yet, is the method used currently at FKFS. A better method for averaging is currently under development at FKFS.



Figure 5.7: Another averaging example, where the 'x' shows the used averaged value.

## 6 Wind Tunnel Setup

The wind tunnel that has been used is the scale model wind tunnel at FKFS.

### 6.1 Information

The scale model wind tunnel, which is of the closed circuit type, has an open test section and is used for the doing measurements of 1:3.5 to 1:5 models. It is equipped with a 5-belt system; a center belt is located between the wheels and the wheels are individually driven by their own belts. The model is fixed to a balance (6-component) with four struts, which together with the wheel rotation units measure the aerodynamic forces. The wind tunnel is also equipped with a turn table for measuring the influence of cross wind. [4]

In table 6.1 the technical data for the FKFS model wind tunnel can be found. Figure 6.1 indicates the layout of the wind tunnel.

Table 6.1: Technical data for the model wind tunnel. [4]

Dimensions of nozzle (WxH)	<i>1,575 m x 1,05 m</i>
Exit area of nozzle	<i>1,654 m<sup>2</sup>/s</i>
Contraction ratio	<i>4,95</i>
Length of open-nozzle test section	<i>2.585 m</i>
Diameter of axial fan	<i>2.0 m</i>
Operating output	<i>335 kW (1050 1/min)</i>
Max. flow velocity	<i>288 km/h</i>
Displacement height of boundary layer in the center of the ground plane (x=0)	
- without boundary layer influence	<i>4.5 mm</i>
- with boundary layer pre-suction	<i>2.4 mm</i>
- with road simulation	<i>Block profile</i>

### 6.2 Setup

For making a Reynold sweep, 5 different wind speeds were used; 140km/h, 160km/h, 180km/h, 200km/h and 220km/h. The ground clearance for the model remained the same as in the CFD simulations. In this case the distances between the wheelhouses and the wheels are 162.0 mm in the front and 161.0 mm in the rear. The measuring time was 2,000 msec. From these numbers an average was made. No cooling of the air flow was used. For

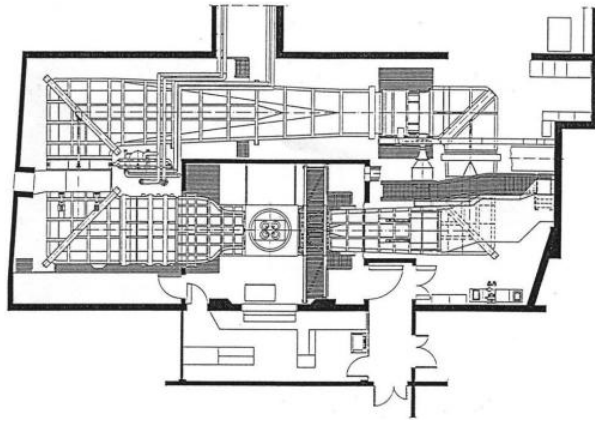


Figure 6.1: A drawing of layout of the model wind tunnel.

all measuring boundary layer pre-suction, tangential blowing for the central belt, and ground simulation were used. The blockage is around 8.5% for this specific car model and wind tunnel. The flow field's velocity was measured in some cases by using a COBRA probe (for more information see the manufacturer's homepage, <http://www.turbulentflow.com.au>). This probe can measure the velocity of all three directions in the flow, however, cannot measure negative velocities. Figure 6.2 displays the car in the wind tunnel. One of the self-made mirrors has been taped on with silver tape.



Figure 6.2: The model car in the wind tunnel.

### 6.3 Rapid Prototyping

The machine used for rapid prototyping is an Objet Eden 260V 3D printer. The printer puts photopolymer materials in ultra-thin layers upon layers onto a build tray until the part is complete. Each photopolymer layer is cured by UV light immediately after being jetted. A supporting material, which supports complicated geometries, is removed by hand and water jetting. This printer has a resolution of 600 dpi in X- and Y-direction and 1600 dpi in Z-direction. Figure 6.3 shows the printer, the mirror with support material around it and an almost clean mirror.

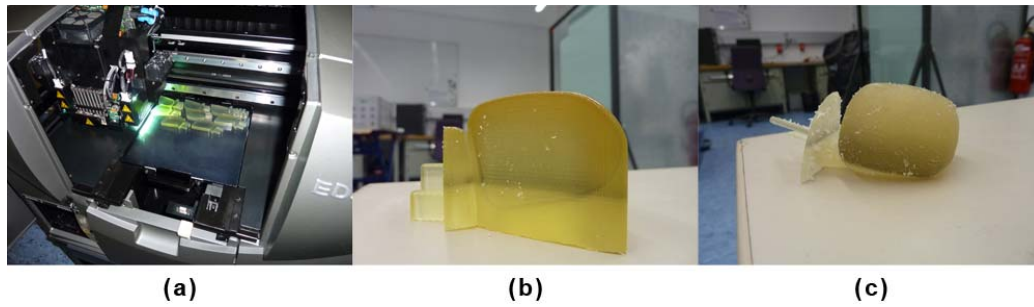


Figure 6.3: (a) A rapid prototyping machine, (b) the mirror with support material around it and (c) an almost clean mirror

## 6.4 Selection of Mirrors for Wind Tunnel Testing

The following mirrors were measured in the wind tunnel:

- Standard mirror
- Without mirror
- Reference mirror
- Reference mirror - Foot 7 mm
- Reference mirror - Gap 4 mm
- Reference mirror - Gap 16 mm
- Reference mirror - Inclination 10 deg
- Reference mirror - Housing curvature medium
- Reference mirror - Inner radius 1 mm
- Reference mirror - Inner radius 10 mm
- Reference mirror - Straight

## 7 Results

The following subsections will present the results of the CFD simulations and wind tunnel testing. A comparison between these two will also be presented. Due to the fact that this thesis is mainly focused on drag reduction, the numbers for lift will not be presented in this section. Detailed results, which include lift data, can be found in appendix C. Please note that all graphs within the result section do not begin at 0.000  $C_d$ , but at a higher value. The value that stands over the bars is the total drag for the configuration in question. The term *drag counts* is used to simplify the way of comparing  $C_d$  values. One drag count is 0.001  $C_d$ . Note: this section will not deal with the uncertainties in the simulations.

### 7.1 CFD

Figure 7.1 bears the results from the simulations of the whole and half car. The simulation results for the half car without mirror and with the reference mirror have been added for comparison purposes. The drag values for all half car simulations have been doubled.

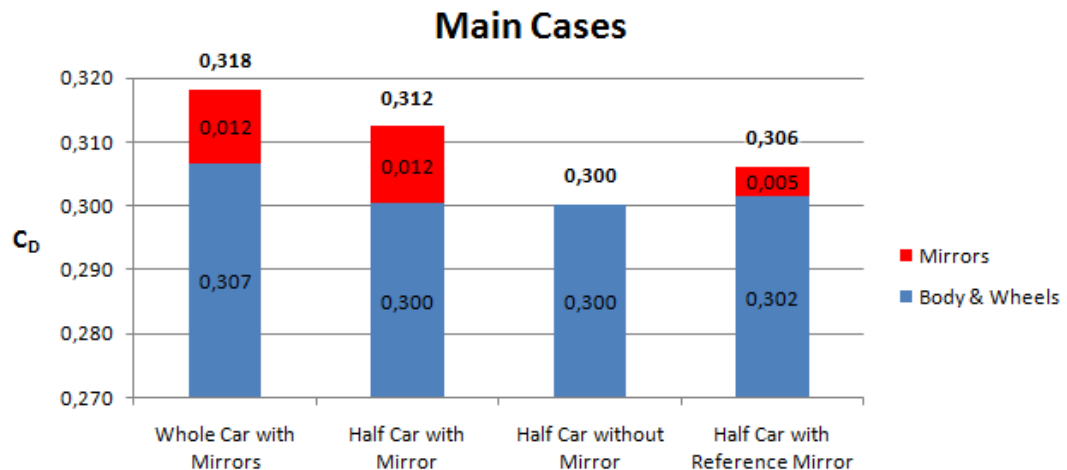


Figure 7.1: Drag comparison between whole and half car.

As visible in figure 7.1 the drag contribution from the body and wheels have been summed up. This summation is due to the insignificant change in the wheels between the different cases. The wheel drag interval contribution was between 54 and 58 drag counts, while mostly remaining at about 55. The larger changes within the body and wheel drag contribution are because of the change in contribution from the body. This figure demonstrates that the drag is not the same for the whole car and the half car. The difference lies in the body and wheels' contribution. Also noteworthy is the reference mirror which has twice as small  $C_d$  value as the standard mirror. As hypothesized, the case without mirror has the least amount of drag.

## Reference Mirror - Gap

Figure 7.2 shows the results from varying the gap distance between the attachment plate and the mirror housing for the reference mirror. There is a vague trend for the  $C_d$  value for the different gap distances; the drag decreases with increasing distance. The difference lies in the contribution from the body. Compared to the reference mirror, the mirror drag contribution is the same for all configurations.

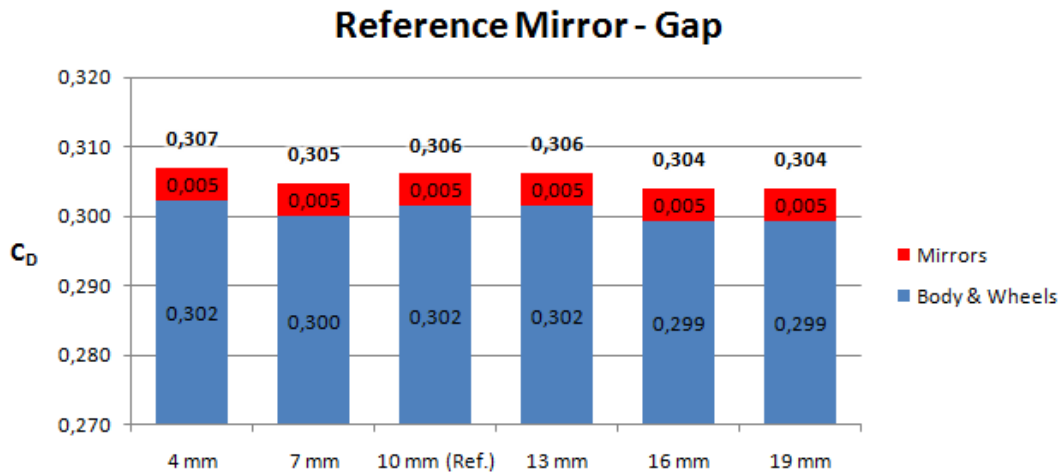


Figure 7.2: Drag comparison between different gap distances for the reference mirror.

## Reference Mirror - Foot

Figure 7.3 illustrates the results from varying the thickness of the foot, which connects the attachment plate and the mirror housing, for the reference mirror. The drag contribution from the mirror remains the same for all configurations. There is no clear trend for the total amount of drag.

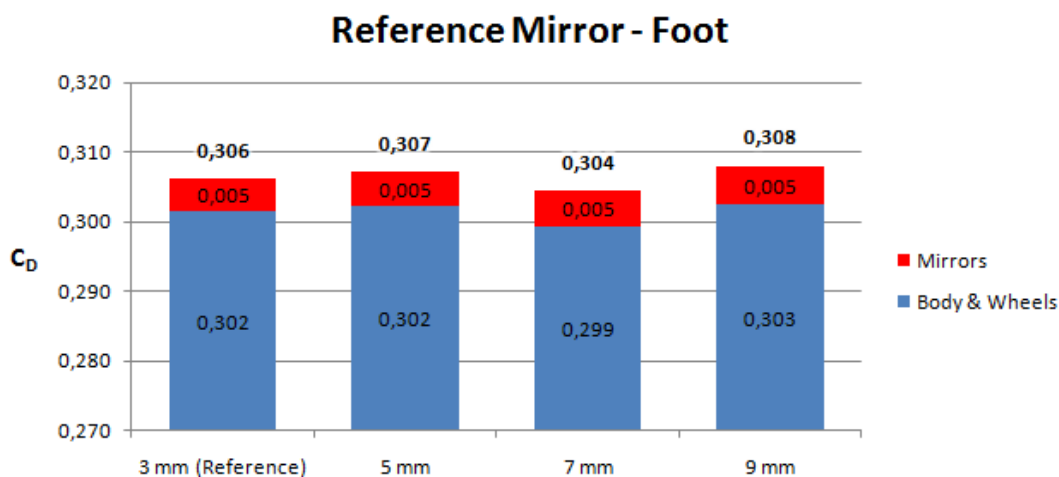


Figure 7.3: Drag comparison between different thicknesses of the foot for the reference mirror.

### Reference Mirror - Inner Radius

Figure 7.4 exhibits the results from varying the inner radius of the mirror housing for the reference mirror. Here a very small increase of the mirror drag contribution for the 1 mm Inner Radius can be observed, however, the rest of the mirrors are the same. It is only the configuration with the largest inner radius that shows a decrease in drag.

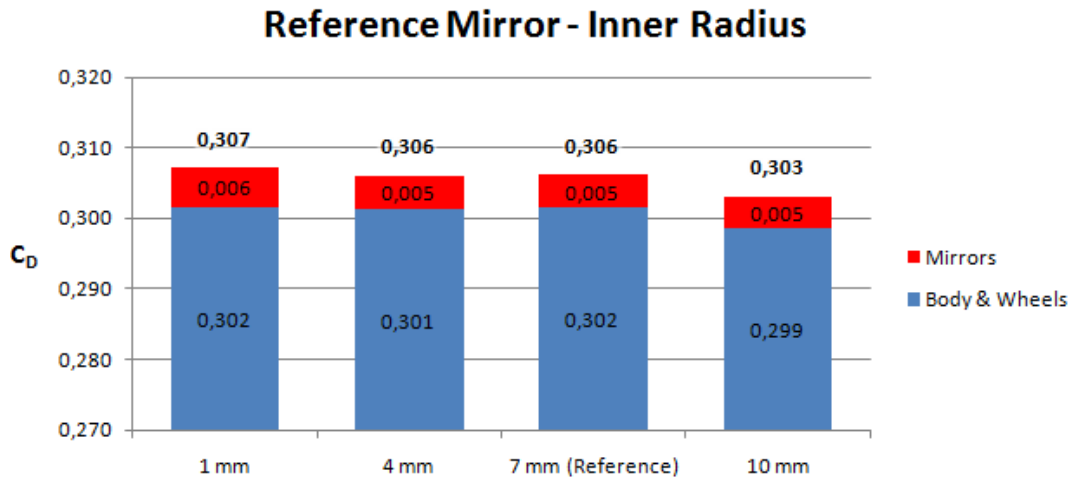


Figure 7.4: Drag comparison between different inner radius of the mirror housing, for the reference mirror.

### Reference Mirror - Inclination

Figure 7.5 shows the results from different inclinations of the mirror housing for the reference mirror. For the inclination there is no clear trend in drag. The two configurations with the greatest difference are -5 deg and 10 deg. These have decreased the drag with 2 respective 5 drag counts compared to the reference case. All the mirrors have the same mirror drag contribution, excluding the case with an inclination of 15 deg.

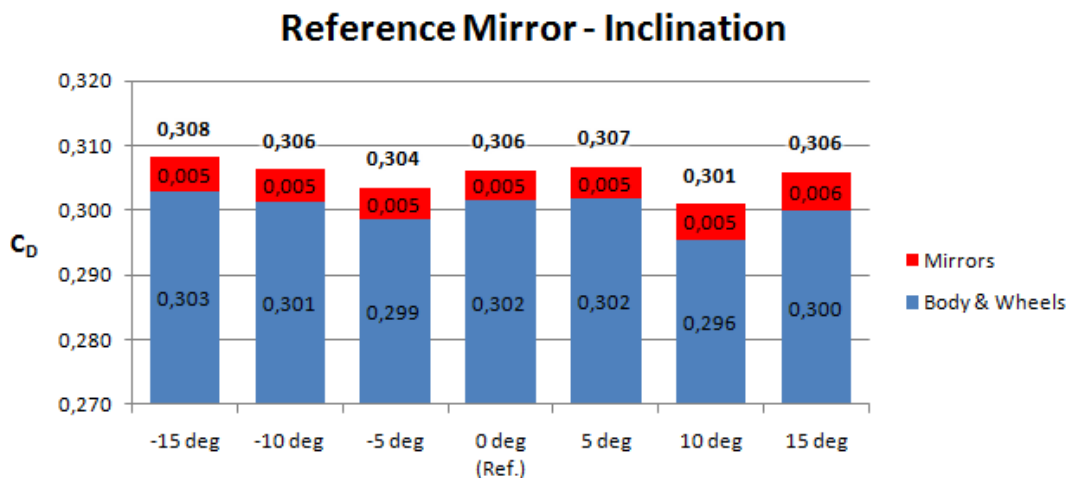


Figure 7.5: Drag comparison between different inclinations of the mirror housing, for the reference mirror.

## Reference Mirror - Housing Curvature

Figure 7.6 presents the results from different curvatures for the mirror housing for the reference mirror. There is a rather large decrease in the total amount of drag for both the flat and medium housing curvature configuration, 5 respective 6 drag counts. The decrease is due to the body and wheels because the mirror drag contribution has increased compared to the reference mirror.

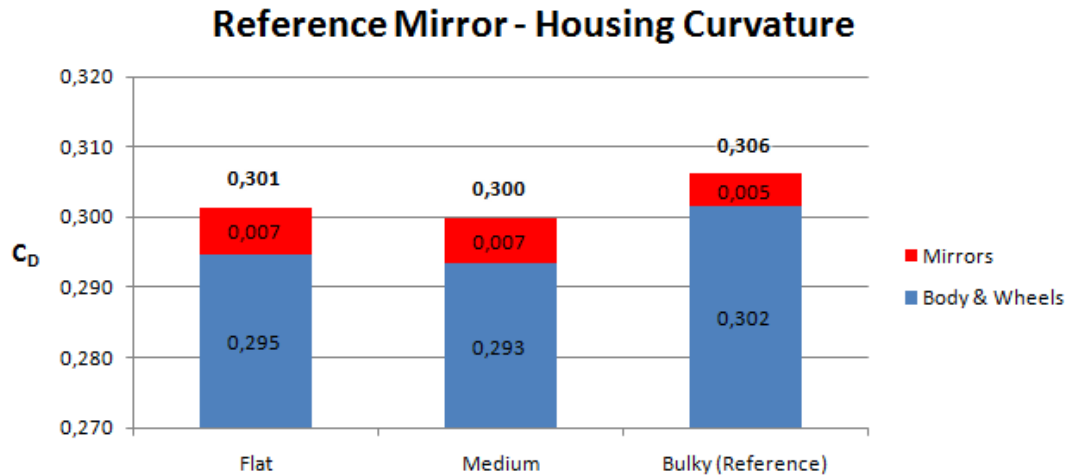


Figure 7.6: Drag comparison between different curvatures of the mirror housing, for the reference mirror.

## Reference Mirror - Single Changes

Figure 7.7 addresses the results of different single changes from the reference mirror. The one change that distinguishes itself from the others is the edge on the under side, with a decrease of 4 drag counts.

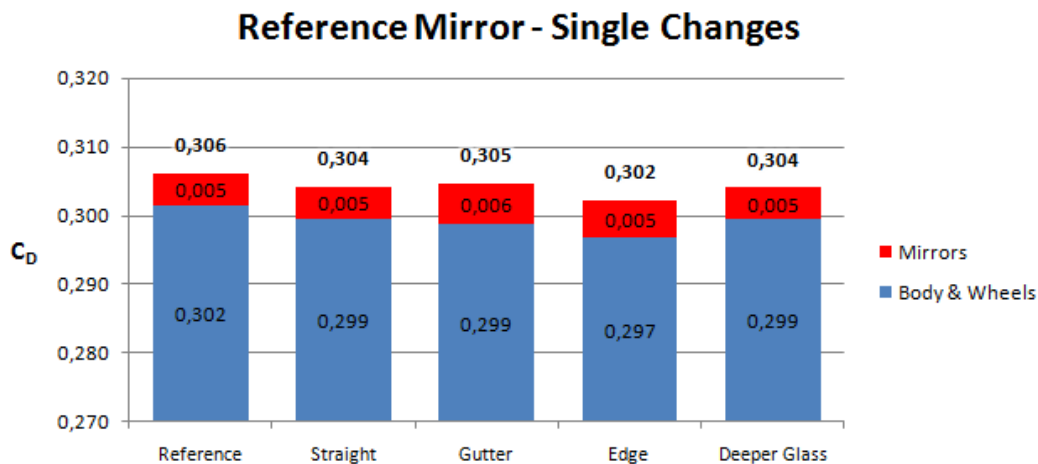


Figure 7.7: Drag comparison between single changes, for the reference mirror.

## Reference Mirror - Combined Changes

Figure 7.8 conveys the results from combined changes for the reference mirror. With the combined changes there are both increases and decreases in drag. With a medium housing curvature, deeper glass, gutter on the upper side, and 16 mm gap there is clear increase of drag (4 drag counts). However, when the gutter and the deeper glass are removed the drag is nearly the same as the reference mirror.

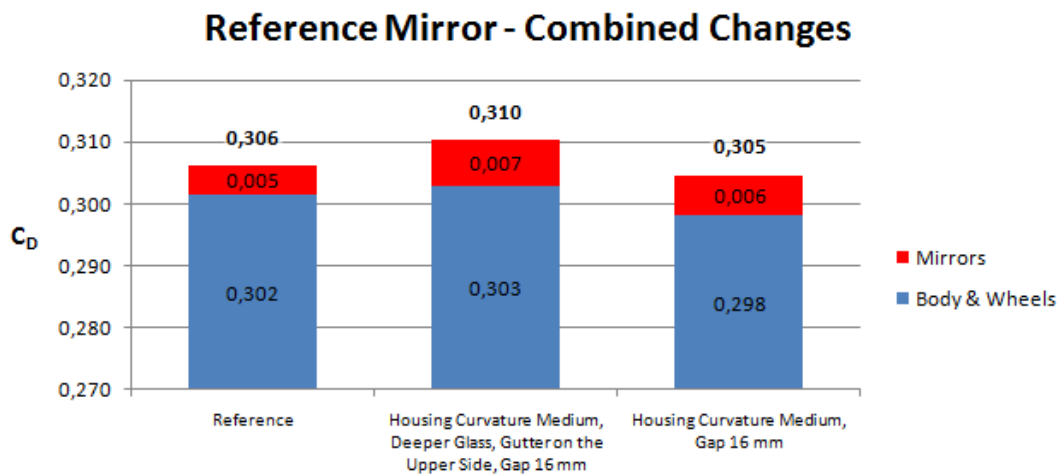


Figure 7.8: Drag comparison between combined changes, for the reference mirror.

## 7.2 Wind Tunnel

The results from the testing of the quarter scale model can be found in figure 7.9. In this figure the drag from the standard mirrors, without mirrors and with the reference mirrors, can be found. The individual contribution, for example of the mirrors, cannot be measured in the wind tunnel, so only the total drag is presented. A more detailed presentation of the result, with belonging lift data, can be found in appendix C. The results of the wind tunnel were first all "scaled" with the same frontal area; that of the standard mirror case. All cases, with exception to the case without mirror, do not bear a noticeable difference (0.3%=1 drag count) by using the same area. The case without mirror differs with 2% which results in about 6 drag counts. Because of this, the results for all cases in this section from the wind tunnel have been scaled with CFD area.

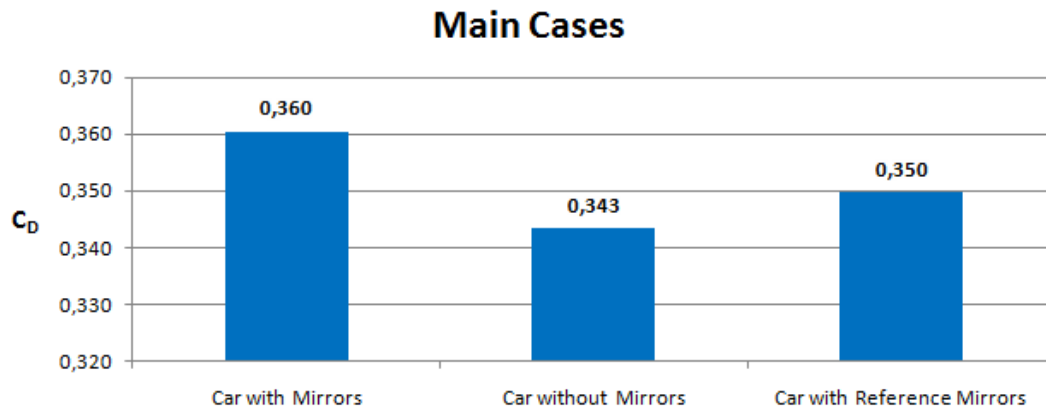


Figure 7.9: Wind tunnel drag comparison between the standard mirrors, without mirrors and the reference mirrors.

Figure 7.10 presents the total drag result after a selection of changes of the reference mirror. The difference between the varying configurations are not large. It is measured around +/- 1 drag counts from the  $C_d$  value of 0.350. There are some mirrors that are worse than the reference, such as the 4 mm gap and the 7 mm thick foot. Both the mirror, with 16 mm gap, and housing curvature medium indicate lower drag than the reference mirror.

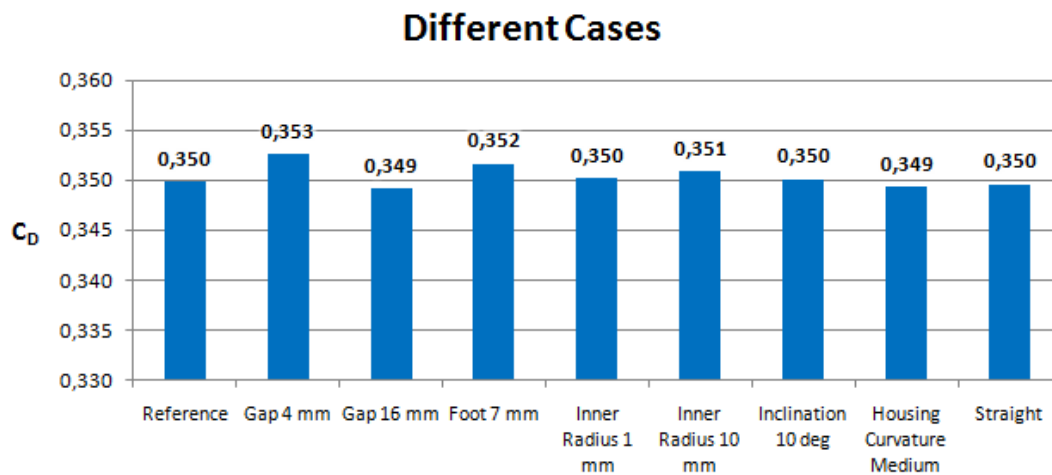


Figure 7.10: Wind tunnel drag comparison between selected changes, for the reference mirror.

### 7.3 Comparison

Figure 7.11 shows the comparison between the results from the wind tunnel and CFD simulations. There is a significant difference between the wind tunnel and CFD results. For the car with the standard mirror it differs 48 drag counts. Without mirrors it differs 43 drag counts, and the reference mirror is 44 drag counts. The CFD simulations seem to underestimate the drag to a great extent (around 13%).

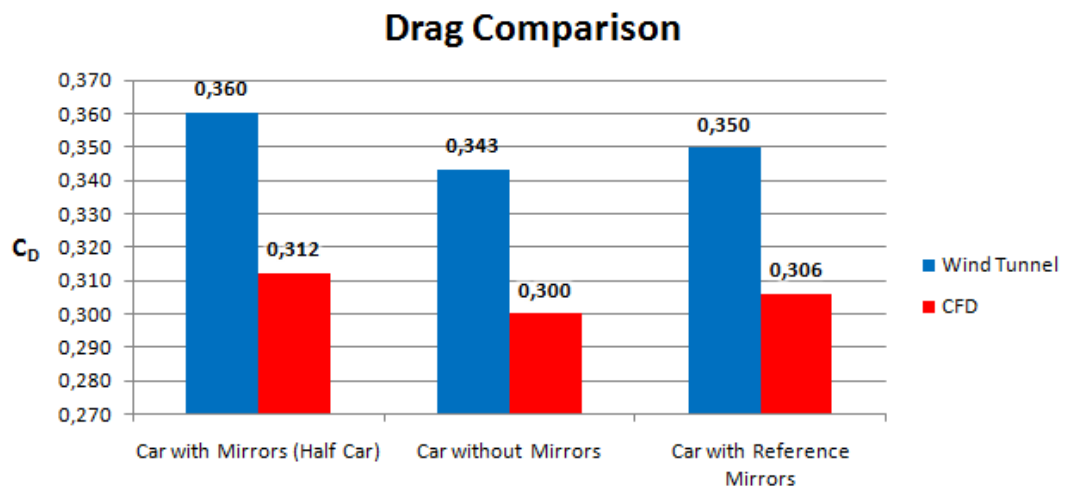


Figure 7.11: Wind tunnel drag results compared with CFD.

In figure 7.12 the difference to the standard mirror in percent is presented. The difference is taken from the respective source. In other words, the CFD results are compared to the CFD simulations for the standard mirror and vice-versa. This is done to illustrate the trends for each change and minimize the influence of the specific values in the wind tunnel tests and CFD simulations. All changes show the same trend; they are all better than the standard mirror. How good they are differs and the difference between CFD and wind tunnel also differs from case to case. Sometimes the wind tunnel gives lower drag and other times we have the opposite case. The difference in no case is bigger than 1.2 percentage points. The case with the largest deviation is the mirror with the inner radius of 1 mm. This can be due to the fact that CFD has hard to handle that sharp corners/edges with current grid.

## Drag Comparison

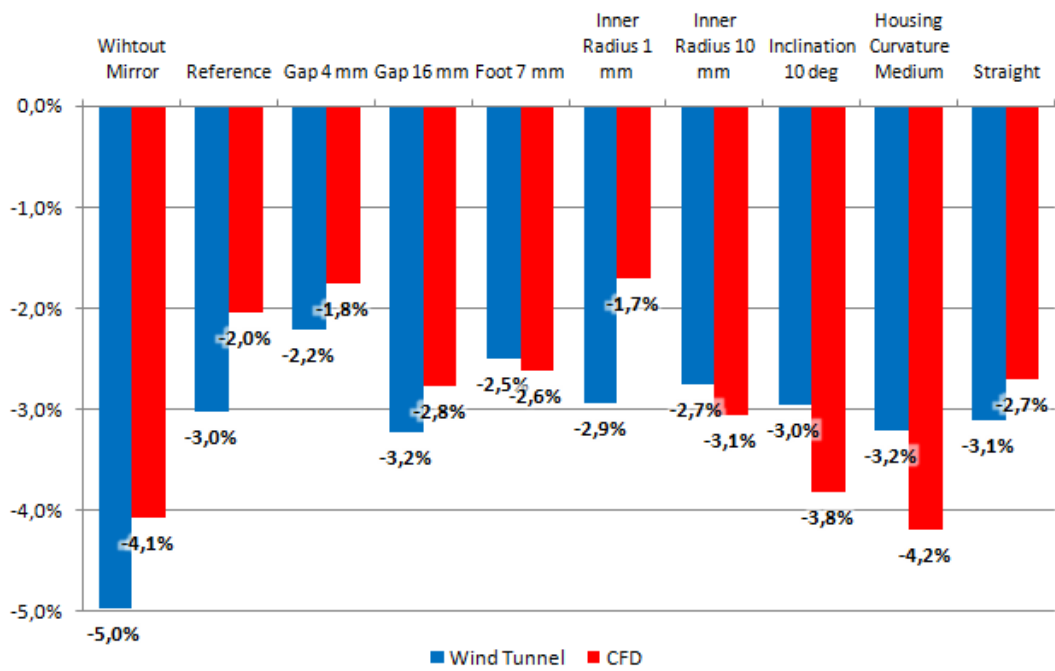


Figure 7.12: Wind tunnel drag results compared with CFD for selected changes. The results are presented in percent compared to the standard mirror.

## 7.4 Reynolds Sweep

Figure 7.13 shows a Reynolds sweep for the standard mirror and reference mirror. While the standard mirror's  $C_d$  value stays more or less the same over the sweep. The reference mirror's  $C_d$  value decreases with the increasing Reynolds number. In this thesis the Reynolds sweep is not considered important due to the CFD simulations and the wind tunnel experiments both being made in quarter scale. For the reference mirror there would probably be a decrease in drag when using a full scale test.

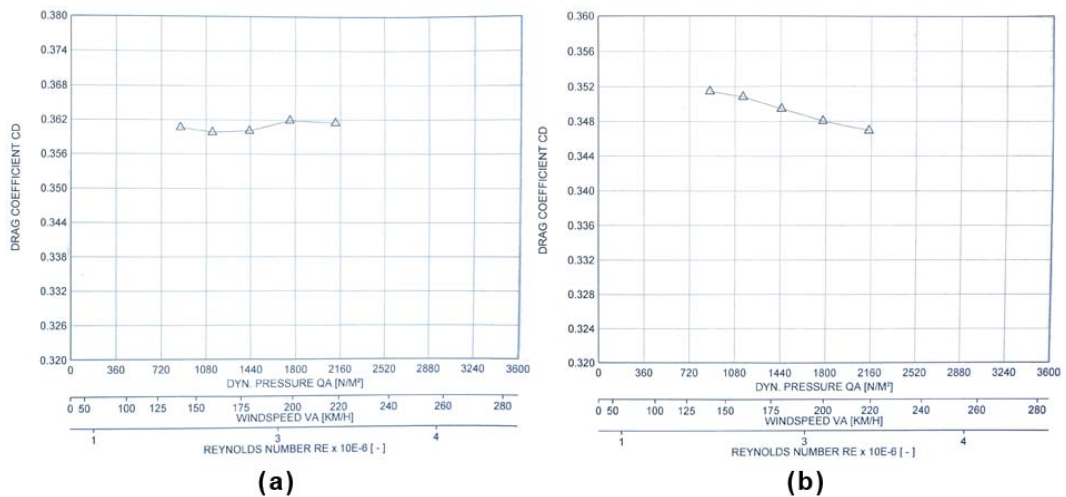


Figure 7.13: A Reynold sweep for (a) the standard mirror and (b) the reference mirror.

## 8 Flow Analysis and Comparison

This section contains the flow analysis of the CFD simulations for different cases. All simulations, excluding the standard mirror, are made by using a symmetry plane. The results will just be shown for half of the car. The different cases are going to be compared to the standard mirror (half car) or the reference mirror. Some cases are also going to be compared to wind tunnel velocity measurements. Not all parameters are going to be dealt with, just a selection. Note: in the figures in this section, the scale for the different properties may be out of range in some cases.

### 8.1 Standard Mirror (Half Car)

In order to see where the large losses in the flow and wakes are, the areas with a total pressure of zero are of interest. In the figure 8.1 the flow separation is represented by iso-surfaces where the total pressure is equal to zero. As shown in the figure there are many different areas with a total pressure of zero (or lower). The largest wakes are formed at the wheels, their archers, and in the rear. The large wake in the rear is created by the roof spoiler, the c-pillar, rear bumper, and the rear wheel. Other wake locations are: plenum, a-pillar, the beginning of the roof, in gaps, and the doorhandles. All these wakes mean losses in flow, which in turn, contribute to increased drag. It can be difficult to see that the standard mirror wake, which is created by the mirror housing itself along with the mirror foot, connects to the window. Moreover, one can see that the rear wake's shape indicates down wash in the rear.

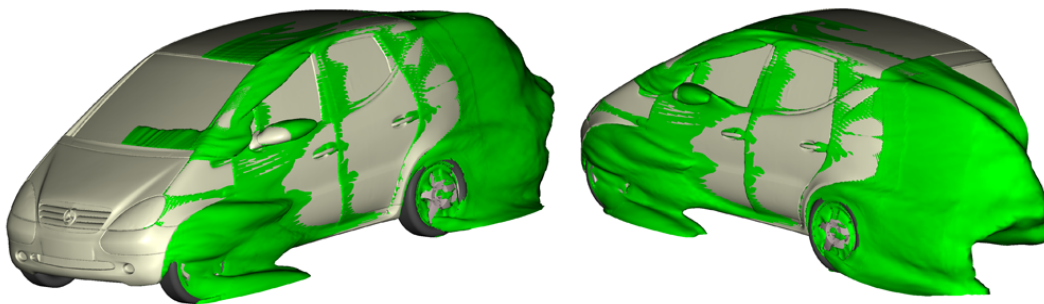


Figure 8.1: Iso-surfaces showing where the total pressure is equal to zero.

Figure 8.2 shows the velocity magnitude of the flow near the symmetry plane from the side. As shown, the flow comes to a stop at the front bumper. In other words, there is a stagnation point at the front bumper. The flow separation at the plenum can also clearly be seen. Both under the car and over the car the flow is accelerated. As with the iso-surface above, one can see that the flow separates on the roof spoiler and at the rear bumper. The velocity arrows indicate that the flow is circulating in the top of the rear wake and that the wake behind the car has a clear down wash. The down wash can also be seen in the wake planes in figure 8.3. The wake planes also show the vorticity from the a-pillar. The wake from the mirror can be seen in the wake planes as a bulging yellow area just above the mirror location.

The reason why it is above the mirror location is because of an upward flow from the mirror.

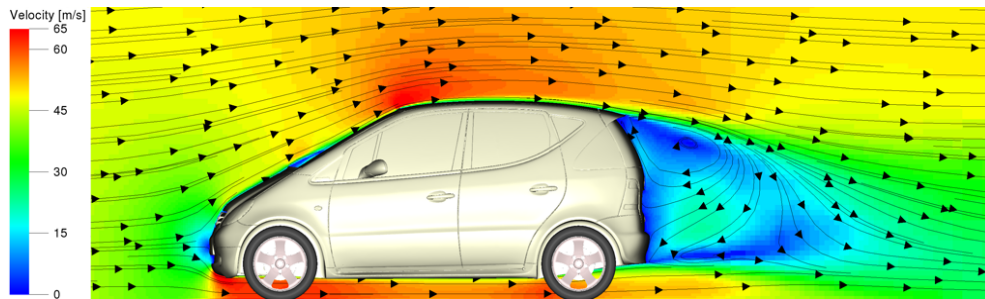


Figure 8.2: Side view of the car showing the velocity magnitude [m/s] in the symmetry plane.

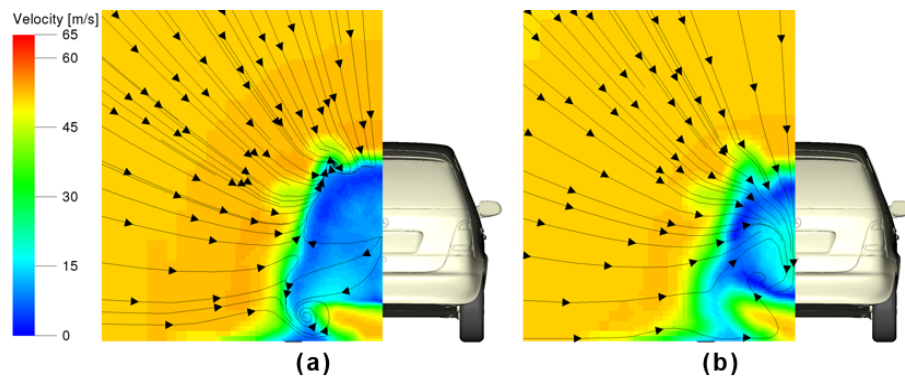


Figure 8.3: Rear view of the car showing the velocity magnitude [m/s] in two wake planes, where (a) is 25 mm and (b) is 90 mm behind the rear bumper.

Figure 8.4 shows the pressure coefficient on the surface of the car. The definition of pressure coefficient: taking the difference between the local pressure in a point along with the free stream static pressure, and then divided the difference with free stream dynamic pressure. This ratio describes how the pressure varies around the vehicle, without taking into consideration the velocity of the vehicle. By looking at the pressure coefficient, the stagnation (high pressure) at the front bumper can be seen. Other surfaces with high pressure are the lower part of the front tire and the mirror. There are also some low pressure areas which indicate accelerated flow. These areas are often "sharp" corners and transitions. In this case the low pressure areas are the front edge of the wheels, the front wheel archer, the a-pillar, the edge of the top of the windscreen, and the mirror. The average pressure coefficient is lower in the rear of the car than in the front, causing pressure drag.

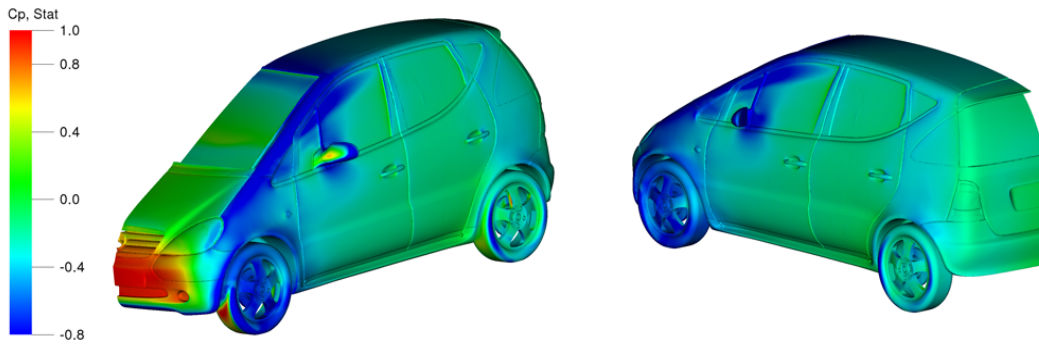


Figure 8.4: Pressure coefficient [-] on the front and the rear of the car.

The total pressure indicates how intense the wake is. The lower the total pressure is, the larger the losses are in the flow. Figure 8.5 shows two wake planes from behind the bumper. One 25 mm and one 90 mm (1/10 of the car.) Here losses in the flow can be observed. The further away from the car, the smaller the losses are. In the wake planes, the influence of the wheels can easily be seen. The changes between the two planes are smaller compared to the change in the wake planes for velocity magnitude.

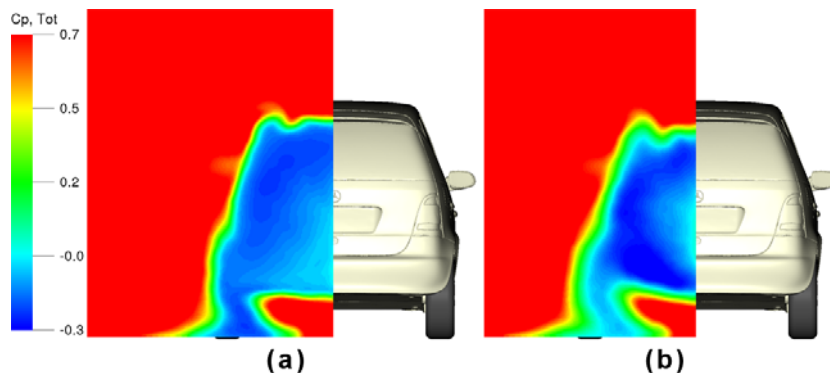


Figure 8.5: Rear view of the car showing the total pressure [-] in two wake planes, where (a) is 25 mm and (b) is 90 mm behind the rear bumper.

Figure 8.6, expresses the total pressure from a side view. This figure is similar to that of the wake planes. The wake formation is similar to a box in shape and has an abrupt end. There is a weakening in the lower part of the wake near the symmetry plane. Figure 8.7 exhibits the total pressure in a plane which is located in the height of the mirror. This plane displays the losses and wake formation from the lower part of a-pillar and the mirror. As previously mentioned, the wake from the mirror's foot reaches the window, which can clearly be seen in this figure. Furthermore one can see from this that the wake starts exactly where the c-pillar begins. This reduces the acceleration of the flow around the c-pillar to almost zero.

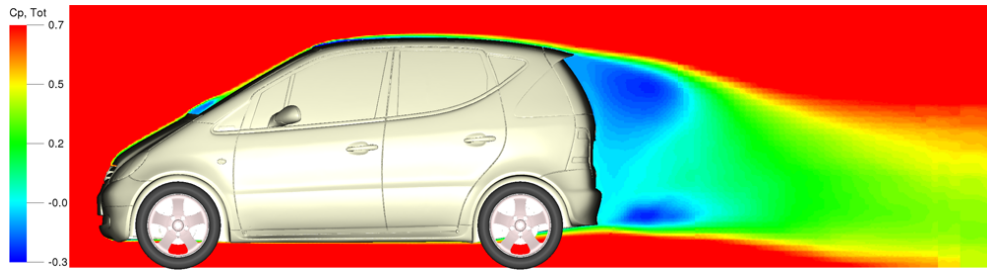


Figure 8.6: Side view of the car showing the total pressure [-] in the symmetry plane.

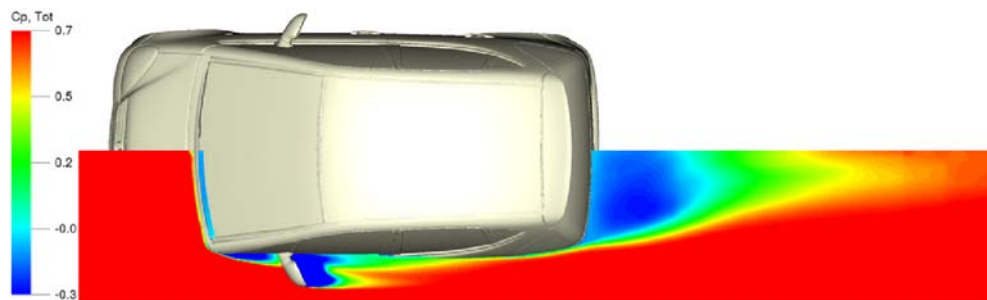


Figure 8.7: Top view of the car showing the total pressure [-] in a plane that cut the mirror in the middle.

As mentioned earlier, the a-pillar suffers from a low pressure coefficient and is a source of vorticities. Vorticity is created due to lower pressure on the top of the car as opposed to underneath. This, therefore, forces a flow from underneath the car to the top. The formation of a vorticity requires a lot of energy, which increases the drag. The a-pillar vorticity can be seen in figure 8.8.

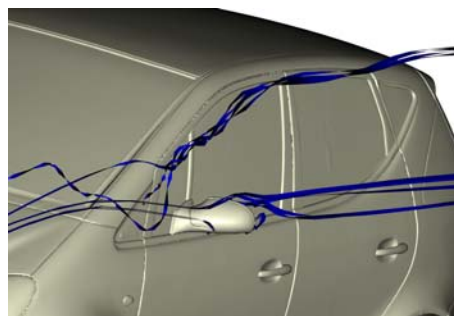


Figure 8.8: The a-pillars vorticity represented with streamlines.

Figure 8.9 shows dimensionless wall distance ( $y^+$ ) on the surface of the car. The wall distance value should be as low as possible as if not, the flow separation can be wrongly predicted, if guesstimated at all. In this case high values of wall distance are located at the tires, front wheel archer, top of the headlamp, and in the beginning of the a-pillar.

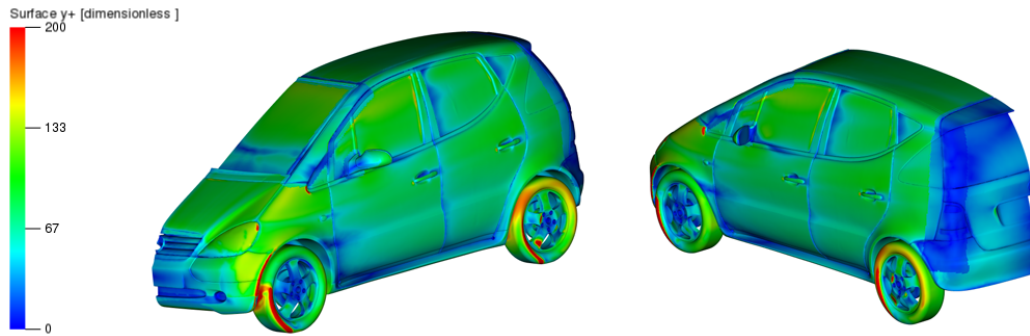


Figure 8.9:  $+y$   $[-]$  on the front and the rear of the car.

## 8.2 Standard Mirror (Whole Car)

Compared to the standard mirror (half car) case (section 8.1), this case has been simulated using the whole car so to see any differences between half car simulations vs whole. Doing whole car simulations takes longer and hence half car simulations are more time efficient.

Figure 8.10 displays the wake formations from a top view. One can see that the wake structures are not symmetrical when comparing the left and right side of the car. The right side of the car has greater wake formations, especially at the rear of the car.

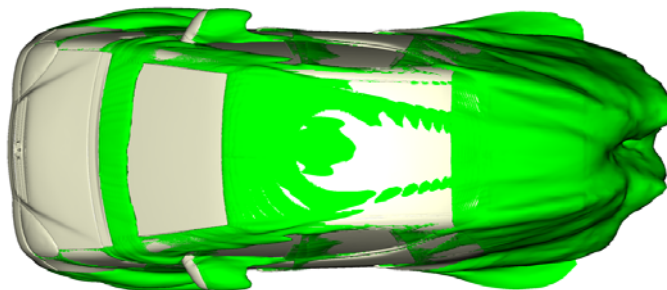


Figure 8.10: Iso-surfaces showing where the total pressure is equal to zero, top view.

The total pressure from a top view (figure 8.11) elucidates the same situation as the iso-surfaces. It can be seen that the right side has a bigger wake area than the left side. Also observable is that the area with the most losses within the rear wake is closer to the rear window at the left side than at the right. Compared with the half car, the left side is similar but for the half car there are less losses close to the symmetry plane. Figure 8.12 illustrates the total pressure in one of the wake planes. One can determine that the area with the least losses is shifted towards the right side. It looks as if the whole car case has more losses in the rear wake than in the case of the half car. This gives increased drag for the whole car compared to the half car.

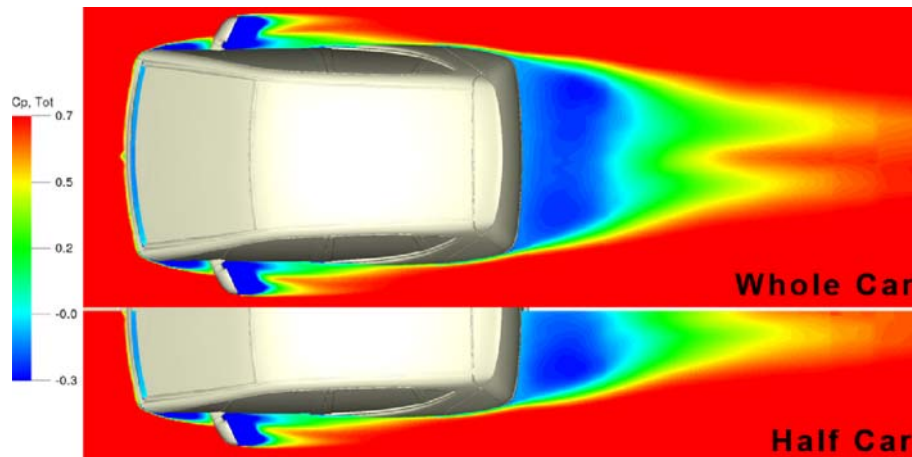


Figure 8.11: Top view of the car showing the total pressure [-] in a plane that cut the mirror in the middle. The half car has been added for comparison.

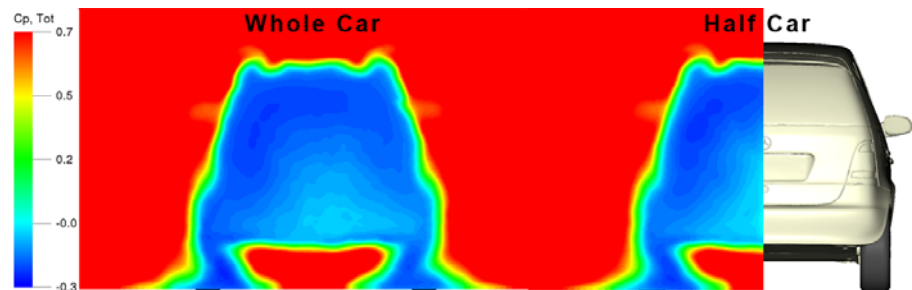


Figure 8.12: Rear view of the car showing the total pressure [-] 90 mm behind the rear bumper. The half car has been added for comparison

When looking at the velocity magnitude in the wake plane located 90 mm behind the rear bumper (figure 8.13), it is clear that the wake structure is asymmetrical. There seems to be a counter-clockwise twist on the wake. This "twist" does not and can not exist in the half car case. Everything on the half car is mirrored to the right side, which makes it completely symmetrical. The symmetry plane works like a splitter.

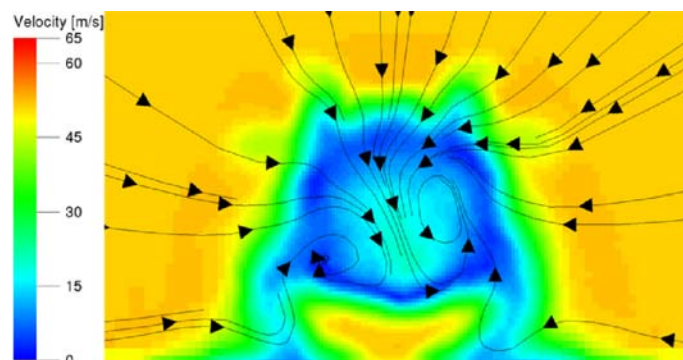


Figure 8.13: Rear view of the car showing the velocity magnitude [m/s] 90 mm behind the rear bumper.

Figure 8.14 shows a comparison of a wake plane between the CFD simulation and the wind tunnel test. The white area in the wind tunnel test

illustrates that there is flow going backwards indicating that there is a wake. The resemblance between these two images is quite good. The vorticity from the a-pillar is there and looks the same. The bulge from the mirror wake is a bit smaller in the wind tunnel image. The biggest differences are in the lower part of the car. The area under the car where the air moves rapidly is smaller in the wind tunnel image. The slow moving air outside the wheels has a bulkier area in the wind tunnel image. It is also shown that the wind tunnel image has a slight twist. The right side seems a little lower than the left and this is probably due to the fact that the car model is slightly crooked, but it is not shown in the CFD simulations.

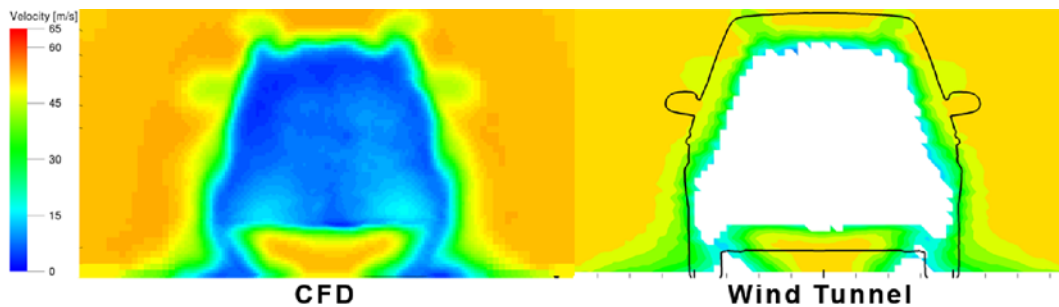


Figure 8.14: Rear view of the car showing the velocity magnitude [m/s] 90 mm behind the rear bumper.

To see how the wake affects the rear of the car, the base pressure (figure 8.15) is a good tool. This figure focusing on the pressure coefficient on the rear's surface, this pressure is often called base pressure. As mentioned before, a higher pressure on the rear surfaces gives a decrease in drag and in other words, high base pressure gives lower drag. The rather small sweep of the scale is to be able of highlighting the differences between the cases. What can be seen is that the base pressure is not symmetrical. It is clear that the right side has a much higher base pressure than the left. This due to the asymmetrical wake and that the right side of the rear wake is not that intensive near the surface of the car as at the left side. When compared to the half car case, the resemblance is rather small. The half car has higher base pressure directly under the Mercedes-Benz emblem, due to less intensive wake in this region. It can clearly be seen that the half car case has a higher total base pressure than the whole car case, which gives the half car case less drag than the whole car case.

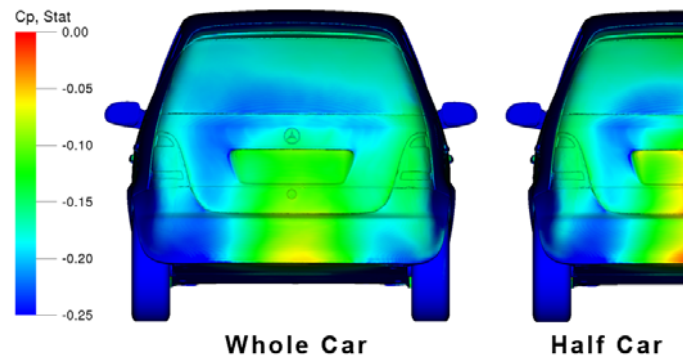


Figure 8.15: Pressure coefficient [-] on the rear of the car, where (a) is the whole car and (b) the half car.

To further investigate where the differences are between the two cases, the force development (in X-direction) can be analyzed in (figure 8.16). One can note that that the force increases at the front of the car and then decreases around the a-pillar area. This is due to the windscreen pulling the car forward (high flow speed and consequent low pressure). After, the force is somewhat constant before it increases again at the end of the car. There are also some influences from the wheels. The difference between the whole car and the half car case is barely noticeable when looking at the force development graph, yet, there is a difference and it is of significant importance. In the rear there is a large increase in force (around 6 drag counts). In the front of the car there is also an increase, however, not as significant (2-3 drag counts).

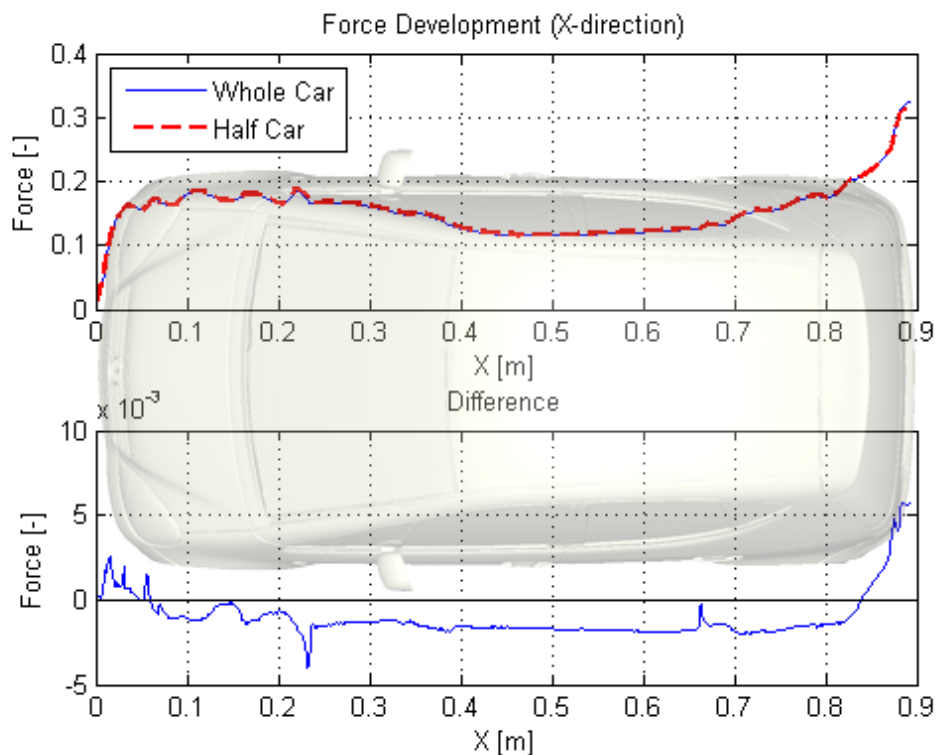


Figure 8.16: Force development, comparing whole car with half car. The difference is whole car - half car.

### 8.3 Without Mirror

In this case the mirror has been removed. This is not a realistic option, but a good way to see the effect of the mirror. The iso-surfaces in figure 8.17 show the wake formations. The difference, apart from no wake from the mirror, is that the wake from the lower part of the a-pillar is longer.

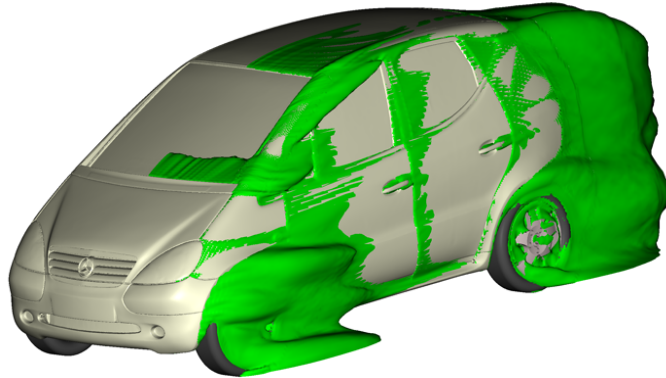


Figure 8.17: Iso-surfaces showing where the total pressure is equal to zero, top view.

By looking at the velocity magnitude one can conclude that the down wash is less significant (figure 8.18). This will affect the base pressure and the losses in the rear wake. Reducing the down wash also has an effect on lift. Under the CFD simulation image there is a measurement from the wind tunnel. The velocity magnitude seems to match rather well, but the wake is longer and has almost no down wash in the CFD simulation. Looking from above (figure 8.19) one can see that the flow is no longer hindered by the mirror. The acceleration of the flow along the side of the car, and in the height of the mirror will affect the wake's appearance.

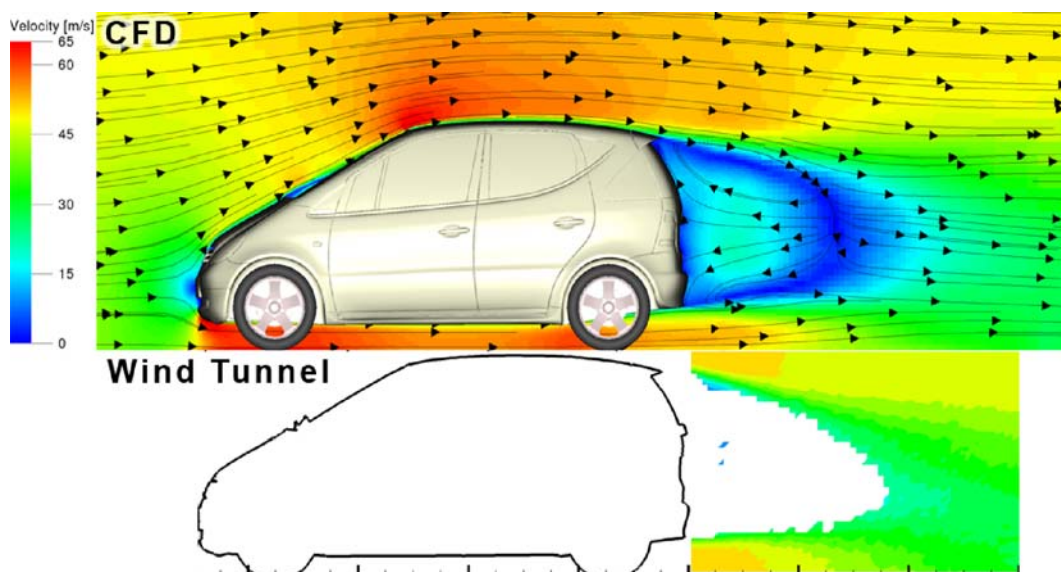


Figure 8.18: Side view of the car showing the velocity magnitude [m/s] in the symmetry plane.

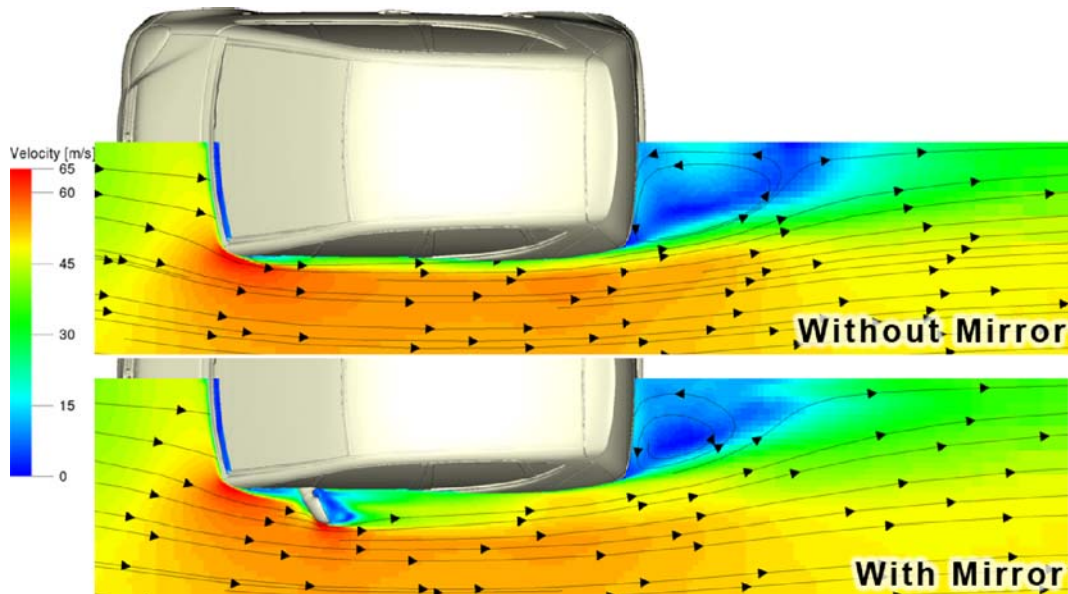


Figure 8.19: Top view of the car showing the velocity magnitude [m/s] in a plane that cut the mirror in the middle.

Due to the change in the rear wake, the losses in the flow have completely changed (figure 8.20). Instead of having a loss isolated in the top of the wake, it is more "evenly" distributed. The losses in the lower part of the rear have increased while the losses close to the rear window have decreased. The absence of the down wash is also clear.

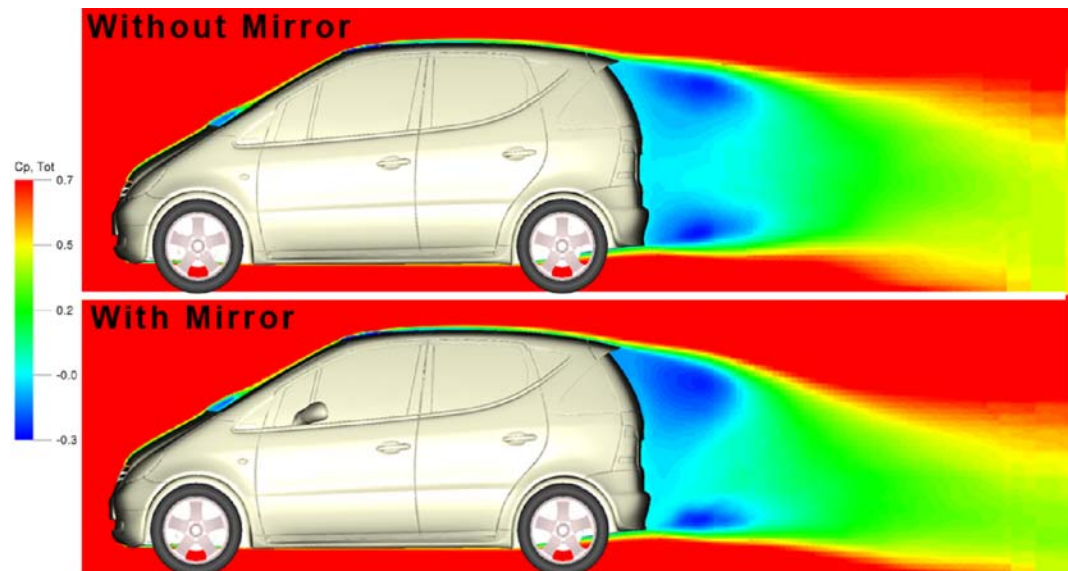


Figure 8.20: Side view of the car showing the total pressure [-] in the symmetry plane.

The base pressure (figure 8.21) is a similar case. The pressure has increased on the rear window, but decreased on the center of the trunk and lower bumper. It would seem that the case without a mirror has higher base pressure than the case with mirror.

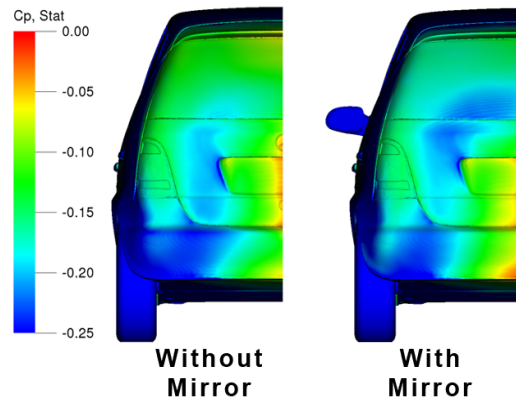


Figure 8.21: Pressure coefficient [-] on the rear of the car.

The force development graph in the X-direction (figure 8.22) shows what large influence the mirror has. At the mirror location there is a massive drop of around 12 drag counts. One can also see the lack of the mirror's influence the rear of the car.

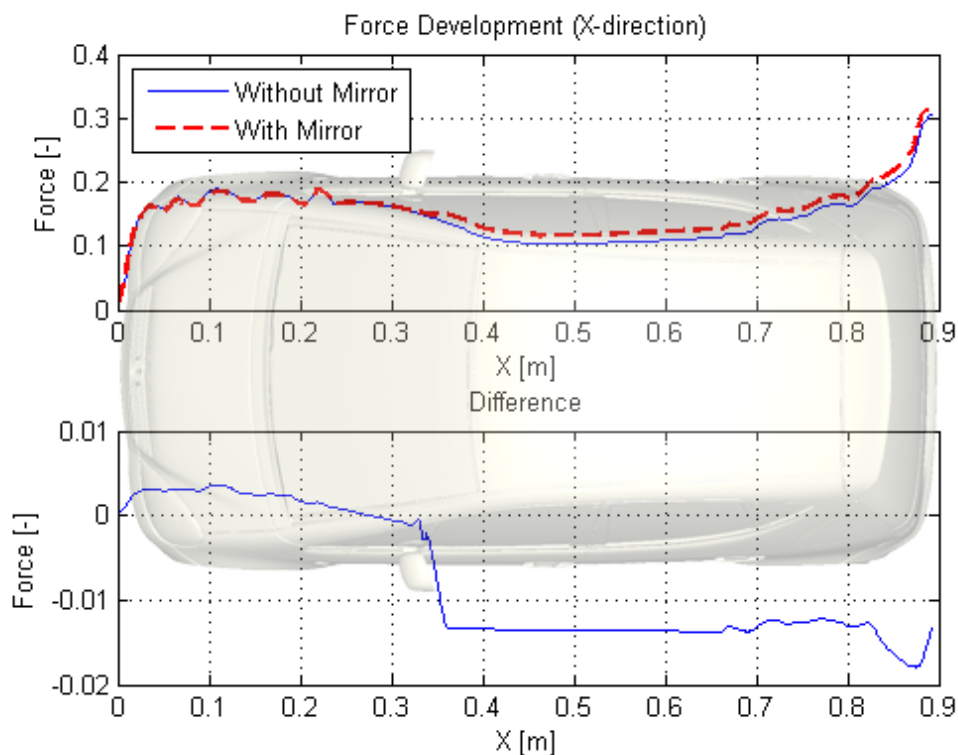


Figure 8.22: Force development, comparison between mirror and without mirror. The difference is without mirror - with mirror.

## 8.4 Reference Mirror

The reference mirror has a gap between the mirror housing and the attachment plate which allows for flow. This can be seen in figure 8.23. There is even an acceleration of the flow at the inside of the mirror housing. This will increase the acceleration of the flow along the side of the car.

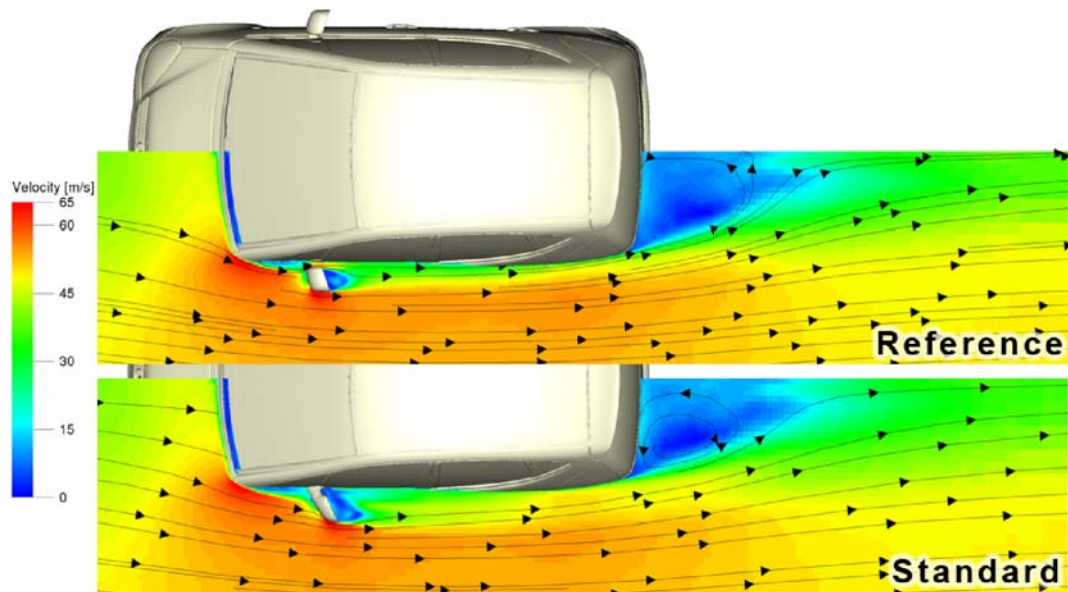


Figure 8.23: Top view of the car showing the velocity magnitude [m/s] in a plane that cut the mirror in the middle.

The wake from the mirror (figure 8.24) is smaller than it was with the standard mirror, which means less drag. It can also be seen that it is separated from the car body. The rear wake's appearance close to the car is the same, but further away the wake is not as wide as for the case with the standard mirror.

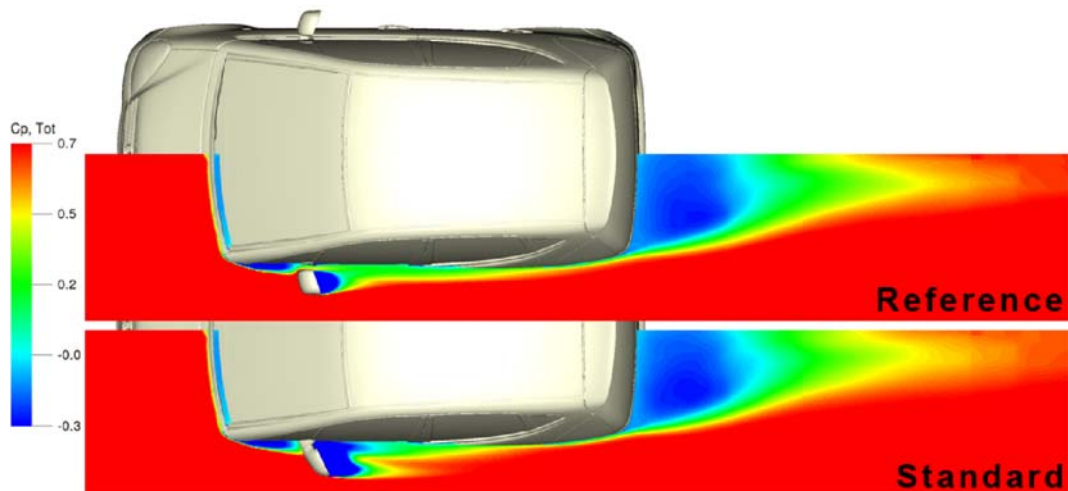


Figure 8.24: Top view of the car showing the total pressure [-] in a plane that cut the mirror in the middle.

The base pressure (figure 8.25) in the reference case shows the same distribution of the low pressure. It seems that the reference case has a lower base pressure than the standard case, which increases the drag.

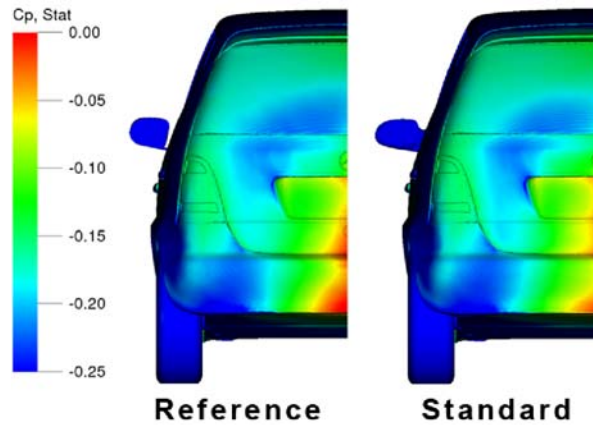


Figure 8.25: Pressure coefficient [-] on the rear of the car.

By looking at the force development in X-direction (figure 8.26) the most significant change occurs at the mirror with a drop of around 8 drag counts. As previously mentioned, the rear wake is also affected by the change of mirror and an increase of 2-3 drag counts can be seen.

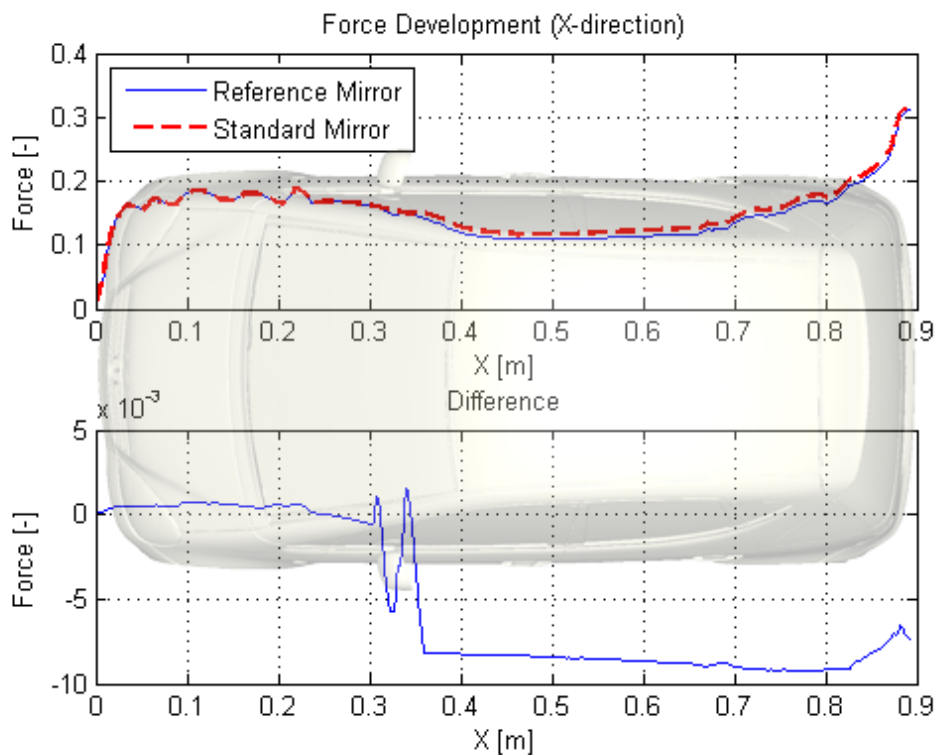


Figure 8.26: Force development, comparing the reference mirror with the whole standard mirror. The difference is reference mirror - standard mirror.

Not only is drag reduction important, but also soiling. There are many ways of investigating soiling. In figure 8.27 particles have been released from a plane that is parallel to the mirror glass and situated just millimeters from the mirror glass. This is an easy and simple way of doing it. The dots symbolize hit points of the particles. The fewer hit points, the less particles have hit the surface which results in a cleaner surface. In this case, only the

driver's window is of interest. As can be seen, the number of particles that hit the window with the standard mirror are generously more than that of the reference mirror. Due to the large mirror foot for the standard mirror, there is an area immediately after the foot with a high density of hit points. This results in poor visibility for the driver. The reference mirror performed well in comparison with the the standard mirror.

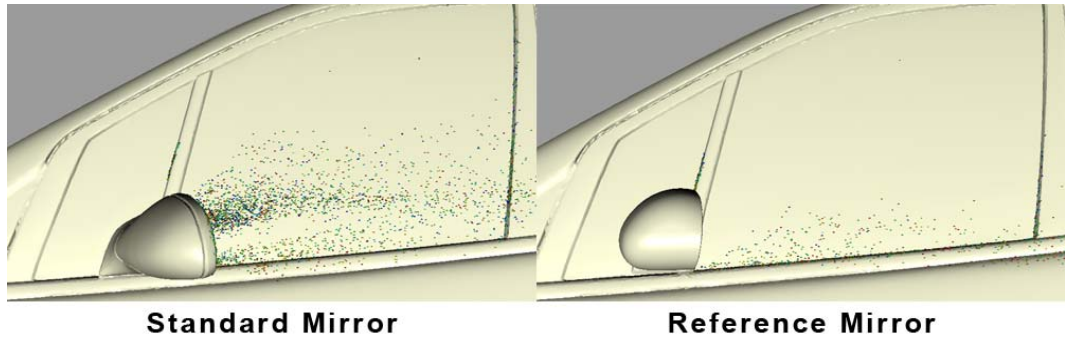


Figure 8.27: Soiling on the driver's window.

## 8.5 Varying the Gap

It seems that the drag drops with increasing gap distance when looking at the  $C_d$  values from the result section. The smallest gap, 4 mm, and the largest gap, 19 mm, are going to be compared to see how the gap affects the flow. The wake structure from the mirror is affected by the gap distance (figure 8.28). With only a small distance, the wake from the mirror will extend to the window. With a large gap distance, the mirror wake stands alone. A larger wake means increased drag.

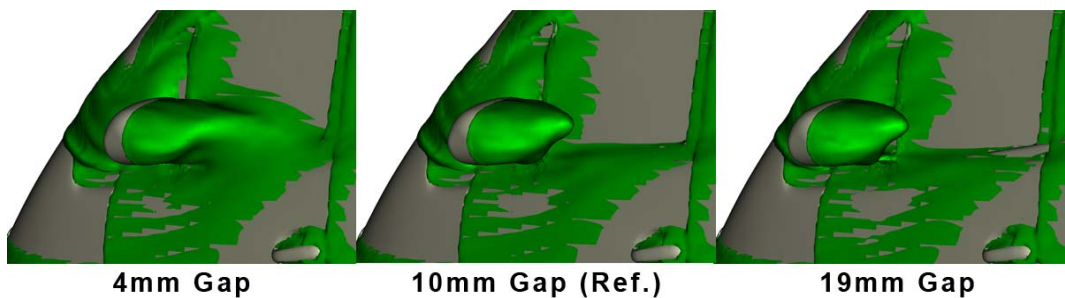


Figure 8.28: Iso-surfaces showing where the total pressure is equal to zero.

Changing the gap distance also affects the rear wake. This can be seen by looking at streamlines released from an area near the mirror (figure 8.29). The streamlines interact in different ways depending on the gap distance. This can result in more energy feed into the wake and possibly giving less drag.

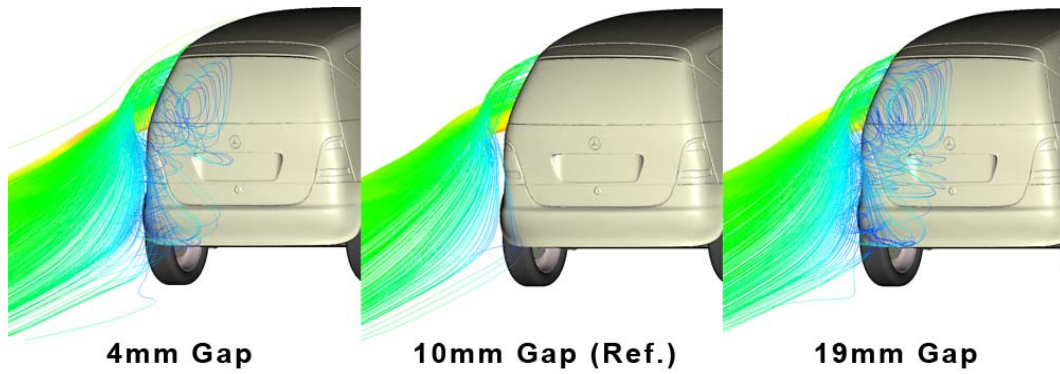


Figure 8.29: Streamlines released from an area near the mirror.

When looking at the force development graph, which in this case shows only the difference between the two different gap distances and the reference mirror (figure 8.30), the largest difference is around the mirror. For the 4 mm gap case, the drag starts to increase in the front of the mirror and then the difference remains constant until the rear of the car where the difference in drag decreases followed by an increase. This is due to the afore mentioned larger wake from the mirror. A larger wake affects the flow along the side of the car and hinder the acceleration of the flow around the a-pillar. For the 19 mm gap mirror it is the other way around. Here the flow is allowed to accelerate around the a-pillar and there is less interference between the mirror and the car body. One should be kept in mind that it is minute changes that are being discussed i.e. around 1 drag count. It seems as though an increase of the gap gives less drag.

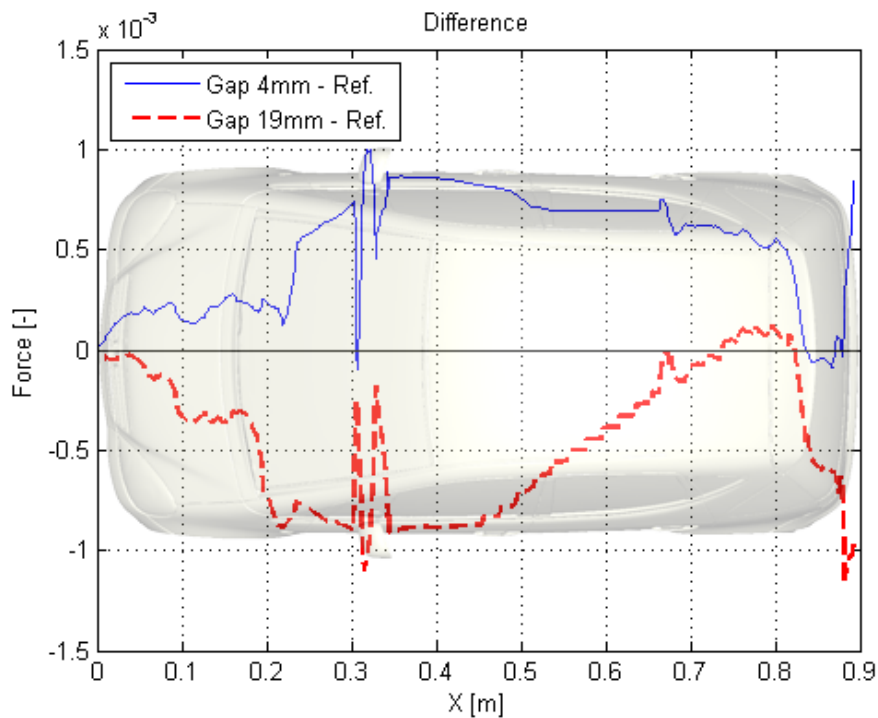


Figure 8.30: Force development difference between 4 mm gap respective 19 mm gap and the reference mirror.

Changing the gap distance also affects the soiling (figure 8.31). Having a small gap, gives, as mentioned earlier, a mirror wake that connects to the car body. This creates more soiling on the window. When the gap distance increases, soiling decreases.

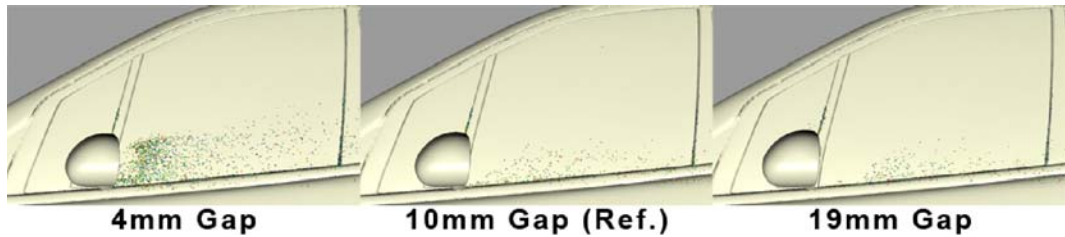


Figure 8.31: Soiling on the driver's window.

## 8.6 Varying the Height of the Foot

Changing the height of the foot is a rather small change, which has the outcome of the mirror wake having an appearance nearly the same for all thicknesses. The difference can be found in the rear wake. By looking at streamlines released around the mirror (figure 8.32) it can clearly be seen, especially for the 7 mm foot case, that the rear wake has been affected by the foot.

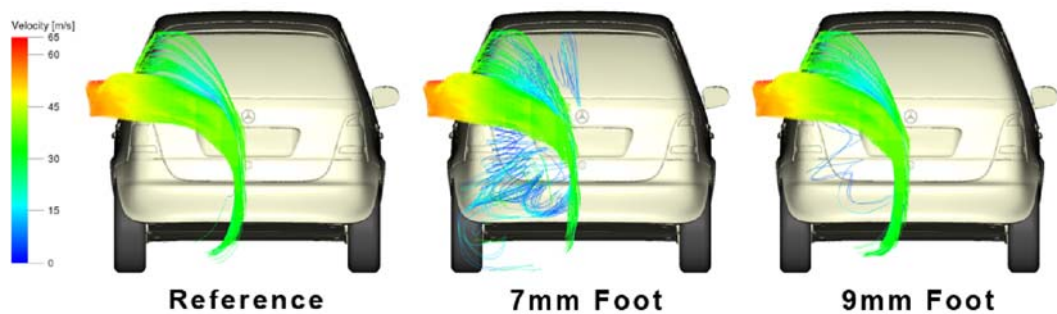


Figure 8.32: Streamlines released from a area near the mirror.

The base pressure (figure 8.33) also tells that the rear wake has been affected by the thicker foot. One can note that the 7 mm foot case has a lower base pressure, which causes lower drag.

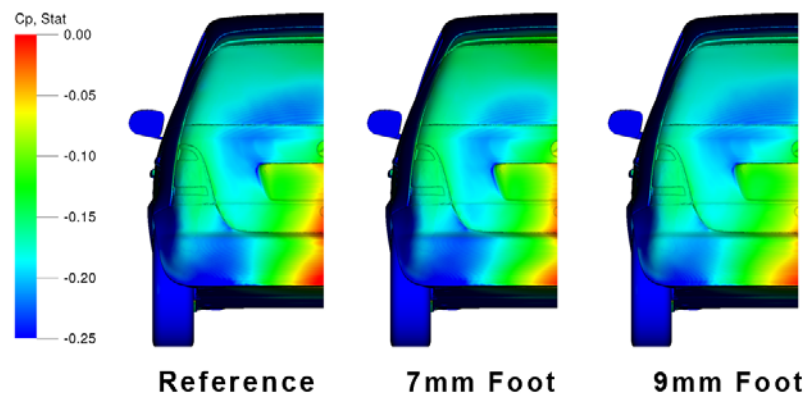


Figure 8.33: Pressure coefficient [-] on the rear of the car.

The force development graph showing the differences from the reference mirror (figure 8.34) illustrates a small difference of less than 1 drag count around the mirror. The real difference is in the rear as mentioned before. Here, the 7 mm foot case decreases its drag by 2 drag counts and the 9 mm foot case which had an increase of 1 drag count from the mirror area increases the drag even more at the rear of the car by an extra 1 drag count.

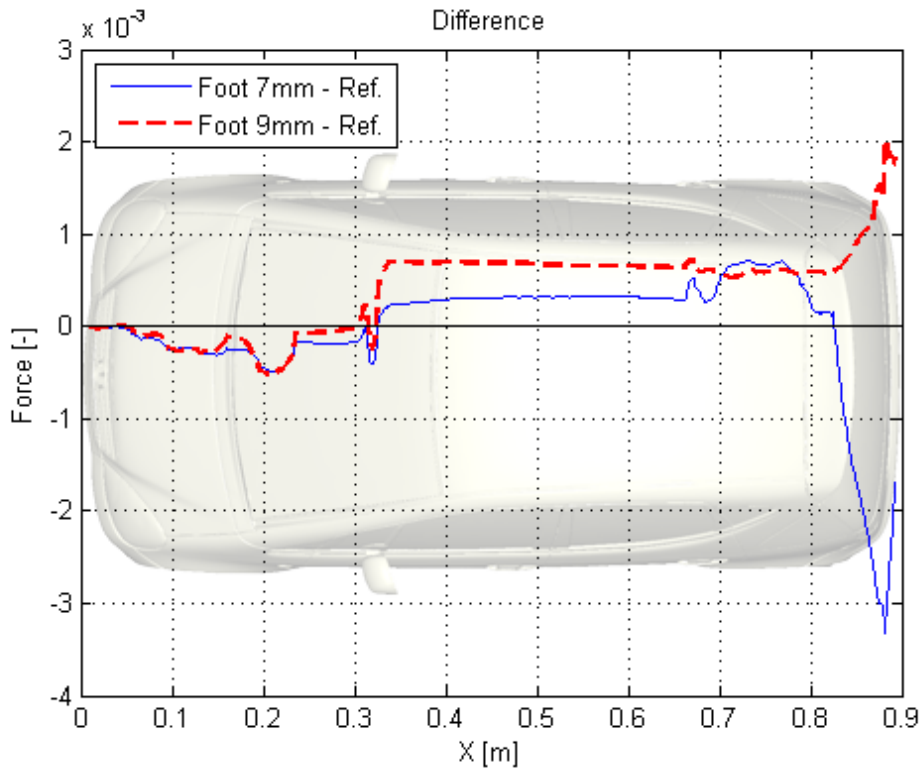


Figure 8.34: Force development difference between 7 mm foot respective 9 mm foot and the reference mirror.

The soiling picture (figure 8.35) shows an increase of hit points directly after the foot where the thickness of the foot increases. This due to a bigger wake after the foot.

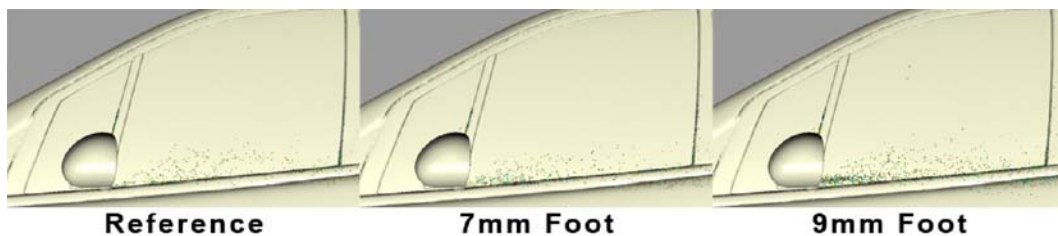


Figure 8.35: Soiling on the driver's window.

## 8.7 Varying the Inner Radius

Changing the inner radius is also a rather small change and it is hard to see the difference in the results, especially when just looking around the area of the mirror. To see even the smallest changes the pressure coefficient on the

surface of the car's body near the mirror can be investigated (figure 8.36). The reference mirror (7 mm inner radius) and the 10 mm inner radius look the same, but the 1 mm inner radius has a lower pressure after the mirror which indicates a change in the wake from the mirror.

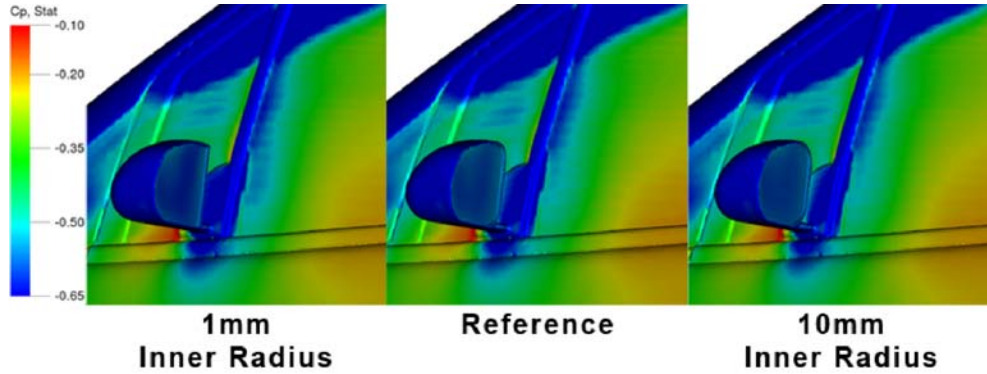


Figure 8.36: Pressure coefficient [-] on the drivers window.

By looking at the base pressure (figure 8.37) the pressure distribution has changed, especially for the 10 mm inner radius case. Here, the pressure near the symmetry plane has decreased, but increased on the rear window.

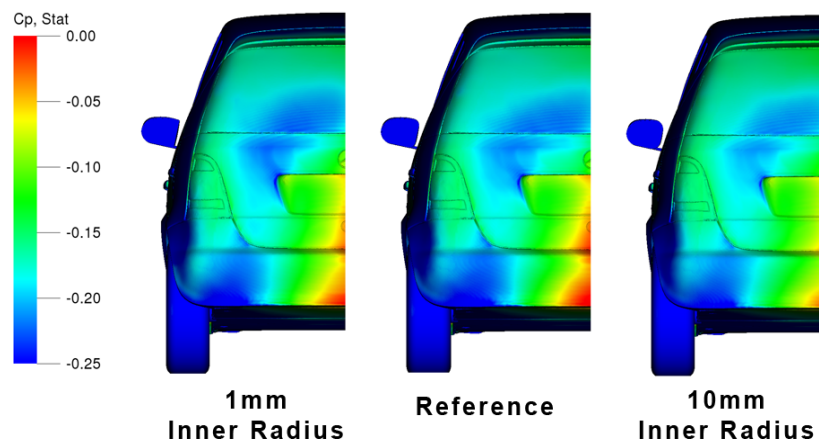


Figure 8.37: Pressure coefficient [-] on the rear of the car.

The above mentioned changes can all be seen in the force development difference graph (figure 8.38). The 1 mm inner radius mirror has an increase in drag (1 drag count) at the mirror location and this difference remains until the end of the car. For the 10 mm inner radius mirror the drop in drag (3 drag counts) is at the rear of the car. It appears that a larger inner radius reduces the drag by affecting the rear of the car.

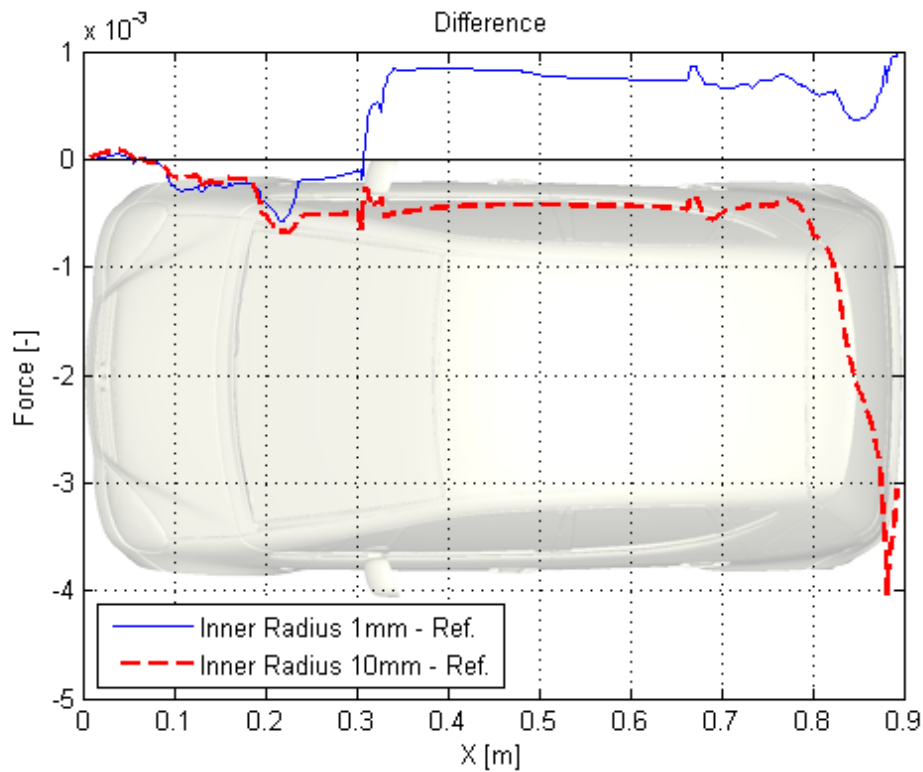


Figure 8.38: Force development difference between 1 mm inner radius respective 10 mm inner radius and the reference mirror.

The change of the inner radius affects the spread of the soiling (figure 8.39). The 1 mm inner radius case gives a larger spread and is more intensive due to the sharp edge. Having a larger radius (10 mm) gives a wider spread compared to the reference case.

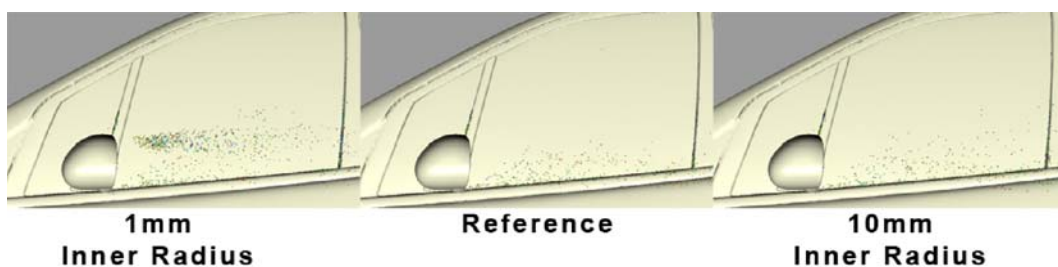


Figure 8.39: Soiling on the driver's window.

## 8.8 Varying the Inclination

Changing the inclination of the inner side of the mirror housing affects the mirror's wake appearance. This can clearly be seen in figure 8.40. For the reference mirror (0 deg inclination) the mirror wake is relative straight. For -15 deg inclination the wake is closer to the window. For the 10 deg inclination the mirror's wake gets further away from the window.

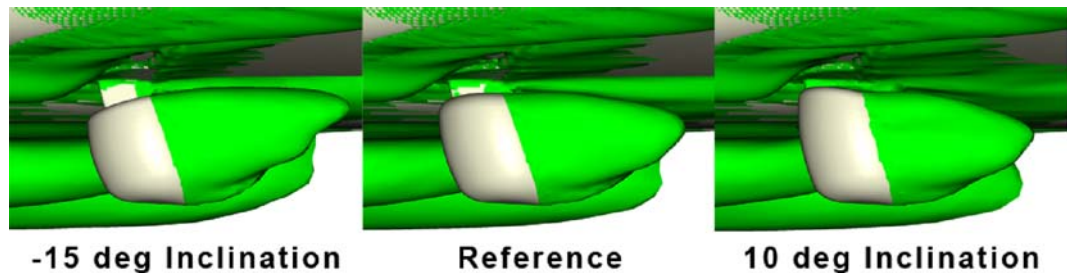


Figure 8.40: Iso-surfaces showing where the total pressure is equal to zero, top view.

Figure 8.41 shows the velocity magnitude. It is clear that the 10 deg inclination effects the mirror wake. The acceleration of the flow along the side of the car is also effected. It seems that the -15 deg inclination case forces the accelerated flow closer to the car body, but for the 10 deg inclination case the, accelerated flow seems to be further away.

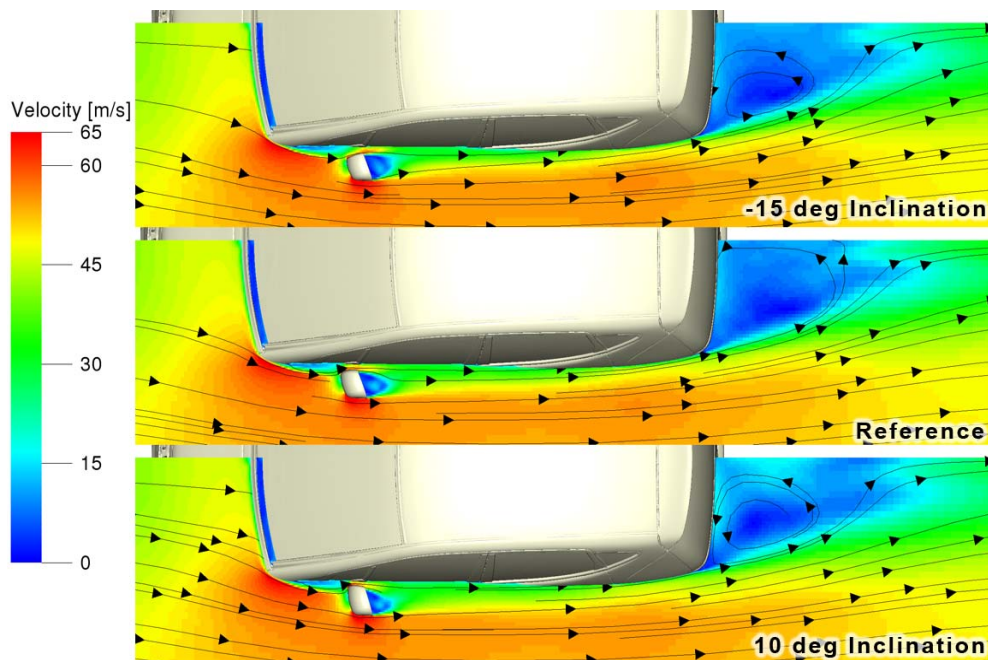


Figure 8.41: Top view of the car showing the velocity magnitude [m/s] in a plane that cut the mirror in the middle.

The base pressure (figure 8.42) for the 10 deg inclination is on average much lower than the reference case. The pressure has increased along the symmetry plane and the low pressure region has changed its appearance. The base pressure for the 10 deg inclination case has decreased significantly; meanwhile, the base pressure for the -15 deg inclination case looks almost the same.

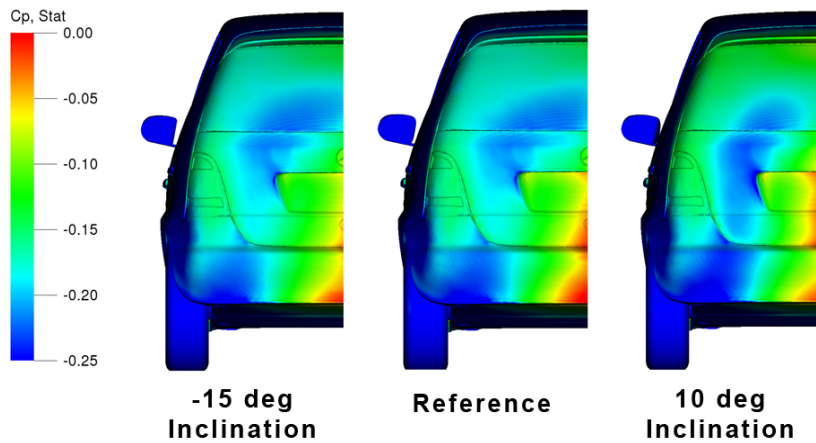


Figure 8.42: Pressure coefficient [-] on the rear of the car.

The force development graph (figure 8.43), shows that the -15 deg inclination change in the mirror wake gives an increase in drag. For the 10 deg inclination, there is a massive decrease in drag (5 drag counts) at the rear.

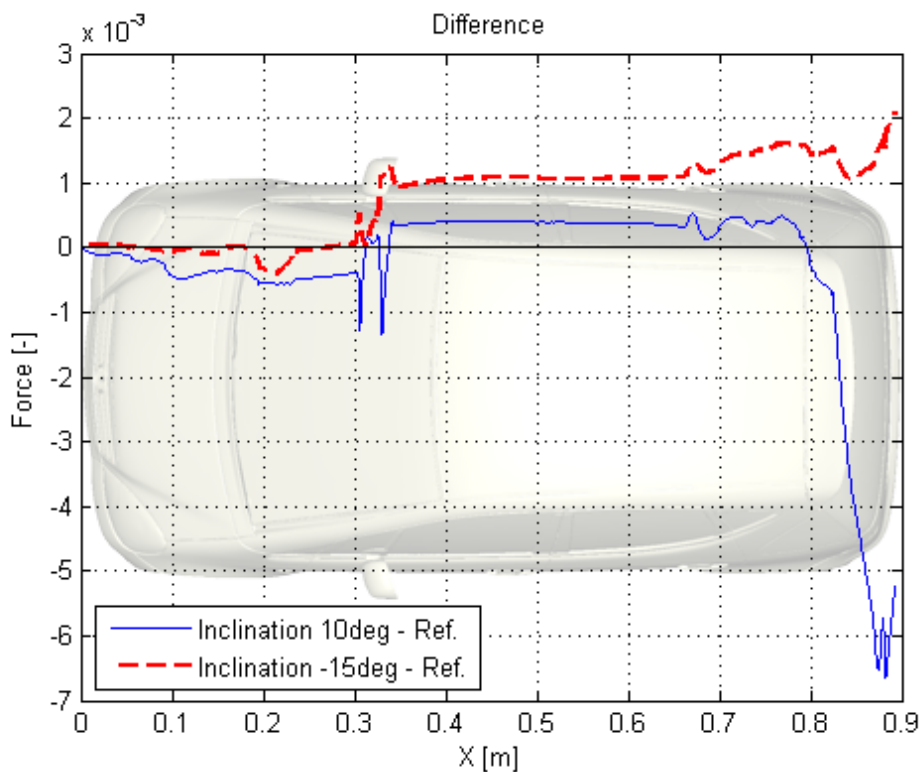


Figure 8.43: Force development difference between 10 deg inclination respective -15 deg inclination and the reference mirror.

The flow is forced against the window with a -15 deg inclination, and it can be noticed by looking at the soiling (figure 8.44). The number of hit points has increased greatly. There is also an increase of hit points for the 10 deg inclination case. This is likely due to the fact that the mirror is closer to the car body, i.e., the gap is smaller, which can be seen in figure 8.40).

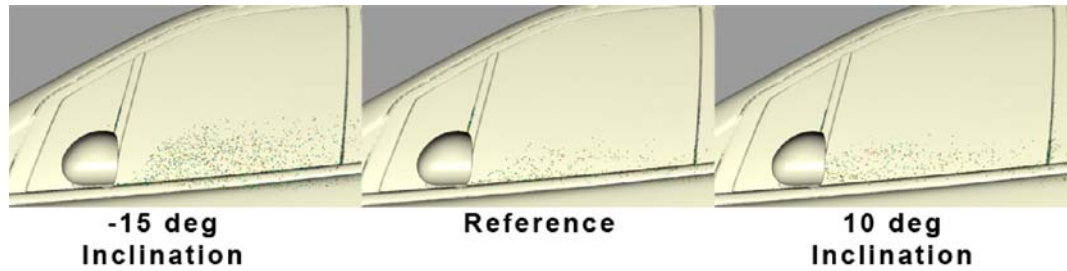


Figure 8.44: Soiling on the driver's window.

## 8.9 Different Housing Curvatures

The mirror wake changes appearance, when altering the mirror housing curvature (figure 8.45). Both the flat and medium housing curvature cases wake appear different in comparison to the reference mirror. The mirror wake itself looks bigger, which increases the drag.

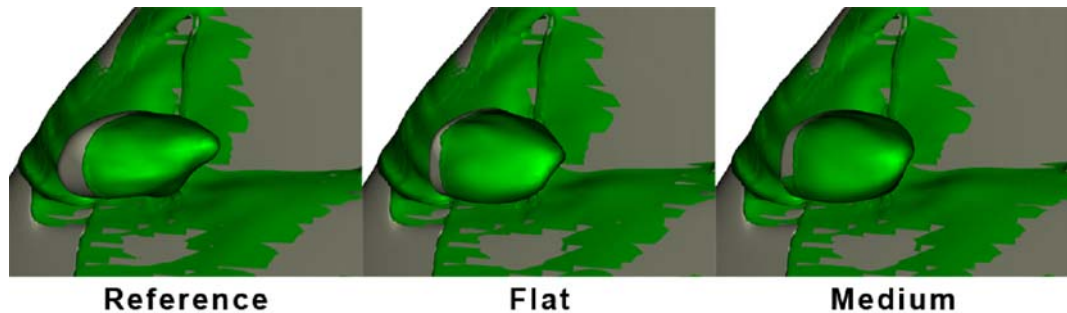


Figure 8.45: Iso-surfaces showing where the total pressure is equal to zero, top view.

An even bigger change can be seen in the base pressure (figure 8.46). The large, low pressure area in the middle has massively decreased for both the flat and medium housing curvature compared to the reference case. The pressure on the top of the rear window has also increased in both cases. This results in less drag.

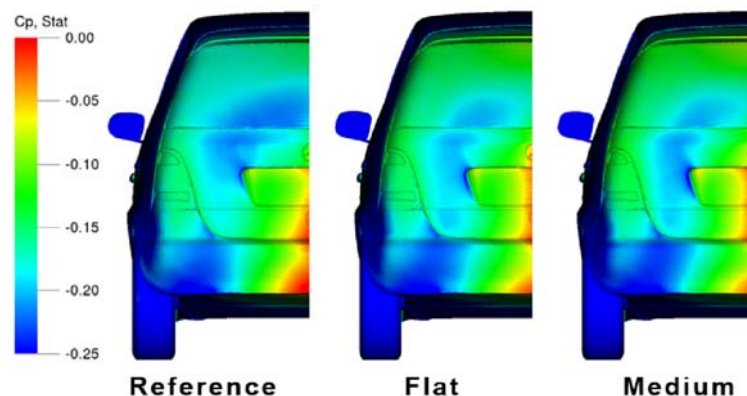


Figure 8.46: Pressure coefficient [-] on the rear of the car.

By looking at the force development graph (figure 8.47), the increase in drag from the mirror wake (1-2 drag counts) can be seen. The two cases

follow each other quite well, with some small differences. In the end, there is a massive drop in drag (6-7 drag counts). This shows how important the mirror is for the rear wake and the car's total amount of drag.

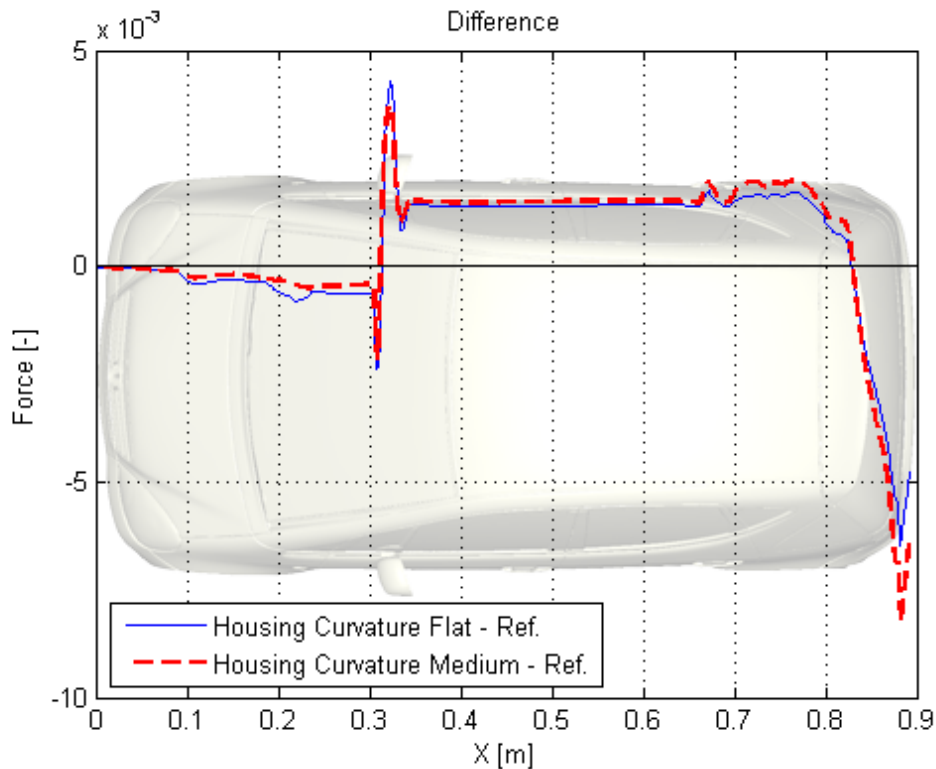


Figure 8.47: Force development difference between flat housing curvature respective medium housing curvature and the reference mirror.

Altering the curvature of the mirror housing completely changes the flow around the mirror, effecting the soiling (figure 8.48). The number of hit points have increased for both the flat and medium housing curvature when compared to the reference case.

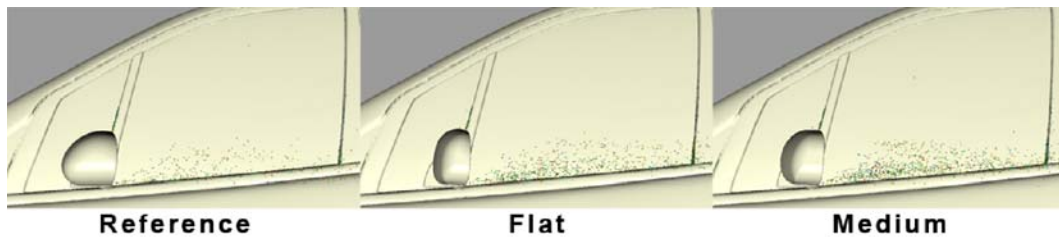


Figure 8.48: Soiling on the driver's window.

## 8.10 Single Changes

The single changes involves small changes to the reference mirror. Figure 8.49 shows the mirror wake formation for the different changes. It is only the deeper glass that has a similar mirror wake formation as the reference mirror. The gutter's and edge's mirror wakes have both changed in shape compared to the reference's. These changes will effect the rear wake.

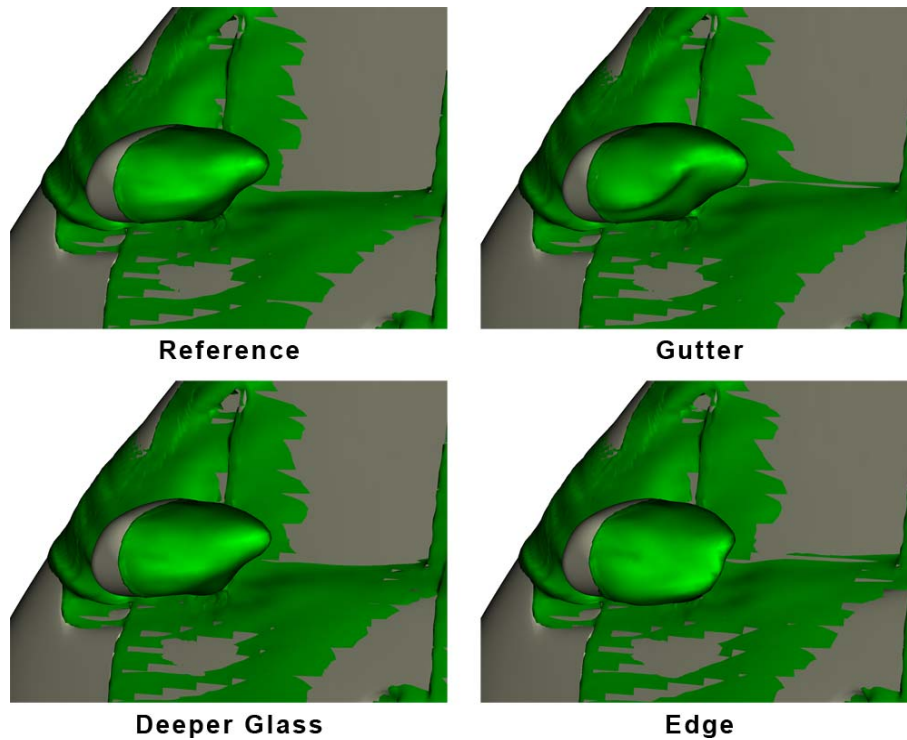


Figure 8.49: Iso-surfaces showing where the total pressure is equal to zero.

Observation of the pressure signature on the driver's window (figure 8.50), shows that both the gutter and edge cases have decreased the pressure above the mirror.

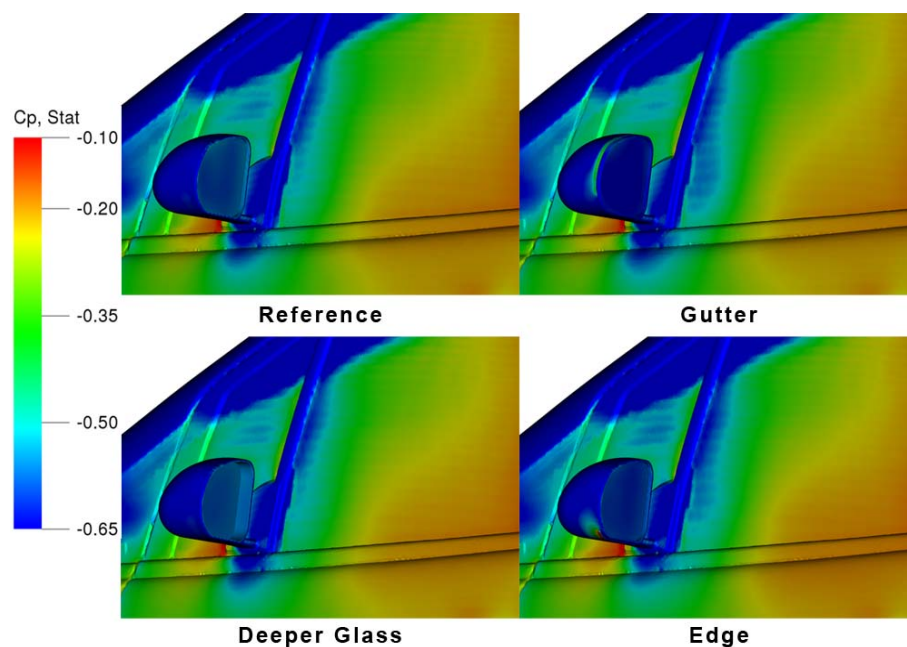


Figure 8.50: Pressure coefficient [-] on the driver's window.

The effect on the rear wake can partly be seen by looking at the total pressure near the symmetry plane (figure 8.51). The wake structures differ a lot from the reference's. For all cases, excluding the edge case, it appears

that the losses have decreased in the upper part of the wake, but increased at the lower part.

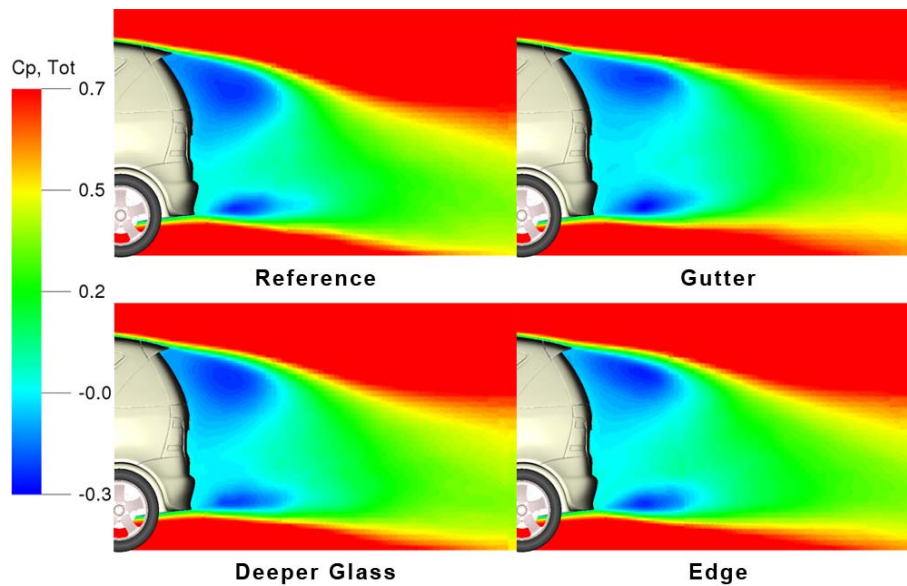


Figure 8.51: Side view of the car showing the total pressure [-] in the symmetry plane.

Observation the base pressure (figure 8.52) indicates the same result as seen in the total pressure images. Interestingly, the mirror with the gutter effects the part of the wake near the rear wheel. The losses have here increased, which gives a lower base pressure in this region. All the cases have a lower base pressure than the reference mirror, which means a decrease in drag.

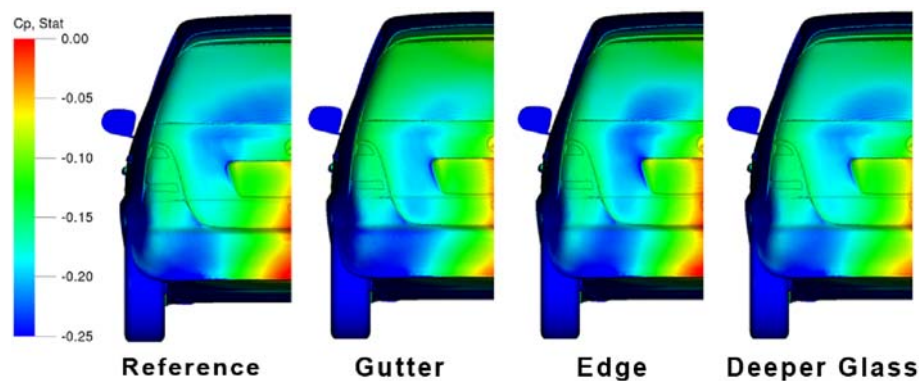


Figure 8.52: Pressure coefficient [-] on the rear.

All the aforementioned results, can be seen in the force development difference graph (8.53). Both the gutter and the edge case have an increase in drag after the mirror, due to the larger mirror wake that they produce. All of the single modifications have a massive decrease in drag at the rear. However, the drag increases rapidly at the very end of the rear.

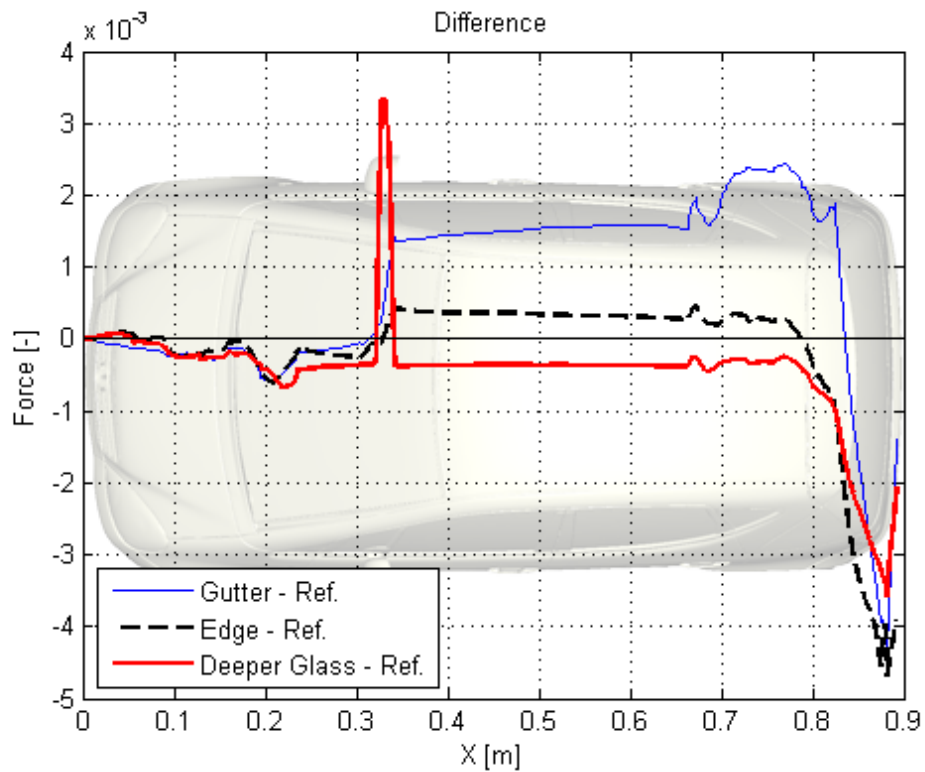


Figure 8.53: Force development difference between the single changes and the reference mirror.

Even small changes effect the soiling (figure 8.54). A deeper glass gives a wider spread of the hit points. Adding a gutter on the top of the mirror seems to increase the number of hit points. The edge also increases the number of hit points.

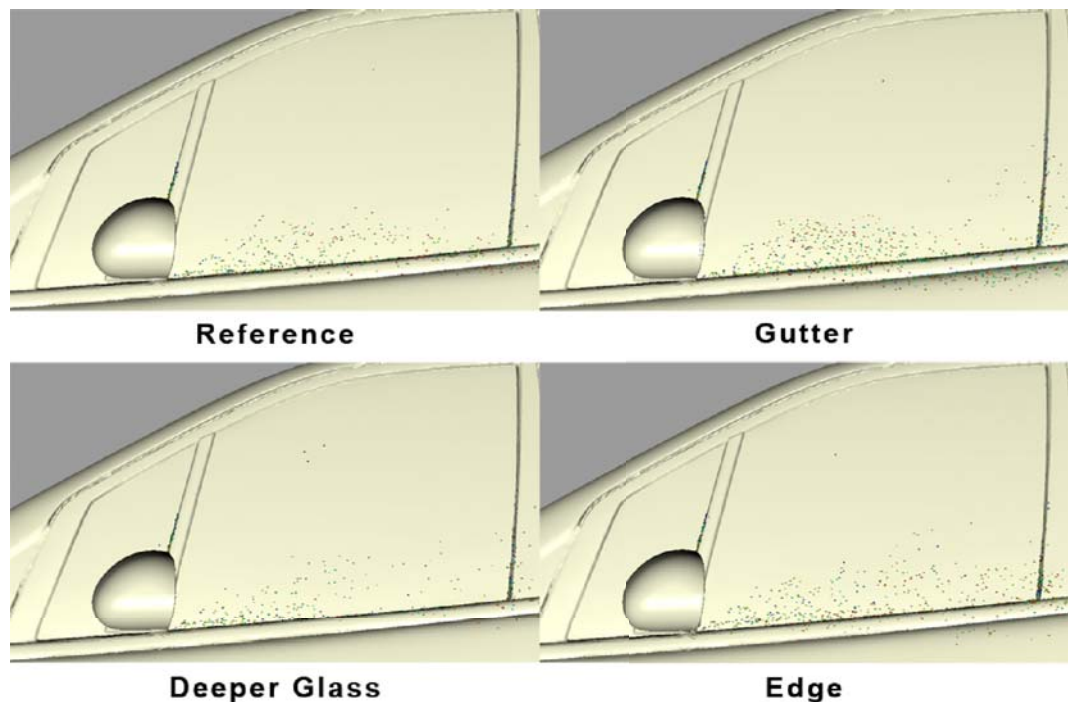


Figure 8.54: Soiling on the driver's window.

## 8.11 Combined Changes

For the combined change, only the force development difference graph (figure 8.55) will be considered. The individual changes have already been discussed. The graph shows that the two combined cases seem to follow each other rather well. The case that contains deeper glass and gutter, has a larger increase after the mirror. This is due to the gutter, whose effect can be seen in figure 8.53. Without the deeper glass and gutter, the drag decreases at the rear of the vehicle. So, there is an increase of drag in one of the cases and in the other there is a decrease compared to the reference mirror.

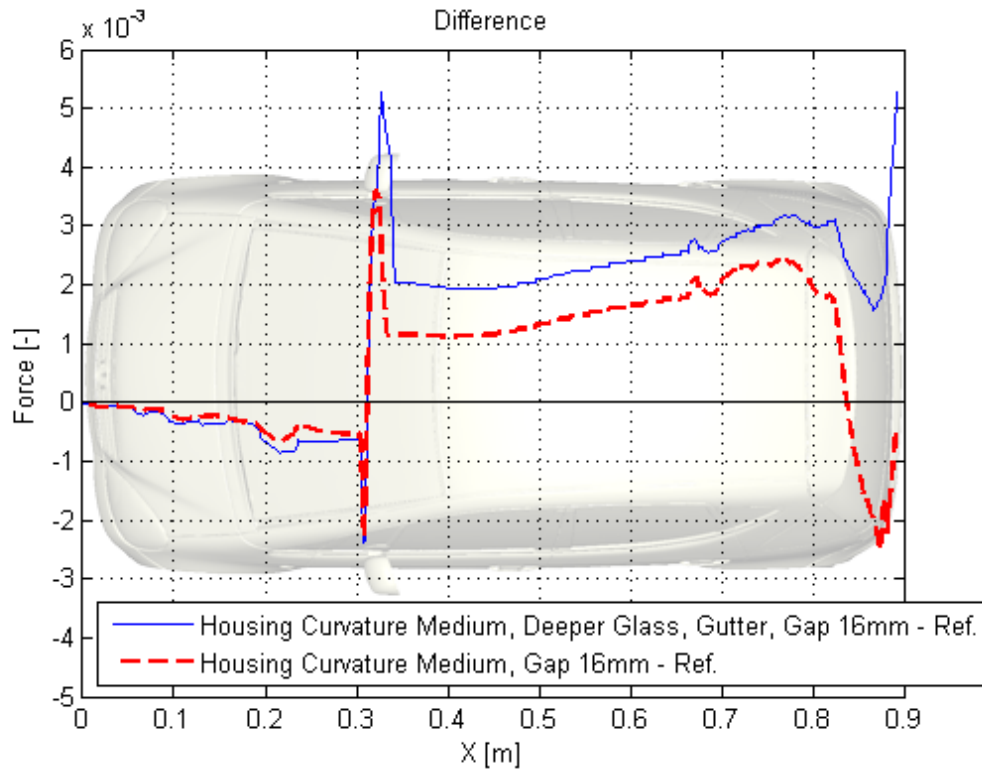


Figure 8.55: Force development difference between the combined changes and the reference mirror.

## 9 Discussion

In the *result* and *flow and analysis* sections, certain problems and question marks have emerged. These will be addressed within this section.

### Half Car vs Whole Car

The CFD result shows a difference between the half car and whole car simulations. The difference in drag is 6 drag counts. The reason behind this difference is found in the combination of the car model being a bit crooked and lack of flow across the middle of the car in the case of the half car. The flow around a car is not symmetric, especially when the car is a bit crooked. This has been very clear in the rear wake, which has a twist. This asymmetrical flow seems to increase the drag, but does not seem to have any larger affect around the mirror area. The uncertainties in the simulation, and averaging process in these cases, have not been of importance because they are both around a mere 1-2 drag count.

### Wind Tunnel vs CFD

The difference between the wind tunnel and CFD results were significant. The average drag from the wind tunnel testing was about 13% (45 drag counts) higher than that of the drag from the CFD simulations. There are some differences in the flow, for example, the rear wake has a different shape and size. By just looking at the velocity magnitude in the wake it is hard to tell how large the loss is in the wake. In this case it seems that the rear wake is larger for CFD simulations. This generally would result in higher drag, yet, perhaps due to a lower wake intensity, the actual drag is lower than the CFD simulations. The flow close to the floor is also different. It can be inferred that the flow under the car has a higher velocity in the CFD simulations. The flow close to the floor outside the tires occupies a much larger area of slow moving air in the wind tunnel as compared with the CFD simulations. This will give the CFD simulations less drag. The lack of windscreen wipers (front and back) for the CFD simulations will also give the CFD simulations less drag. The blockage in the wind tunnel increases the drag for the wind tunnel tests.

Another source causing less drag for the CFD simulations can be caused by incorrectly predicted flow separations and reattachments. Additionally, it is possible that not all flow phenomenas have been captured. The flow separation at the a-pillar and the reattachment just before the mirror holds a major role for drag contribution from the mirror. This could be the reason why the trends for the different cases compared to the standard mirror for the CFD simulations and the wind tunnel tests differ. A more suitable mesh around the lower part of the A-pillar and around the front wheel archer could have had improved the results by giving more accurate flow separations in these areas. All of the aforementioned reasons contribute to the difference between the wind tunnel tests and CFD simulations.

One should note that the aim of this thesis is not to obtain CFD results

equal to those of the wind tunnel results. The aim is to observe the trends. The trends all go in the desired direction; a decrease of drag. The wind tunnel results were more coherent, meanwhile, the CFD simulation results demonstrated more variation. The reason behind the variation can be the uncertainties in the CFD simulations.

## Mirror Design Optimization

Comparing minute changes to the mirror is hard and sometimes impossible due to too large uncertainties in the simulations. By using most of the time the same averaging interval gives a fairly good result overall, but can sometimes leave large deviations. In most cases the uncertainties were around 1-2 drag counts, but could in some cases be as large as 3 drag counts. When comparing different cases, the uncertainties can become even greater due to the fact that the uncertainties can add up (underestimation and overestimation). Some suspicious results from a few cases had to be rerun. The results from the reruns could be totally different compared to the first runs. In some cases the down wash was gone in the rear, but returned in the rerun.

Due to these reasons, a difference of 1-2 drag counts between two mirrors has no real value. Only when two different cases have a difference of over 3 drag counts can it be assumed that the increase/decrease in drag is valid. This makes it very difficult to see what happens when changing one parameter a couple millimeters (about 1 cm in full scale). There may or may not be a trend in the results. It is impossible to tell sometimes. By combining different modifications it has been clear that aerodynamics is not linear. Combining two modifications that separately give low drag values can together give worse drag.

Disregarding the simulation and averaging uncertainties, the drag contribution from the mirror has been reduced by 12 drag counts (standard mirror) down to zero contribution (reference mirror with housing curvature medium). This is only valid for the CFD simulations. The wind tunnel tests also show a decrease in drag contribution for the modified mirrors, but not as large as that of the CFD simulations. Some modifications did not show a trend at all. The flow at the rear was also affected. In some cases, the larger decreases in drag were due to the lower base pressure in the rear from "up wash effect" of the mirror. The flow that goes around the mirror affects the flow around the entire c-pillar which has a major influence on the rear wake.

All modification cases not only affect the drag but also the soiling. It has been seen that small changes can vary the spread and amount of hit points rather heavily. Compared to the standard mirror, the mirrors with the lowest drag contribution experiences less soiling. This means that reducing the drag reduction can also have a positive effect on the problem of soiling. (Remark: a deeper study in soiling has to be done to get a complete overview of the soiling situation for the mirror.)

## 10 Conclusion

The mirror plays a major part when it comes to drag contribution for the entire car and therefore mirror optimization is a vital component to consider. Mirror design optimization is no easy feat due to problems such as CFD simulation uncertainties. The result from smaller changes (1-2 drag counts difference) can, many times, not be trusted. Only with larger changes, eg. 3+ drag counts difference, can the results be considered trustworthy. This omits fine tuning, which probably has to be done in a full scale wind tunnel (correct separation for laminar/turbulent boundary layers). To find a good mirror design a combination of wind tunnel testing and CFD simulations are necessary.

### 10.1 Future Work

For future work it is advisable to look additionally into aeroacoustics, more extensive soiling investigation, and development of a better averaging method.

## References

- [1] EUR Lex Access to European Union law. Directive 2003/97/EC. <http://eur-lex.europa.eu/LexUriServ/LexUriServ.do?uri=CELEX:32003L0097:en:NOT>, 2011.
- [2] R. H. Barnard. *Road Vehicle Aerodynamic Design*. MechAero Publishing, second edition, 2001.
- [3] Internationale Angelegenheiten Universität Stuttgart homepage. <http://www.ia.uni-stuttgart.de>, 2010.
- [4] FKFS homepage. <http://www.fkfs.de/>, 2011.
- [5] W. H. Hucho. *Aerodynamik des Automobils*. Wieweg+ Teubner, fifth edition, 2005.
- [6] H. K. Versteeg and W. Malalasekera. *An Introduction to Computational Fluid Dynamics, The Finite Volume Method*. Pearson Prentice Hall, second edition, 2007.
- [7] W. H. Rae J. B. Barlow and A. Pope. *Low-speed wind tunnel testing*. Wiley-interscience, third edition, 1999.
- [8] Lecture: Wind tunnels, Course: MTF235 - Road vehicle aerodynamics, School: Chalmers University of Technology. [https://www.student.chalmers.se/sys/FileHandling/downloadFile?folderName=6893hout&path=Lecture\\_notes&fileId=Wind\\_tunnel.pdf](https://www.student.chalmers.se/sys/FileHandling/downloadFile?folderName=6893hout&path=Lecture_notes&fileId=Wind_tunnel.pdf), 2010.



# Appendices

## A PowerCASE Parameters

The setup/parameters in the following tables have been used for all cases. Some parameters that appear in the template have been left out to be used as only a default. In Table A.1 the parameters for the case tab in Aero Wind Tunnel are presented. Both the characteristic length and area are set to be decided by the program itself. In this case the characteristic length is 0.398599 m and the characteristic area is 0.139632  $m^2$ . Table A.2 illustrates the main wind tunnel parameters. The scale model sets the ratio for the dimensions for the wind tunnels. The tunnel length, which is set by the largest VR region's length, in this case is equal to 24.32 m.

Table A.1: Aero Wind Tunnel: Case

Parameters	Value	Unit
Velocity	50	[m/s]
Viscosity	1.49e-05	[ $m^2/s$ ]
Characteristic Length	Body Height	[-]
Characteristic Area via	Body Projection	[-]
Resolution Specified at VR	9	[-]
Resolution via	Voxel Size	[-]
Voxel size	0.625	[mm]

Table A.2: Aero Wind Tunnel: Wind Tunnel

Parameters	Values	Unit
Air Flow Direction	+X	[-]
Up Direction	+Z	[-]
Blockage	0.1	[%]
Tunnel Aspect Ratio	Body Ratio	[-]
Tunnel Length	Maximum VR Length	[m]

The template also sets some global parameters, which can be found in table A.3.

Table A.3: PowerCASE: Global Parameters

<b>Parameters</b>	<b>Values</b>	<b>Unit</b>
Characteristic Pressure	<i>101325</i>	[Pa]
Characteristic Temperature	<i>25</i>	[degC]
Characteristic Viscosity	<i>1.49e-05</i>	[m <sup>2</sup> /s]
Resolution*	<i>637.8</i>	[-]
Max Expected Velocity	<i>50*1.3</i>	[m/s]
Simulation Time	<i>500000</i>	[timestep]
Gas Molecular Weight	<i>28.97</i>	[kg/kmol]
Gas Specific Heat Ratio	<i>1.4</i>	[-]
Constant-pressure Specific Heat	<i>1007</i>	[J/(kg * degK)]
Default Turbulence Intensity	<i>0.01</i>	[-]
Default Turbulence Length Scale	<i>5</i>	[mm]

\*cells along char length

In Table A.4 the configuration for the floor is presented. The parameters are set to fit the scale model wind tunnel dimensions. The wheel axis height values are measured in ANSA. To increase the fines of grid different Variable Resolution (VR) regions were created. Table A.5 presents the Offset for each VR zone from the constructed VRs.

Table A.4: Aero Wind Tunnel: Floor

<b>Parameters</b>	<b>Value</b>	<b>Unit</b>
Front Wheel Axis Height	<i>73.6</i>	[mm]
Rear Wheel Axis Height	<i>73.6</i>	[mm]
Prescribed Boundary Layer Location	<i>0</i>	[m]
Prescribed Boundary Layer Height	<i>0</i>	[m]
Center Belt Length	<i>1.75</i>	[m]
Center Belt Width	<i>0.225</i>	[m]
Wheel Belt Length	<i>0.092</i>	[m]
Wheel Belt Width	<i>0.0715</i>	[m]

Table A.5: Aero Wind Tunnel: VR

	<b>Offset</b>	<b>Unit</b>
VR6	<i>1</i>	[Local Voxels]
VR7	<i>10</i>	[Local Voxels]
VR8	<i>6</i>	[Local Voxels]

Table A.6: Aero Wind Tunnel: Boundary Condition

<b>Part</b>	<b>Type</b>	<b>Roughness</b>	<b>Velocity</b>
Ceiling	<i>Friction less</i>	-	-
Floor	<i>Friction less</i>	-	-
Walls	<i>Friction less</i>	-	-
Moving belt (center)	<i>Sliding wall</i>	<i>0 (smooth)</i>	<i>50 m/s (x-dir)</i>
Wheel belts	<i>Sliding wall</i>	<i>0 (smooth)</i>	<i>50 m/s (x-dir)</i>
Wheel faces	<i>Rotating wall</i>	<i>0 (smooth)</i>	<i>661 rad/s (angular)</i>
Inlet	<i>Velocity</i>	-	<i>50 m/s (x-dir)</i>
Outlet	<i>Static pressure, Free flow direction</i>	-	-



## B Mirror Glass Investigation

Every different car manufacturer has its own approach when it comes to mirror design. Mirrors from the same car manufacture often have the same design. The size can differ to fit the car type and regulations. To get an idea of the size of the mirror glasses, a number of mirrors from different car manufacturers have been investigated.

### Selection of Mirrors

The different mirrors that have been selected to participate in this investigation have been chosen by the following criteria:

- Be fitted on a common car type (not bigger than a sedan)
- Satisfy today's regulations (EC component type-approval mark, see figure B.1)\*
- Be on a car of model year 2010/2011

\*Note: Unfortunately, the majority of the cars had the directive 02.



Figure B.1: The E-mark on a left mirror on a BMW 3-serie.

### The Different Cars

The following cars and their mirrors were chosen:

- Audi A1
- Audi A3 (Sportback)
- Audi A5 (Sportback)
- Audi TT (cabriolet)
- BWM 1-serie (5-doors, 118i)
- BWM 3-serie (Coupe, E92)
- BMW Z4
- Mercedes-Benz A-Class (A180 CDI, W169)
- Mercedes-Benz C-Class (C250 CGI)

### Measuring the Glass Area

The measuring procedure was as follows. The objects were photographed at different dealerships around Stuttgart. The photos was taken as perpendicu-

lar as possible in order to measure the area without influence of perspective skewness. A measuring tape was taped on to the glass (see figure B.2) to make it possible to later calculate the glass area when post processing. Post processing was made with Photoshop from Adobe. The area was calculated in the amount of pixels and then a pixel length (and width) in centimeters was calculated with the help of the measuring tape. Only the middle of the measuring tape was used due to the fact that ends where not always perpendicular to the camera. Note: Permission was granted from all of the car dealerships.



Figure B.2: Photo of a Audi A1 mirror, taken at the Audi Dealership Zentrum Stuttgart.

Both the right and left mirror were photographed, in almost all cases, to decrease the error of perspective skewness and because simulations for this these use the same mirror for both left and right side. The average of the left and right mirror glasses are then weighted with a factor which depends on the car type. The more similar the car type is to a Mercedes-Benz A-class (W168), the higher factor it gets. The following factors were used: 5 ("same" car), 1.5 (same car type), 1 (similar car type) and 0.5 (not a similar car type).

## Result

The averaged area and the weights can be seen in table B.1. The weighted average area was calculated to  $157 \text{ cm}^2$ . This results in a mirror glass area of  $9.8 \text{ cm}^2$  when it comes to model scale (1:4). (To cope with that some mirrors had the directive 02, a larger area has been used).

Table B.1: Mirror glass area for different cars.

<b>Car</b>	<b>Averaged Area [<math>cm^2</math>]</b>	<b>Weight</b>
A-class	<i>144</i>	5
C-class	<i>163</i>	0.5
A1	<i>152</i>	1.5
A3	<i>176</i>	1
A5	<i>181</i>	0.5
TT	<i>168</i>	0.5
1-serie	<i>170</i>	1.5
3-serie	<i>164</i>	0.5
z4	<i>155</i>	1

All of the investigated mirrors were aspherical on the driver side, but just the half of them were aspherical on the passenger side.



# C Detailed Results

## CFD Results

<b>Base Cases</b>															
	Whole car with Mirrors			Half Car Without Mirror			Half Car With Mirror			Half Car With Reference Mirror					
	Drag	Lift		Drag	Lift		Drag	Lift		Drag	Lift				
Body	0.251	-0.144		0.495	-0.218		0.246	-0.162		0.247	-0.148				
Wheels	0.056	0.023		0.115	0.024		0.054	0.022		0.055	0.022				
Mirrors	0.012	-0.009		0.000	0.000		0.012	-0.009		0.005	-0.001				
<b>Total</b>	<b>0.318</b>	<b>-0.131</b>		<b>0.610</b>	<b>-0.194</b>		<b>0.312</b>	<b>-0.149</b>		<b>0.306</b>	<b>-0.127</b>				
<b>Gap</b>															
	Gap_4mm			Gap_7mm			Gap_10mm (Reference)			Gap_13mm			Gap_16mm		
	Drag	Lift		Drag	Lift		Drag	Lift		Drag	Lift		Drag	Lift	
Body	0.248	-0.153		0.242	-0.206		0.247	-0.148		0.247	-0.149		0.238	-0.177	
Wheels	0.055	0.023		0.056	0.023		0.055	0.022		0.055	0.023		0.055	0.022	
Mirrors	0.005	0.000		0.005	0.000		0.005	-0.001		0.005	-0.001		0.005	-0.002	
<b>Total</b>	<b>0.307</b>	<b>-0.130</b>		<b>0.302</b>	<b>-0.184</b>		<b>0.306</b>	<b>-0.127</b>		<b>0.306</b>	<b>-0.128</b>		<b>0.298</b>	<b>-0.157</b>	
<b>Gap...</b>															
	Gap_19mm														
	Drag	Lift													
Body	0.245	-0.151													
Wheels	0.054	0.023													
Mirrors	0.005	-0.002													
<b>Total</b>	<b>0.304</b>	<b>-0.130</b>													
<b>Foot</b>															
	Foot_3mm (Reference)			Foot_5mm			Foot_7mm			Foot_9mm					
	Drag	Lift		Drag	Lift		Drag	Lift		Drag	Lift				
Body	0.247	-0.148		0.247	-0.167		0.251	-0.139		0.248	-0.147				
Wheels	0.055	0.022		0.055	0.022		0.054	0.023		0.054	0.022				
Mirrors	0.005	-0.001		0.005	-0.001		0.005	-0.001		0.005	-0.001				
<b>Total</b>	<b>0.306</b>	<b>-0.127</b>		<b>0.307</b>	<b>-0.145</b>		<b>0.310</b>	<b>-0.118</b>		<b>0.308</b>	<b>-0.126</b>				
<b>Inner Radius</b>															
	InnerRadius_1mm			InnerRadius_4mm			InnerRadius_7mm (Ref.)			InnerRadius_10mm					
	Drag	Lift		Drag	Lift		Drag	Lift		Drag	Lift				
Body	0.247	-0.152		0.246	-0.153		0.247	-0.148		0.244	-0.160				
Wheels	0.054	0.023		0.055	0.023		0.055	0.022		0.054	0.023				
Mirrors	0.006	-0.001		0.005	-0.001		0.005	-0.001		0.005	-0.001				
<b>Total</b>	<b>0.307</b>	<b>-0.131</b>		<b>0.306</b>	<b>-0.131</b>		<b>0.306</b>	<b>-0.127</b>		<b>0.303</b>	<b>-0.138</b>				
<b>Housing Curvature</b>															
	Reference			Housing_Curvature_Flat			Housing_Curvature_Medium								
	Drag	Lift		Drag	Lift		Drag	Lift							
Body	0.247	-0.148		0.240	-0.170		0.238	0.475							
Wheels	0.055	0.022		0.055	0.023		0.056	0.111							
Mirrors	0.005	-0.001		0.007	0.000		0.007	0.013							
<b>Total</b>	<b>0.306</b>	<b>-0.127</b>		<b>0.301</b>	<b>-0.147</b>		<b>0.300</b>	<b>0.600</b>							
<b>Inclination</b>															
	Reference			Inclination_5deg			Inclination_10deg			Inclination_15deg			Inclination_minus_5deg		
	Drag	Lift		Drag	Lift		Drag	Lift		Drag	Lift		Drag	Lift	
Body	0.247	-0.148		0.247	0.000		0.240	-0.173		0.245	-0.152		0.244	-0.153	
Wheels	0.055	0.022		0.055	0.022		0.055	0.023		0.055	0.023		0.054	0.023	
Mirrors	0.005	-0.001		0.005	0.000		0.005	-0.001		0.006	-0.001		0.005	-0.001	
<b>Total</b>	<b>0.306</b>	<b>-0.127</b>		<b>0.307</b>	<b>0.022</b>		<b>0.301</b>	<b>-0.151</b>		<b>0.306</b>	<b>-0.131</b>		<b>0.304</b>	<b>-0.131</b>	
<b>Inclination...</b>															
	Inclination_minus_10deg			Inclination_minus_15deg											
	Drag	Lift		Drag	Lift										
Body	0.246	-0.156		0.248	-0.156										
Wheels	0.055	0.022		0.055	0.023										
Mirrors	0.005	-0.001		0.005	-0.002										
<b>Total</b>	<b>0.306</b>	<b>-0.136</b>		<b>0.308</b>	<b>-0.135</b>										
<b>Single Changes</b>															
	Reference			Gutter			Edge			Straight			Deeper_Glass		
	Drag	Lift		Drag	Lift		Drag	Lift		Drag	Lift		Drag	Lift	
Body	0.247	-0.148		0.243	-0.181		0.242	-0.163		0.244	-0.185		0.245	-0.159	
Wheels	0.055	0.022		0.056	0.022		0.054	0.023		0.056	0.023		0.054	0.023	
Mirrors	0.005	-0.001		0.006	-0.004		0.005	0.002		0.005	-0.001		0.005	-0.001	
<b>Total</b>	<b>0.306</b>	<b>-0.127</b>		<b>0.305</b>	<b>-0.163</b>		<b>0.302</b>	<b>-0.139</b>		<b>0.304</b>	<b>-0.163</b>		<b>0.304</b>	<b>-0.137</b>	
<b>Combined Changes</b>															
	Reference			H.C.medium Deeper Glass Gutter Gap16mm			Housing Curvature medium Gap 16mm								
	Drag	Lift		Drag	Lift		Drag	Lift							
Body	0.247	-0.148		0.248	-0.162		0.243	-0.169							
Wheels	0.055	0.022		0.055	0.023		0.055	0.023							
Mirrors	0.005	-0.001		0.007	-0.004		0.006	-0.002							
<b>Total</b>	<b>0.306</b>	<b>-0.127</b>		<b>0.310</b>	<b>-0.143</b>		<b>0.305</b>	<b>-0.149</b>							

# Wind Tunnel Results

Case	Run	Velocity km/h	CD	CZ	CZ_front	CZ_rear	CS	CS_front	CS_rear
			Drag coeff.	Lift coeff.	Front axle coeff.	Rear axle coeff.	Side force coeff.	Front axle coeff.	Rear Axle coeff.
Standard Mirror	1	140.3	<b>0.361</b>	<b>0.0393</b>	-0.0650	0.1042	0.0026	-0.0020	0.0046
	2	159.6	<b>0.360</b>	<b>0.0396</b>	-0.0640	0.1036	0.0006	-0.0027	0.0033
	3	<b>179.7</b>	<b>0.360</b>	<b>0.0419</b>	<b>-0.0619</b>	<b>0.1038</b>	<b>0.0003</b>	<b>-0.0025</b>	<b>0.0028</b>
	4	199.3	<b>0.359</b>	<b>0.0426</b>	-0.0612	0.1038	-0.0008	-0.0028	0.0020
	5	219.2	<b>0.357</b>	<b>0.0434</b>	-0.0606	0.1040	-0.0009	-0.0029	0.0019
Without Mirrors	1	140.3	<b>0.340</b>	<b>0.0525</b>	-0.0636	0.1161	0.0010	-0.0036	0.0046
	2	159.8	<b>0.338</b>	<b>0.0585</b>	-0.0567	0.1153	0.0013	-0.0019	0.0033
	3	<b>179.8</b>	<b>0.337</b>	<b>0.0594</b>	<b>-0.0553</b>	<b>0.1148</b>	<b>0.0008</b>	<b>-0.0019</b>	<b>0.0027</b>
	4	199.6	<b>0.337</b>	<b>0.0611</b>	-0.0545	0.1156	-0.0002	-0.0024	0.0022
	5	219.5	<b>0.336</b>	<b>0.0620</b>	-0.0536	0.1156	-0.0009	-0.0027	0.0018
Reference	1	140.5	<b>0.351</b>	<b>0.0419</b>	-0.0654	0.1074	0.0020	-0.0015	0.0036
	2	159.6	<b>0.351</b>	<b>0.0436</b>	-0.0640	0.1076	0.0017	-0.0017	0.0033
	3	<b>179.7</b>	<b>0.349</b>	<b>0.0465</b>	<b>-0.0618</b>	<b>0.1083</b>	<b>-0.0003</b>	<b>-0.0023</b>	<b>0.0020</b>
	4	199.5	<b>0.348</b>	<b>0.0499</b>	-0.0599	0.1098	-0.0010	-0.0028	0.0018
	5	219.4	<b>0.347</b>	<b>0.0537</b>	-0.0576	0.1114	-0.0011	-0.0026	0.0015
Inclination 10deg	1	140.2	<b>0.353</b>	<b>0.0438</b>	-0.0644	0.1082	0.0030	-0.0009	0.0039
	2	159.6	<b>0.352</b>	<b>0.0465</b>	-0.0621	0.1086	0.0027	-0.0011	0.0039
	3	<b>179.5</b>	<b>0.350</b>	<b>0.0497</b>	<b>-0.0596</b>	<b>0.1093</b>	<b>0.0019</b>	<b>-0.0015</b>	<b>0.0034</b>
	4	199.4	<b>0.348</b>	<b>0.0528</b>	-0.0577	0.1105	-0.0004	-0.0020	0.0016
	5	219.3	<b>0.347</b>	<b>0.0565</b>	-0.0555	0.1120	-0.0014	-0.0022	0.0008
Foot 7mm	1	140.3	<b>0.353</b>	<b>0.0442</b>	-0.0646	0.1087	0.0027	-0.0014	0.0041
	2	159.6	<b>0.352</b>	<b>0.0450</b>	-0.0632	0.1082	0.0025	-0.0013	0.0039
	3	<b>179.7</b>	<b>0.351</b>	<b>0.0493</b>	<b>-0.0602</b>	<b>0.1096</b>	<b>0.0001</b>	<b>-0.0024</b>	<b>0.0025</b>
	4	199.2	<b>0.349</b>	<b>0.0512</b>	-0.0588	0.1100	-0.0008	-0.0027	0.0019
	5	219.3	<b>0.347</b>	<b>0.0555</b>	-0.0565	0.1119	-0.0007	-0.0028	0.0021
Gap 16mm	1	140.1	<b>0.353</b>	<b>0.0337</b>	-0.0757	0.1095	0.0002	-0.0049	0.0050
	2	159.6	<b>0.350</b>	<b>0.0429</b>	-0.0650	0.1079	0.0021	-0.0015	0.0036
	3	<b>179.7</b>	<b>0.349</b>	<b>0.0465</b>	<b>-0.0624</b>	<b>0.1090</b>	<b>-0.0004</b>	<b>-0.0027</b>	<b>0.0023</b>
	4	199.2	<b>0.347</b>	<b>0.0487</b>	-0.0608	0.1095	-0.0003	-0.0026	0.0023
	5	219.4	<b>0.346</b>	<b>0.0512</b>	-0.0591	0.1103	-0.0010	-0.0027	0.0017
Housing Curvature Medium	1	140.4	<b>0.354</b>	<b>0.0514</b>	-0.0586	0.1099	0.0016	-0.0015	0.0031
	2	159.8	<b>0.351</b>	<b>0.0527</b>	-0.0567	0.1094	0.0021	-0.0013	0.0034
	3	<b>179.9</b>	<b>0.349</b>	<b>0.0550</b>	<b>-0.0560</b>	<b>0.1110</b>	<b>0.0001</b>	<b>-0.0022</b>	<b>0.0023</b>
	4	199.5	<b>0.347</b>	<b>0.0549</b>	-0.0562	0.1111	0.0006	-0.0021	0.0027
	5	219.2	<b>0.347</b>	<b>0.0563</b>	-0.0554	0.1117	-0.0007	-0.0025	0.0018
Inner Radius 1mm	1	140.2	<b>0.352</b>	<b>0.0439</b>	-0.0650	0.1089	0.0039	-0.0006	0.0046
	2	159.8	<b>0.351</b>	<b>0.0465</b>	-0.0628	0.1092	0.0030	-0.0007	0.0037
	3	<b>179.7</b>	<b>0.350</b>	<b>0.0501</b>	<b>-0.0604</b>	<b>0.1105</b>	<b>0.0004</b>	<b>-0.0017</b>	<b>0.0022</b>
	4	199.2	<b>0.349</b>	<b>0.0517</b>	-0.0590	0.1107	-0.0002	-0.0019	0.0017
	5	219.4	<b>0.348</b>	<b>0.0538</b>	-0.0576	0.1114	-0.0004	-0.0020	0.0016
Straight	1	140.2	<b>0.351</b>	<b>0.0445</b>	-0.0650	0.1094	0.0022	-0.0014	0.0036
	2	159.6	<b>0.350</b>	<b>0.0451</b>	-0.0636	0.1087	0.0007	-0.0018	0.0025
	3	<b>179.6</b>	<b>0.349</b>	<b>0.0484</b>	<b>-0.0614</b>	<b>0.1098</b>	<b>-0.0008</b>	<b>-0.0028</b>	<b>0.0019</b>
	4	199.4	<b>0.348</b>	<b>0.0505</b>	-0.0597	0.1102	-0.0004	-0.0028	0.0023
	5	219.3	<b>0.347</b>	<b>0.0529</b>	-0.0581	0.1111	-0.0009	-0.0029	0.0020
Inner Radius 10mm	1	140.2	<b>0.355</b>	<b>0.0256</b>	-0.0849	0.1105	-0.0013	-0.0073	0.0060
	2	159.7	<b>0.351</b>	<b>0.0437</b>	-0.0642	0.1078	0.0009	-0.0020	0.0029
	3	<b>179.8</b>	<b>0.350</b>	<b>0.0467</b>	<b>-0.0619</b>	<b>0.1087</b>	<b>-0.0009</b>	<b>-0.0028</b>	<b>0.0019</b>
	4	199.2	<b>0.349</b>	<b>0.0490</b>	-0.0604	0.1094	-0.0007	-0.0028	0.0021
	5	219.4	<b>0.347</b>	<b>0.0525</b>	-0.0583	0.1108	-0.0015	-0.0030	0.0015
Gap 4mm	1	140.2	<b>0.358</b>	<b>0.0209</b>	-0.0916	0.1125	0.0042	-0.0015	0.0057
	2	159.7	<b>0.353</b>	<b>0.0470</b>	-0.0622	0.1092	0.0013	-0.0022	0.0034
	3	<b>179.6</b>	<b>0.352</b>	<b>0.0499</b>	<b>-0.0602</b>	<b>0.1102</b>	<b>-0.0001</b>	<b>-0.0028</b>	<b>0.0026</b>
	4	199.3	<b>0.351</b>	<b>0.0518</b>	-0.0587	0.1105	-0.0005	-0.0030	0.0026
	5	219.2	<b>0.349</b>	<b>0.0537</b>	-0.0573	0.1110	-0.0010	-0.0031	0.0021

Case	Run	CM	CN	CL	Reynolds	Temp	Baro	Rho	PVK	QA
		Pitch moment coeff.	Yaw moment coeff.	Roll moment coeff.	number	°C	hPa		N/m <sup>2</sup>	Dyn. Pres. Pa
Standard Mirror	1	-0.0846	-0.0033	0.0011	2.23E+06	20.24	977.02	1.1612	859.7	880.3
	2	-0.0838	-0.0030	0.0001	2.53E+06	20.45	977.01	1.1604	1114.9	1141.1
	3	<b>-0.0828</b>	<b>-0.0027</b>	<b>-0.0002</b>	<b>2.85E+06</b>	<b>20.77</b>	<b>977.02</b>	<b>1.1591</b>	<b>1412.2</b>	<b>1444.6</b>
	4	-0.0825	-0.0024	-0.0007	3.14E+06	21.32	977.00	1.1569	1734.5	1773.2
	5	-0.0823	-0.0024	-0.0005	3.45E+06	21.91	977.02	1.1546	2096.4	2142.2
Without Mirrors	1	-0.0898	-0.0041	0.0017	2.23E+06	20.15	977.31	1.1619	862.2	882.8
	2	-0.0860	-0.0026	0.0007	2.54E+06	20.50	977.30	1.1605	1117.4	1143.6
	3	<b>-0.0851</b>	<b>-0.0023</b>	<b>0.0002</b>	<b>2.84E+06</b>	<b>20.95</b>	<b>977.28</b>	<b>1.1587</b>	<b>1414.3</b>	<b>1446.8</b>
	4	-0.0850	-0.0023	-0.0002	3.15E+06	21.48	977.28	1.1566	1737.5	1776.4
	5	-0.0846	-0.0022	-0.0004	3.44E+06	22.18	977.28	1.1539	2099.7	2145.5
Reference	1	-0.0864	-0.0026	0.0005	2.23E+06	20.31	977.50	1.1615	861.9	882.5
	2	-0.0858	-0.0025	0.0001	2.54E+06	20.36	977.51	1.1613	1116.6	1142.8
	3	<b>-0.0851</b>	<b>-0.0022</b>	<b>-0.0006</b>	<b>2.84E+06</b>	<b>21.03</b>	<b>977.53</b>	<b>1.1587</b>	<b>1412.6</b>	<b>1445.0</b>
	4	-0.0849	-0.0023	-0.0009	3.14E+06	21.78	977.55	1.1558	1734.8	1773.5
	5	-0.0845	-0.0021	-0.0009	3.43E+06	22.55	977.55	1.1528	2094.8	2140.5
Inclination 10deg	1	-0.0863	-0.0024	0.0006	2.21E+06	21.62	977.65	1.1565	856.7	877.2
	2	-0.0853	-0.0025	0.0002	2.51E+06	21.92	977.64	1.1553	1109.7	1135.7
	3	<b>-0.0845</b>	<b>-0.0025</b>	<b>0.0002</b>	<b>2.81E+06</b>	<b>22.32</b>	<b>977.62</b>	<b>1.1538</b>	<b>1404.6</b>	<b>1436.9</b>
	4	-0.0841	-0.0018	-0.0006	3.11E+06	22.93	977.61	1.1514	1727.2	1765.8
	5	-0.0837	-0.0015	-0.0009	3.42E+06	23.21	977.63	1.1503	2089.3	2134.9
Foot 7mm	1	-0.0867	-0.0028	0.0004	2.21E+06	21.61	977.80	1.1567	856.3	876.8
	2	-0.0857	-0.0026	0.0000	2.51E+06	21.90	977.82	1.1556	1110.3	1136.4
	3	<b>-0.0849</b>	<b>-0.0025</b>	<b>-0.0008</b>	<b>2.82E+06</b>	<b>22.29</b>	<b>977.81</b>	<b>1.1541</b>	<b>1406.0</b>	<b>1438.3</b>
	4	-0.0844	-0.0023	-0.0012	3.11E+06	22.86	977.82	1.1519	1727.4	1766.0
	5	-0.0842	-0.0024	-0.0011	3.41E+06	23.52	977.82	1.1493	2087.3	2132.9
Gap 16mm	1	-0.0926	-0.0050	0.0000	2.20E+06	22.24	978.06	1.1546	854.4	874.8
	2	-0.0864	-0.0026	-0.0008	2.50E+06	22.60	978.04	1.1532	1107.1	1133.1
	3	<b>-0.0857</b>	<b>-0.0025</b>	<b>-0.0017</b>	<b>2.81E+06</b>	<b>23.00</b>	<b>978.04</b>	<b>1.1516</b>	<b>1401.8</b>	<b>1433.9</b>
	4	-0.0852	-0.0025	-0.0016	3.10E+06	23.51	978.03	1.1496	1723.1	1761.6
	5	-0.0847	-0.0022	-0.0016	3.40E+06	24.03	978.03	1.1476	2083.4	2129.0
Housing Curvature Medium	1	-0.0843	-0.0023	-0.0001	2.23E+06	20.71	978.11	1.1607	860.8	881.4
	2	-0.0830	-0.0023	-0.0004	2.53E+06	20.86	978.13	1.1601	1115.1	1141.3
	3	<b>-0.0835</b>	<b>-0.0023</b>	<b>-0.0009</b>	<b>2.84E+06</b>	<b>21.41</b>	<b>978.09</b>	<b>1.1579</b>	<b>1411.7</b>	<b>1444.1</b>
	4	-0.0837	-0.0024	-0.0009	3.13E+06	22.10	978.09	1.1552	1733.6	1772.4
	5	-0.0836	-0.0021	-0.0011	3.42E+06	22.95	978.07	1.1518	2092.6	2138.3
Inner Radius 1mm	1	-0.0869	-0.0026	0.0008	2.21E+06	21.50	978.03	1.1575	857.6	878.0
	2	-0.0860	-0.0022	0.0004	2.52E+06	21.73	978.02	1.1565	1111.6	1137.7
	3	<b>-0.0855</b>	<b>-0.0020</b>	<b>-0.0003</b>	<b>2.82E+06</b>	<b>22.20</b>	<b>978.01</b>	<b>1.1547</b>	<b>1407.1</b>	<b>1439.4</b>
	4	-0.0848	-0.0018	-0.0006	3.11E+06	22.88	977.99	1.1520	1728.1	1766.7
	5	-0.0845	-0.0018	-0.0007	3.41E+06	23.46	978.00	1.1498	2088.8	2134.4
Straight	1	-0.0872	-0.0025	-0.0001	2.20E+06	21.92	978.09	1.1559	856.2	876.7
	2	-0.0861	-0.0021	-0.0010	2.51E+06	22.17	978.04	1.1548	1109.7	1135.7
	3	<b>-0.0856</b>	<b>-0.0024</b>	<b>-0.0015</b>	<b>2.81E+06</b>	<b>22.65</b>	<b>978.04</b>	<b>1.1530</b>	<b>1404.3</b>	<b>1436.5</b>
	4	-0.0850	-0.0025	-0.0014	3.11E+06	23.21	978.00	1.1507	1725.8	1764.3
	5	-0.0846	-0.0024	-0.0014	3.41E+06	23.75	978.02	1.1487	2087.1	2132.7
Inner Radius 10mm	1	-0.0977	-0.0067	0.0011	2.21E+06	21.30	977.53	1.1576	857.5	878.0
	2	-0.0860	-0.0025	-0.0003	2.52E+06	21.61	977.55	1.1564	1111.6	1137.7
	3	<b>-0.0853</b>	<b>-0.0024</b>	<b>-0.0009</b>	<b>2.82E+06</b>	<b>22.09</b>	<b>977.54</b>	<b>1.1546</b>	<b>1407.2</b>	<b>1439.5</b>
	4	-0.0849	-0.0025	-0.0010	3.11E+06	22.71	977.51	1.1521	1729.0	1767.6
	5	-0.0845	-0.0022	-0.0010	3.42E+06	23.35	977.53	1.1496	2089.1	2134.7
Gap 4mm	1	-0.1021	-0.0036	0.0008	2.20E+06	21.91	977.39	1.1551	854.9	875.3
	2	-0.0857	-0.0028	-0.0007	2.50E+06	22.23	977.39	1.1538	1109.1	1135.1
	3	<b>-0.0852</b>	<b>-0.0027</b>	<b>-0.0011</b>	<b>2.81E+06</b>	<b>22.67</b>	<b>977.39</b>	<b>1.1521</b>	<b>1402.9</b>	<b>1435.1</b>
	4	-0.0846	-0.0028	-0.0012	3.11E+06	23.22	977.37	1.1500	1724.4	1763.0
	5	-0.0842	-0.0026	-0.0013	3.40E+06	23.75	977.35	1.1479	2084.6	2130.1



# D PowerCASE Case Summary (Example)

PowerFLOW 4.2c PowerCASE Summary

Case: Mirror\_lc.case

Date: Thu Dec 9 12:13:40 2010

User: hiwiae21

Host: ivk190

Path: /daten/hiwiae21/Sim/Half\_car\_with\_mirror\_lc

## PREPARATION INFO

Check Case completed.

o The following parts are not used for any purpose:

Mirror\_left\_help\_box

Mirror\_right\_help\_box

o The following automatic VR levels will be ignored:

6

## SIMULATION INFO

Type: 3D, External Flow, Turbulence Modeling, Isothermal, Ideal Gas

Characteristic Properties:

Pressure: 101325 Pa

Temperature: 25 degC

Density: 1.184 kg/m<sup>3</sup>

Velocity: 50 m/s

Viscosity: 1.49e-05 m<sup>2</sup>/s

Spec. Heat Ratio: 1.4

Speed of Sound: 346.1 m/s

Real Mach #: 0.1445

Sim. Mach #: 0.31497 (Char. Lattice Velocity = 0.18185)

Length: 0.3986 m (Resolution = 637.8)

Area: 0.1396 m<sup>2</sup>

Molec. Weight: 28.97 kg/kmol

Specific Heat: 1007 J/(kg\*degK)

Reynolds #: 1.33758e+06

Physical Time Scaling: 1 timestep = 2.228e-06 sec

Simulation volume: Part "\_Simulation-Volume"

Simulation volume size:

LatticeLength: 3.891e+04 x 3.891e+04 x 3.994e+04

meters: 24.32 x 24.32 x 24.96

Symmetry Planes:

LatticeLength: Y = 0, Active side: Negative

meters: Y = 0, Active side: Negative

Grid Configuration -- 10 resolution levels

Level 1 (0.320 m/voxel): \_Simulation-Volume

Level 2 (0.160 m/voxel): \_VR\_01

Level 3 (0.080 m/voxel): \_VR\_02

Level 4 (0.040 m/voxel): \_VR\_03

Level 5 (0.020 m/voxel): \_VR\_04

Level 6 (0.010 m/voxel): \_VR\_05, \_VR\_05-BL

Level 7 (5.00e-03 m/voxel): \_VR\_06-Construct VR06

Level 8 (2.50e-03 m/voxel): \_VR\_07-Construct VR07, Mirror\_right\_VR7, Mirror\_left\_VR7

Level 9 (1.25e-03 m/voxel): \_VR\_08-Construct VR08, Mirror\_right\_VR8, Mirror\_left\_VR8

Level 10 (6.25e-04 m/voxel): Cpillar\_right\_VR9, Bumper\_low\_VR9, Apillar\_left\_VR9, Apillar\_right\_VR9, ...

Cpillar\_left\_VR9, Mirror\_left\_VR9, Mirror\_right\_VR9, Spoiler\_rear\_VR9, Edge\_roof\_VR9

Minimum Grid Level Thicknesses

Default: 2 Local Voxels

Simulation duration: 500000 timesteps (1.114 sec)

Checkpoint interval: 1e+05 timesteps

Case defines the rotating reference frame "Rotation.Wheel.front.left" as follows:

Part: MRF\_wheel\_front\_left

Type: Stationary Mesh (MRF)

Angular Velocity: 661.4 rad/sec

Boundary Definition: Axisymmetric Part

Case defines the rotating reference frame "Rotation.Wheel.front.right" as follows:

Part: MRF\_wheel\_front\_right

Type: Stationary Mesh (MRF)

Angular Velocity: -661.4 rad/sec

Boundary Definition: Axisymmetric Part

Case defines the rotating reference frame "Rotation.Wheel.rear.left" as follows:

Part: MRF\_wheel\_rear\_left

Type: Stationary Mesh (MRF)

Angular Velocity: 661.4 rad/sec

Boundary Definition: Axisymmetric Part

Case defines the rotating reference frame "Rotation.Wheel.rear.right" as follows:

Part: MRF\_wheel\_rear\_right

Type: Stationary Mesh (MRF)

Angular Velocity: -661.4 rad/sec

Boundary Definition: Axisymmetric Part

No gravity force defined for this case.

## GEOMETRY SUMMARY

16 Imported parts (1673544 facets)

25 Created parts (1852 facets)

16 Offset parts

68 Faces

1629512 facets used for boundary conditions

See "GEOMETRY DETAILS" below for specific Part and Face information

## FLUID INFO

### FLUID REGIONS

Segment "Vehicle Definition/Vehicle Wrap":

"Construct\_VR8"

Initial Conditions:

Pressure: 101325 Pa

```

Relative to C-SYS: default_csyes
Relative to Ref Frame: Global Body-Fixed
Velocity: [ 0, 0, 0 ] m/s
Turbulence: 0.01, 0.005 m
Region "VR_04" Initial Conditions
Pressure: 101325 Pa
Relative to C-SYS: default_csyes
Relative to Ref Frame: Global Body-Fixed
Velocity: [ 50, 0, 0 ] m/s
Turbulence: 0.01, 0.005 m
Region "Simulation.Volume" Initial Conditions
Pressure: 101325 Pa
Relative to C-SYS: default_csyes
Relative to Ref Frame: Global Body-Fixed
Velocity: [ 50, 0, 0 ] m/s
Turbulence: 0.01, 0.005 m
POROUS MEDIA AND FAN REGIONS:
Segment "Vehicle Definition/Porous Media":
Initial Conditions:
Pressure: 101325 Pa
Relative to C-SYS: default_csyes
Relative to Ref Frame: Global Body-Fixed
Velocity: [ 5, 0, 0 ] m/s
Turbulence: 0.01, 0.005 m
Porous Media Description:
Resistance Coefficients [X, Y, Z]:
Viscous [500, Infinite, Infinite] 1/s
Inertial [100, 0.0, 0.0] 1/m
-----
SOLID/BOUNDARY INFO
-----
The following boundary conditions have been applied:
Inlet: Velocity:
Part "_Inlet":
Face "_Inlet"
Relative to C-SYS: default_csyes
Relative to Ref Frame: Global Body-Fixed
Velocity: [ 50, 0, 0 ] m/s
Turbulence: 0.01, 0.005 m
Outlet: Static Pressure, Free Flow Direction:
Part "_Outlet":
Face "_Outlet"
Pressure: 101325 Pa
Use Reflection Damping: No
Wall:
Part "_Floor_Friction":
Face "_Floor_Friction"
Relative to Ref Frame: Global Body-Fixed
Surf. Rough. Height: 0 m (smooth)
Parent "wheel faces/unassigned":
Face "Body.Vehicle.Body"
Relative to Ref Frame: Global Body-Fixed
Surf. Rough. Height: 0 m (smooth)
Face "Body.Vehicle.Body_bumper_front_low"
Relative to Ref Frame: Global Body-Fixed
Surf. Rough. Height: 0 m (smooth)
Face "Body.Vehicle.Body_apillar_right"
Relative to Ref Frame: Global Body-Fixed
Surf. Rough. Height: 0 m (smooth)
Face "Body.Vehicle.Body_apillar_left"
Relative to Ref Frame: Global Body-Fixed
Surf. Rough. Height: 0 m (smooth)
Face "Body.Vehicle.Body_cpillar_right"
Relative to Ref Frame: Global Body-Fixed
Surf. Rough. Height: 0 m (smooth)
Face "Body.Vehicle.Body_cpillar_left"
Relative to Ref Frame: Global Body-Fixed
Surf. Rough. Height: 0 m (smooth)
Face "Body.Vehicle.Body_edge_roof"
Relative to Ref Frame: Global Body-Fixed
Surf. Rough. Height: 0 m (smooth)
Face "Body.Vehicle.Body_spoiler_rear"
Relative to Ref Frame: Global Body-Fixed
Surf. Rough. Height: 0 m (smooth)
Parent "wheel faces/unassigned":
Face "Mirror_left.Vehicle.Body_mirror_lc_left"
Relative to Ref Frame: Global Body-Fixed
Surf. Rough. Height: 0 m (smooth)
Parent "wheel faces/unassigned":
Face "Mirror_right.Vehicle.Body_mirror_lc_right"
Relative to Ref Frame: Global Body-Fixed
Surf. Rough. Height: 0 m (smooth)
Parent "wheel faces/unassigned":
Face "Suspension_shaft_front_left.Suspension_shaft_front_left"
Relative to Ref Frame: Global Body-Fixed
Surf. Rough. Height: 0 m (smooth)
Parent "wheel faces/unassigned":
Face "Suspension_shaft_front_right.Suspension_shaft_front_right"
Relative to Ref Frame: Global Body-Fixed
Surf. Rough. Height: 0 m (smooth)
Parent "wheel faces/unassigned":
Face "Suspension_shaft_rear_left.Suspension_shaft_rear_left"
Relative to Ref Frame: Global Body-Fixed
Surf. Rough. Height: 0 m (smooth)
Parent "wheel faces/unassigned":
Face "Suspension_shaft_rear_right.Suspension_shaft_rear_right"
Relative to Ref Frame: Global Body-Fixed
Surf. Rough. Height: 0 m (smooth)
Frictionless Wall:
Part "_Ceiling" (all faces)

```

```

Part "_Wall.1" (all faces)
Part "_Wall.2" (all faces)
Part "_Floor" (all faces)
Sliding Wall:
Part "_Moving.Belt":
Face "_Moving.Belt"
Relative to C-SYS: _Moving.Belt_CSYS
Relative to Ref Frame: Global Body-Fixed
Velocity: [ 50, 0, 0 ] m/s
Surf. Rough. Height: 0 m (smooth)
Part "_Wheel.Belt.Front.Left":
Face "_Wheel.Belt.Front.Left"
Relative to C-SYS: _Moving.Belt_CSYS
Relative to Ref Frame: Global Body-Fixed
Velocity: [ 50, 0, 0 ] m/s
Surf. Rough. Height: 0 m (smooth)
Part "_Wheel.Belt.Front.Right":
Face "_Wheel.Belt.Front.Right"
Relative to C-SYS: _Moving.Belt_CSYS
Relative to Ref Frame: Global Body-Fixed
Velocity: [ 50, 0, 0 ] m/s
Surf. Rough. Height: 0 m (smooth)
Part "_Wheel.Belt.Rear.Left":
Face "_Wheel.Belt.Rear.Left"
Relative to C-SYS: _Moving.Belt_CSYS
Relative to Ref Frame: Global Body-Fixed
Velocity: [ 50, 0, 0 ] m/s
Surf. Rough. Height: 0 m (smooth)
Part "_Wheel.Belt.Rear.Right":
Face "_Wheel.Belt.Rear.Right"
Relative to C-SYS: _Moving.Belt_CSYS
Relative to Ref Frame: Global Body-Fixed
Velocity: [ 50, 0, 0 ] m/s
Surf. Rough. Height: 0 m (smooth)
Rotating Wall:
Parent "wheel faces/front wheel faces":
Face "Front_wheel.left.Wheels.rim.front.left"
Axis: _Front.Wheel.Axis
Angular Velocity: 661.4 rad/sec
Relative to Ref Frame: Global Body-Fixed
Surf. Rough. Height: 0 m (smooth)
Face "Front_wheel.left.Wheels.tire.front.left"
Axis: _Front.Wheel.Axis
Angular Velocity: 661.4 rad/sec
Relative to Ref Frame: Global Body-Fixed
Surf. Rough. Height: 0 m (smooth)
Parent "wheel faces/front wheel faces":
Face "Front_wheel.right.Wheels.rim.front.right"
Axis: _Front.Wheel.Axis
Angular Velocity: 661.4 rad/sec
Relative to Ref Frame: Global Body-Fixed
Surf. Rough. Height: 0 m (smooth)
Face "Front_wheel.right.Wheels.tire.front.right"
Axis: _Front.Wheel.Axis
Angular Velocity: 661.4 rad/sec
Relative to Ref Frame: Global Body-Fixed
Surf. Rough. Height: 0 m (smooth)
Parent "wheel faces/rear wheel faces":
Face "Rear_wheel.left.Wheels.rim.rear.left"
Axis: _Rear.Wheel.Axis
Angular Velocity: 661.4 rad/sec
Relative to Ref Frame: Global Body-Fixed
Surf. Rough. Height: 0 m (smooth)
Face "Rear_wheel.left.Wheels.tire.rear.left"
Axis: _Rear.Wheel.Axis
Angular Velocity: 661.4 rad/sec
Relative to Ref Frame: Global Body-Fixed
Surf. Rough. Height: 0 m (smooth)
Parent "wheel faces/rear wheel faces":
Face "Rear_wheel.right.Wheels.rim.rear.right"
Axis: _Rear.Wheel.Axis
Angular Velocity: 661.4 rad/sec
Relative to Ref Frame: Global Body-Fixed
Surf. Rough. Height: 0 m (smooth)
Face "Rear_wheel.right.Wheels.tire.rear.right"
Axis: _Rear.Wheel.Axis
Angular Velocity: 661.4 rad/sec
Relative to Ref Frame: Global Body-Fixed
Surf. Rough. Height: 0 m (smooth)

```

-----  
COUPLING DETAILS  
-----

```

IMPORT MODELS:
No import models defined.
COUPLING WALLS:
No walls defined.
-----

```

MEASUREMENT INFO  
-----

```

STANDARD MEASUREMENTS:
Window "Fluid_Meas":
Parts: Segment "Meas Regions/Main":
_VR_04"
Start Time: 0
End Time: last timestep
Period: 4000 timesteps (round to closest)
Frequency: 112.2 Hz
Time Averaging: 4000 timesteps
Building Block: 2x2x2 Voxels
Spatial Averaging: 1.25 mm

```

First Frame: 0 - 4000 timesteps (Approximate)  
 File per Frame: No  
 Options:  
 Fluid: Standard (with Turbulence Properties)  
 Porous: None  
 Surface: Standard (no HTC (Near Wall Temp))  
 COMPOSITE MEASUREMENTS:  
 Window "Composite\_Meas":  
 Parts: Segment "Meas Regions/Main":  
 "\_VR\_04"  
 Start Time: 0  
 End Time: last timestep  
 Period: 4 timesteps (round to closest)  
 Frequency: 1.122e+05 Hz  
 Time Averaging: 4 timesteps  
 Screen Invalid: Yes  
 Min Valid Cp: -10.08 (PowerFLOW default)  
 Max Valid Cp: 10.08 (PowerFLOW default)  
 Default Ref. Point: "Moment\_Point"  
 Options:  
 Fluid: None  
 Surface: Force, Calc. Moments  
 PROBES:  
 No probes defined.  
 SAMPLED FACE MEASUREMENTS:  
 No sampled face measurements defined.  
 Note: See PowerCASE User's Guide for details on how measurement  
 times are affected by grid scales.

-----  
 GEOMETRY DETAILS  
 -----

PART/FACE BOUND INFORMATION:

Part (all faces): | Min Bound | Max Bound |  
 Face | (m) | (m) |

._Ceiling	-11.86, -12.16, 10.85	12.46, 12.16, 12.16
._Ceiling	-11.86, -12.16, 10.85	12.46, 12.16, 12.16
._Floor	-11.86, -12.16, -12.8	12.46, 12.16, -0.0036
._Floor	-11.86, -12.16, -12.8	12.46, 12.16, -0.0036
._Floor_Friction	0.301, -0.3995, -0.3243	1.381, 0.4005, -0.0036
._Floor_Friction	0.301, -0.3995, -0.3243	1.381, 0.4005, -0.0036
._Inlet	-11.86, -6.432, -0.0036	-10.58, 6.433, 10.85
._Inlet	-11.86, -6.432, -0.0036	-10.58, 6.433, 10.85
._Moving_Belt	-0.574, -0.112, -0.0536	1.176, 0.113, -0.0036
._Moving_Belt	-0.574, -0.112, -0.0536	1.176, 0.113, -0.0036
._Outlet	11.18, -6.432, -0.0036	12.46, 6.433, 10.85
._Outlet	11.18, -6.432, -0.0036	12.46, 6.433, 10.85
._Simulation_Volume	-11.86, -12.16, -12.8	12.46, 12.16, 12.16
._Simulation_Volume	-11.86, -12.16, -12.8	12.46, 12.16, 12.16
._VR_01	-5.459, -5.2, -5.164	6.061, 5.2, 5.556
._VR_01	-5.459, -5.2, -5.164	6.061, 5.2, 5.556
._VR_02	-2.899, -2.64, -2.604	4.461, 2.64, 2.996
._VR_02	-2.899, -2.64, -2.604	4.461, 2.64, 2.996
._VR_03	-1.619, -1.36, -1.324	3.181, 1.36, 1.716
._VR_03	-1.619, -1.36, -1.324	3.181, 1.36, 1.716
._VR_04	-0.9785, -0.7195, -0.6843	2.141, 0.7205, 1.076
._VR_04	-0.9785, -0.7195, -0.6843	2.141, 0.7205, 1.076
._VR_05	-0.6585, -0.3995, -0.3243	1.381, 0.4005, 0.7157
._VR_05	-0.6585, -0.3995, -0.3243	1.381, 0.4005, 0.7157
._VR_05_BL	0.301, -0.3995, -0.3243	1.381, 0.4005, 0.0964
._VR_05_BL	0.301, -0.3995, -0.3243	1.381, 0.4005, 0.0964
._VR_06_Construct VR0	-0.5219, -0.3338, -0.01368	1.328, 0.3362, 0.585
._VR_06_Construct V	-0.5219, -0.3338, -0.01368	1.328, 0.3362, 0.585
._VR_07_Construct VR0	-0.2932, -0.2486, -0.03287	0.9069, 0.2502, 0.4803
._VR_07_Construct V	-0.2932, -0.2486, -0.03287	0.9069, 0.2502, 0.4803
._VR_08_Construct VR0	-0.166, -0.2267, -0.03217	0.7688, 0.2283, 0.4212
._VR_08_Construct V	-0.166, -0.2267, -0.03217	0.7688, 0.2283, 0.4212
._Wall_1	-11.86, -12.16, -0.0036	12.46, -6.432, 10.85
._Wall_1	-11.86, -12.16, -0.0036	12.46, -6.432, 10.85
._Wall_2	-11.86, 6.433, -0.0036	12.46, 12.16, 10.85
._Wall_2	-11.86, 6.433, -0.0036	12.46, 12.16, 10.85
._Wheel_Belt_Front_Le	-0.0475, -0.2184, -0.0536	0.0445, -0.1469, -0.0036
._Wheel_Belt_Front_Le	-0.0475, -0.2184, -0.0536	0.0445, -0.1469, -0.0036
._Wheel_Belt_Front_Ri	-0.0475, 0.1469, -0.0536	0.0445, 0.2184, -0.0036
._Wheel_Belt_Front_Ri	-0.0475, 0.1469, -0.0536	0.0445, 0.2184, -0.0036
._Wheel_Belt_Rear_Lef	0.5575, -0.2172, -0.0536	0.6495, -0.1457, -0.0036
._Wheel_Belt_Rear_Lef	0.5575, -0.2172, -0.0536	0.6495, -0.1457, -0.0036
._Wheel_Belt_Rear_L	0.5575, -0.2172, -0.0536	0.6495, -0.1457, -0.0036
._Wheel_Belt_Rear_Rig	0.5575, 0.1457, -0.0536	0.6495, 0.2172, -0.0036
._Wheel_Belt_Rear_Rig	0.5575, 0.1457, -0.0536	0.6495, 0.2172, -0.0036
._Wheel_Belt_Rear_R	0.5575, 0.1457, -0.0536	0.6495, 0.2172, -0.0036
._Wheel_Belt_Rear_R	0.5575, 0.1457, -0.0536	0.6495, 0.2172, -0.0036
._Apillar_left_VR9	0.02403, -0.1895, 0.243	0.2629, -0.1269, 0.3757
._Apillar_left_VR9	0.02403, -0.1895, 0.243	0.2629, -0.1269, 0.3757
._Apillar_right_VR9	0.02243, 0.129, 0.2428	0.2594, 0.1904, 0.3754
._Apillar_right_VR9	0.02243, 0.129, 0.2428	0.2594, 0.1904, 0.3754
._Body	-0.1449, -0.2131, 0.03889	0.7478, 0.2146, 0.393
._Body	-0.1449, -0.2131, 0.03889	0.7478, 0.2146, 0.393
._Body_Vehicle_Body_	0.02505, -0.187, 0.2433	0.2623, -0.1285, 0.3731
._Body_Vehicle_Body_	0.02505, -0.187, 0.2433	0.2623, -0.1285, 0.3731
._Body_Vehicle_Body_	0.02445, 0.131, 0.2443	0.2579, 0.1878, 0.373
._Body_Vehicle_Body_	0.02445, 0.131, 0.2443	0.2579, 0.1878, 0.373
._Body_Vehicle_Body_	-0.1412, -0.1951, 0.04128	-0.08748, 0.1941, 0.07032
._Body_Vehicle_Body_	-0.1412, -0.1951, 0.04128	-0.08748, 0.1941, 0.07032
._Body_Vehicle_Body_	0.651, -0.2024, 0.1135	0.734, -0.105, 0.3543
._Body_Vehicle_Body_	0.651, -0.2024, 0.1135	0.734, -0.105, 0.3543
._Body_Vehicle_Body_	0.6486, 0.1244, 0.1084	0.7297, 0.2036, 0.351
._Body_Vehicle_Body_	0.6486, 0.1244, 0.1084	0.7297, 0.2036, 0.351
._Body_Vehicle_Body_	0.2344, -0.1296, 0.3683	0.2547, 0.1319, 0.3779
._Body_Vehicle_Body_	0.2344, -0.1296, 0.3683	0.2547, 0.1319, 0.3779
._Body_Vehicle_Body_	0.6411, -0.1409, 0.3399	0.6985, 0.1444, 0.3772
._Body_Vehicle_Body_	0.6411, -0.1409, 0.3399	0.6985, 0.1444, 0.3772
._Bumper_low_VR9	-0.1437, -0.1975, 0.03877	-0.08642, 0.1966, 0.07271
._Bumper_low_VR9	-0.1437, -0.1975, 0.03877	-0.08642, 0.1966, 0.07271
._Construct_VR6	-0.5168, -0.3288, -0.008568	1.323, 0.3312, 0.58
._Construct_VR6	-0.5168, -0.3288, -0.008568	1.323, 0.3312, 0.58
._Construct_VR6_Defa	-0.5168, -0.3288, -0.008568	1.323, 0.3312, 0.58
._Construct_VR6_Defa	-0.5168, -0.3288, -0.008568	1.323, 0.3312, 0.58
._Construct_VR7	-0.268, -0.2236, -0.007161	0.8817, 0.2252, 0.4553
._Construct_VR7	-0.268, -0.2236, -0.007161	0.8817, 0.2252, 0.4553
._Construct_VR7_Defa	-0.268, -0.2236, -0.007161	0.8817, 0.2252, 0.4553
._Construct_VR7_Defa	-0.268, -0.2236, -0.007161	0.8817, 0.2252, 0.4553
._Construct_VR8	-0.1585, -0.2192, -0.0246	0.7613, 0.2208, 0.4137
._Construct_VR8	-0.1585, -0.2192, -0.0246	0.7613, 0.2208, 0.4137
._Construct_VR8.0	-0.1585, -0.2192, -0.0246	0.7613, 0.2208, 0.4137
._Construct_VR8.0	-0.1585, -0.2192, -0.0246	0.7613, 0.2208, 0.4137

Cpillar_left_VR9		0.6475,	-0.2046,	0.113		0.7363,	-0.1049,	0.3552	
Cpillar_left_VR9		0.6475,	-0.2046,	0.113		0.7363,	-0.1049,	0.3552	
Cpillar_right_VR9		0.648,	0.1238,	0.1079		0.7319,	0.2056,	0.3527	
Cpillar_right_VR9		0.648,	0.1238,	0.1079		0.7319,	0.2056,	0.3527	
Edge_roof_VR9		0.232,	-0.133,	0.367		0.2555,	0.1347,	0.3805	
Edge_roof_VR9		0.232,	-0.133,	0.367		0.2555,	0.1347,	0.3805	
Front_wheel_left		-0.07709,	-0.207,	-0.0056		0.07409,	-0.1582,	0.1456	
Front_wheel_left.W		-0.0561,	-0.207,	0.0154		0.0531,	-0.1633,	0.1246	
Front_wheel_left.W		-0.07709,	-0.207,	-0.0056		0.07409,	-0.1582,	0.1456	
Front_wheel_right		-0.07709,	0.1582,	-0.0056		0.07409,	0.207,	0.1456	
Front_wheel_right		-0.0561,	0.1633,	0.0154		0.0531,	0.207,	0.1246	
Front_wheel_right		-0.07709,	0.1582,	-0.0056		0.07409,	0.207,	0.1456	
Mirror_left		0.1595,	-0.2357,	0.24		0.1995,	-0.1808,	0.2787	
Mirror_left.Vehicl		0.1595,	-0.2357,	0.24		0.1995,	-0.1808,	0.2787	
Mirror_left_box		0.1573,	-0.2508,	0.2364		0.2777,	-0.1756,	0.2842	
Mirror_left_box		0.1573,	-0.2508,	0.2364		0.2777,	-0.1756,	0.2842	
Mirror_left_help_box		0.1573,	-0.2508,	0.2364		0.2777,	-0.1756,	0.2842	
Mirror_left_help-b		0.1573,	-0.2508,	0.2364		0.2777,	-0.1756,	0.2842	
Mirror_left_VR7		0.1473,	-0.2608,	0.2264		0.2877,	-0.1656,	0.2942	
Mirror_left_VR7		0.1473,	-0.2608,	0.2264		0.2877,	-0.1656,	0.2942	
Mirror_left_VR8		0.1523,	-0.2558,	0.2314		0.2827,	-0.1706,	0.2892	
Mirror_left_VR8		0.1523,	-0.2558,	0.2314		0.2827,	-0.1706,	0.2892	
Mirror_left_VR9		0.157,	-0.2382,	0.2369		0.2021,	-0.1777,	0.2812	
Mirror_left_VR9		0.157,	-0.2382,	0.2369		0.2021,	-0.1777,	0.2812	
Mirror_right		0.1595,	0.1818,	0.24		0.1995,	0.2367,	0.2787	
Mirror_right.Vehicl		0.1595,	0.1818,	0.24		0.1995,	0.2367,	0.2787	
Mirror_right_box		0.1573,	0.1763,	0.2359		0.2777,	0.2515,	0.2836	
Mirror_right_box		0.1573,	0.1763,	0.2359		0.2777,	0.2515,	0.2836	
Mirror_right_help-bo		0.1573,	0.1763,	0.2359		0.2777,	0.2515,	0.2836	
Mirror_right_help-		0.1573,	0.1763,	0.2359		0.2777,	0.2515,	0.2836	
Mirror_right_VR7		0.1473,	0.1663,	0.2259		0.2877,	0.2615,	0.2936	
Mirror_right_VR7		0.1473,	0.1663,	0.2259		0.2877,	0.2615,	0.2936	
Mirror_right_VR8		0.1523,	0.1713,	0.2309		0.2827,	0.2565,	0.2886	
Mirror_right_VR8		0.1523,	0.1713,	0.2309		0.2827,	0.2565,	0.2886	
Mirror_right_VR9		0.157,	0.1787,	0.2369		0.2021,	0.2392,	0.2812	
Mirror_right_VR9		0.157,	0.1787,	0.2369		0.2021,	0.2392,	0.2812	
MRF_wheel_front_left		-0.0561,	-0.2077,	0.0154		0.0531,	-0.1857,	0.1246	
MRF_wheel_front_le		-0.0561,	-0.2077,	0.0154		0.0531,	-0.1857,	0.1246	
MRF_wheel_front_right		-0.0561,	0.1863,	0.0154		0.0531,	0.2083,	0.1246	
MRF_wheel_front_ri		-0.0561,	0.1863,	0.0154		0.0531,	0.2083,	0.1246	
MRF_wheel_rear_left		0.5489,	-0.2067,	0.0154		0.658,	-0.1847,	0.1246	
MRF_wheel_rear_lef		0.5489,	-0.2067,	0.0154		0.658,	-0.1847,	0.1246	
MRF_wheel_rear_right		0.5489,	0.1853,	0.0154		0.658,	0.2073,	0.1246	
MRF_wheel_rear_rig		0.5489,	0.1853,	0.0154		0.658,	0.2073,	0.1246	
Rear_wheel_left		0.5279,	-0.2058,	-0.0056		0.679,	-0.157,	0.1456	
Rear_wheel_left.Wh		0.5489,	-0.2058,	0.0154		0.658,	-0.1621,	0.1246	
Rear_wheel_left.Wh		0.5279,	-0.2058,	-0.0056		0.679,	-0.157,	0.1456	
Rear_wheel_right		0.5279,	0.157,	-0.0056		0.679,	0.2058,	0.1456	
Rear_wheel_right.W		0.5489,	0.1621,	0.0154		0.658,	0.2058,	0.1246	
Rear_wheel_right.W		0.5279,	0.157,	-0.0056		0.679,	0.2058,	0.1456	
Spoiler_rear_VR9		0.6395,	-0.143,	0.338		0.7011,	0.1462,	0.3796	
Spoiler_rear_VR9		0.6395,	-0.143,	0.338		0.7011,	0.1462,	0.3796	
Suspension_shaft_fro		-0.03448,	-0.1901,	0.03705		0.03147,	-0.1352,	0.1029	
Suspension_shaft.f		-0.03448,	-0.1901,	0.03705		0.03147,	-0.1352,	0.1029	
Suspension_shaft_fro		-0.03448,	0.1357,	0.03705		0.03147,	0.1906,	0.1029	
Suspension_shaft.f		-0.03448,	0.1357,	0.03705		0.03147,	0.1906,	0.1029	
Suspension_shaft_rea		0.5705,	-0.1893,	0.03705		0.6364,	-0.1493,	0.1029	
Suspension_shaft.r		0.5705,	-0.1893,	0.03705		0.6364,	-0.1493,	0.1029	
Suspension_shaft_rea		0.5705,	0.1481,	0.03705		0.6364,	0.1893,	0.1029	
Suspension_shaft.r		0.5705,	0.1481,	0.03705		0.6364,	0.1893,	0.1029	
PART/FACE SIZE INFORMATION:									
Part (all faces):     Total Area   Bounding Box Size									
Face		# Facets		(m^2)		(m)			
<hr/>									
.Ceiling		12		1250		24.32,	24.32,	1.306	
.Ceiling		12		1250		24.32,	24.32,	1.306	
.Floor		12		2345		24.32,	24.32,	12.8	
.Floor		12		2345		24.32,	24.32,	12.8	
.Floor_Friction		12		2.935		1.08,	0.8,	0.3207	
.Floor_Friction		12		2.935		1.08,	0.8,	0.3207	
.Inlet		12		340		1.28,	12.87,	10.85	
.Inlet		12		340		1.28,	12.87,	10.85	
.Moving_Belt		12		0.985		1.75,	0.225,	0.05	
.Moving_Belt		12		0.985		1.75,	0.225,	0.05	
.Outlet		12		340		1.28,	12.87,	10.85	
.Outlet		12		340		1.28,	12.87,	10.85	
.Simulation_Volume		12		3498		24.32,	24.32,	24.96	
.Simulation_Volume		12		3498		24.32,	24.32,	24.96	
.VR_01		12		709.6		11.52,	10.4,	10.72	
.VR_01		12		709.6		11.52,	10.4,	10.72	
.VR_02		12		219.3		7.36,	5.28,	5.6	
.VR_02		12		219.3		7.36,	5.28,	5.6	
.VR_03		12		71.83		4.8,	2.72,	3.04	
.VR_03		12		71.83		4.8,	2.72,	3.04	
.VR_04		12		25.04		3.12,	1.44,	1.76	
.VR_04		12		25.04		3.12,	1.44,	1.76	
.VR_05		12		9.171		2.04,	0.8,	1.04	
.VR_05		12		9.171		2.04,	0.8,	1.04	
.VR_05.BL		12		3.311		1.08,	0.8,	0.4207	
.VR_05.BL		12		3.311		1.08,	0.8,	0.4207	
.VR_06_Construct VR06		N/A		N/A		1.85,	0.67,	0.5987	
.VR_06_Construct VR06		N/A		N/A		1.85,	0.67,	0.5987	
.VR_07_Construct VR07		N/A		N/A		1.2,	0.4988,	0.5131	
.VR_07_Construct VR07		N/A		N/A		1.2,	0.4988,	0.5131	
.VR_08_Construct VR08		N/A		N/A		0.9349,	0.455,	0.4534	
.VR_08_Construct VR08		N/A		N/A		0.9349,	0.455,	0.4534	
.Wall.1		12		891.4		24.32,	5.728,	10.85	
.Wall.1		12		891.4		24.32,	5.728,	10.85	
.Wall.2		12		891.4		24.32,	5.727,	10.85	
.Wall.2		12		891.4		24.32,	5.727,	10.85	

```

-Wheel.Belt_Front_Left: | 12 | 0.02951 | 0.092, 0.0715, 0.05 |
-Wheel.Belt_Front_Left: | 12 | 0.02951 | 0.092, 0.0715, 0.05 |
-Wheel.Belt_Front_Right: | 12 | 0.02951 | 0.092, 0.0715, 0.05 |
-Wheel.Belt_Front_Right: | 12 | 0.02951 | 0.092, 0.0715, 0.05 |
-Wheel.Belt_Rear_Left: | 12 | 0.02951 | 0.092, 0.0715, 0.05 |
-Wheel.Belt_Rear_Left: | 12 | 0.02951 | 0.092, 0.0715, 0.05 |
-Wheel.Belt_Rear_Right: | 12 | 0.02951 | 0.092, 0.0715, 0.05 |
-Wheel.Belt_Rear_Right: | 12 | 0.02951 | 0.092, 0.0715, 0.05 |
Apillar_left_VR9: | N/A | N/A | 0.2389, 0.06259, 0.1328 |
Apillar_left_VR9 | N/A | N/A | 0.2389, 0.06259, 0.1328 |
Apillar_right_VR9: | N/A | N/A | 0.2369, 0.06141, 0.1326 |
Apillar_right_VR9 | N/A | N/A | 0.2369, 0.06141, 0.1326 |
Body: | 1283356 | 1.306 | 0.8927, 0.4277, 0.3541 |
Body.Vehicle_Body | 1182234 | 1.221 | 0.8927, 0.4277, 0.3541 |
Body.Vehicle_Body_apillar_left | 17214 | 0.01156 | 0.2373, 0.05847, 0.1298 |
Body.Vehicle_Body_apillar_right | 17294 | 0.01116 | 0.2335, 0.05683, 0.1287 |
Body.Vehicle_Body_bumper_front_low | 17719 | 0.01566 | 0.05374, 0.3892, 0.02904 |
Body.Vehicle_Body_cpillar_left | 15446 | 0.01551 | 0.08297, 0.0974, 0.2408 |
Body.Vehicle_Body_cpillar_right | 12913 | 0.01313 | 0.0811, 0.07912, 0.2426 |
Body.Vehicle_Body_edge_roof | 4940 | 0.00297 | 0.0203, 0.2616, 0.009514 |
Body.Vehicle_Body_spoiler_rear | 15596 | 0.01504 | 0.05736, 0.2853, 0.03733 |
Bumper_low_VR9: | N/A | N/A | 0.05731, 0.3942, 0.03394 |
Bumper_low_VR9 | N/A | N/A | 0.05731, 0.3942, 0.03394 |
Construct_VR6: | 10160 | 4.227 | 1.839, 0.66, 0.5885 |
Construct_VR6.Default | 10160 | 4.227 | 1.839, 0.66, 0.5885 |
Construct_VR7: | 10160 | 1.959 | 1.15, 0.4488, 0.4624 |
Construct_VR7.Default | 10160 | 1.959 | 1.15, 0.4488, 0.4624 |
Construct_VR8: | 8784 | 1.417 | 0.9199, 0.44, 0.4383 |
Construct_VR8.0 | 8784 | 1.417 | 0.9199, 0.44, 0.4383 |
Cpillar_left_VR9: | N/A | N/A | 0.08883, 0.09972, 0.2422 |
Cpillar_left_VR9 | N/A | N/A | 0.08883, 0.09972, 0.2422 |
Cpillar_right_VR9: | N/A | N/A | 0.08384, 0.08184, 0.2449 |
Cpillar_right_VR9 | N/A | N/A | 0.08384, 0.08184, 0.2449 |
Edge_roof_VR9: | N/A | N/A | 0.02347, 0.2677, 0.01342 |
Edge_roof_VR9 | N/A | N/A | 0.02347, 0.2677, 0.01342 |
Front_wheel_left: | 48816 | 0.06578 | 0.1512, 0.04877, 0.1512 |
Front_wheel_left.Wheels_rim_front_left | 24956 | 0.02845 | 0.1092, 0.04375, 0.1092 |
Front_wheel_left.Wheels_tire_front_left | 23860 | 0.03733 | 0.1512, 0.04874, 0.1512 |
Front_wheel_right: | 48816 | 0.06578 | 0.1512, 0.04877, 0.1512 |
Front_wheel_right.Wheels_rim_front_right | 24956 | 0.02845 | 0.1092, 0.04375, 0.1092 |
Front_wheel_right.Wheels_tire_front_right | 23860 | 0.03733 | 0.1512, 0.04874, 0.1512 |
Mirror_left: | 59754 | 0.005915 | 0.04001, 0.05494, 0.03863 |
Mirror_left.Vehicle_Body_mirror_lc_left | 59754 | 0.005915 | 0.04001, 0.05494, 0.03863 |
Mirror_left_box: | 12 | 0.03678 | 0.1204, 0.07518, 0.04775 |
Mirror_left_box | 12 | 0.03678 | 0.1204, 0.07518, 0.04775 |
Mirror_left_help_box: | 7536 | 0.01512 | 0.1204, 0.07518, 0.04775 |
Mirror_left_help_box.Vehicle_Body_mirror_left | 7536 | 0.01512 | 0.1204, 0.07518, 0.04775 |
Mirror_left_VR7: | N/A | N/A | 0.1404, 0.09518, 0.06775 |
Mirror_left_VR7 | N/A | N/A | 0.1404, 0.09518, 0.06775 |
Mirror_left_VR8: | N/A | N/A | 0.1304, 0.08518, 0.05775 |
Mirror_left_VR8 | N/A | N/A | 0.1304, 0.08518, 0.05775 |
Mirror_left_VR9: | N/A | N/A | 0.04512, 0.06056, 0.04427 |
Mirror_left_VR9 | N/A | N/A | 0.04512, 0.06056, 0.04427 |
Mirror_right: | 59754 | 0.005915 | 0.04001, 0.05494, 0.03863 |
Mirror_right.Vehicle_Body_mirror_lc_right | 59754 | 0.005915 | 0.04001, 0.05494, 0.03863 |
Mirror_right_box: | 12 | 0.03675 | 0.1204, 0.07516, 0.04769 |
Mirror_right_box | 12 | 0.03675 | 0.1204, 0.07516, 0.04769 |
Mirror_right_help_box: | 7536 | 0.01512 | 0.1204, 0.07516, 0.04769 |
Mirror_right_help_box.Vehicle_Body_mirror_right | 7536 | 0.01512 | 0.1204, 0.07516, 0.04769 |
Mirror_right_VR7: | N/A | N/A | 0.1404, 0.09516, 0.06769 |
Mirror_right_VR7 | N/A | N/A | 0.1404, 0.09516, 0.06769 |
Mirror_right_VR8: | N/A | N/A | 0.1304, 0.08516, 0.05769 |
Mirror_right_VR8 | N/A | N/A | 0.1304, 0.08516, 0.05769 |
Mirror_right_VR9: | N/A | N/A | 0.04512, 0.06056, 0.04427 |
Mirror_right_VR9 | N/A | N/A | 0.04512, 0.06056, 0.04427 |
MRF_wheel_front_left: | 400 | 0.02626 | 0.1092, 0.022, 0.1092 |
MRF_wheel_front_left | 400 | 0.02626 | 0.1092, 0.022, 0.1092 |
MRF_wheel_front_right: | 400 | 0.02626 | 0.1092, 0.022, 0.1092 |
MRF_wheel_front_right | 400 | 0.02626 | 0.1092, 0.022, 0.1092 |
MRF_wheel_rear_left: | 400 | 0.02626 | 0.1092, 0.022, 0.1092 |
MRF_wheel_rear_left | 400 | 0.02626 | 0.1092, 0.022, 0.1092 |
MRF_wheel_rear_right: | 400 | 0.02626 | 0.1092, 0.022, 0.1092 |
MRF_wheel_rear_right | 400 | 0.02626 | 0.1092, 0.022, 0.1092 |
Rear_wheel_left: | 48816 | 0.06578 | 0.1512, 0.04877, 0.1512 |
Rear_wheel_left.Wheels_rim_rear_left | 24956 | 0.02845 | 0.1092, 0.04375, 0.1092 |
Rear_wheel_left.Wheels_tire_rear_left | 23860 | 0.03733 | 0.1512, 0.04874, 0.1512 |
Rear_wheel_right: | 48816 | 0.06578 | 0.1512, 0.04877, 0.1512 |
Rear_wheel_right.Wheels_rim_rear_right | 24956 | 0.02845 | 0.1092, 0.04375, 0.1092 |
Rear_wheel_right.Wheels_tire_rear_right | 23860 | 0.03733 | 0.1512, 0.04874, 0.1512 |
Spoiler_rear_VR9: | N/A | N/A | 0.06157, 0.2892, 0.04156 |
Spoiler_rear_VR9 | N/A | N/A | 0.06157, 0.2892, 0.04156 |
Suspension_shaft_front_left: | 8136 | 0.01338 | 0.06595, 0.05485, 0.06589 |
Suspension_shaft_front_left.Suspension_shaft_front_left | 8136 | 0.01338 | 0.06595, 0.05485, 0.06589 |
Suspension_shaft_front_right: | 8136 | 0.01338 | 0.06595, 0.05485, 0.06589 |
Suspension_shaft_front_right.Suspension_shaft_front_right | 8136 | 0.01338 | 0.06595, 0.05485, 0.06589 |
Suspension_shaft_rear_left: | 7448 | 0.01118 | 0.06595, 0.03999, 0.06589 |
Suspension_shaft_rear_left.Suspension_shaft_rear_left | 7448 | 0.01118 | 0.06595, 0.03999, 0.06589 |
Suspension_shaft_rear_right: | 7520 | 0.01193 | 0.06595, 0.04119, 0.06589 |
Suspension_shaft_rear_right.Suspension_shaft_rear_right | 7520 | 0.01193 | 0.06595, 0.04119, 0.06589 |
COORDINATE SYSTEM INFORMATION:
C-SYS_VR_Build_CSYS
Relative to C-SYS: "default.csys"
Origin: [ 0.3015, 0.0005, 0.1957 ] m
X-Axis Vector: [ 1, 0, 0 ]
Y-Axis Vector: [ 0, 1, 0 ]
Z-Axis Vector: [ 0, 0, 1 ]
C-SYS_Moving_Belt_CSYS
Relative to C-SYS: "default.csys"
Origin: [ 0.301, 0.0005, -0.0036 ] m
X-Axis Vector: [ 1, 0, 0 ]

```

Y-Axis Vector: [ 0, 1, 0 ]  
 Z-Axis Vector: [ 0, 0, 1 ]  
 C-SYS \_Base\_Vehicle\_Angle\_CSYS  
 Relative to C-SYS: "\_Moving\_Belt\_CSYS"  
 Origin: [ 0, 0, -0.002 ] m  
 X-Axis Vector: [ 1, 0, 0 ]  
 Y-Axis Vector: [ 0, 1, 0 ]  
 Z-Axis Vector: [ 0, 0, 1 ]  
 C-SYS \_Wheel\_Import\_CSYS  
 Relative to C-SYS: "\_Base\_Vehicle\_Angle\_CSYS"  
 Origin: [ -0.301, -0.0005, 0.0036 ] m  
 X-Axis Vector: [ 1, 0, 0 ]  
 Y-Axis Vector: [ 0, 1, 0 ]  
 Z-Axis Vector: [ 0, 0, 1 ]  
 C-SYS \_Wheelbase\_Center\_CSYS  
 Relative to C-SYS: "\_Moving\_Belt\_CSYS"  
 Origin: [ 0, 0, -0.002 ] m  
 X-Axis Vector: [ 1, 0, 0 ]  
 Y-Axis Vector: [ 0, 1, 0 ]  
 Z-Axis Vector: [ 0, 0, 1 ]  
 C-SYS \_Body\_Import\_CSYS  
 Relative to C-SYS: "\_Wheelbase\_Center\_CSYS"  
 Origin: [ -0.301, -0.0005, 0.0036 ] m  
 X-Axis Vector: [ 1, 0, 0 ]  
 Y-Axis Vector: [ 0, 1, 0 ]  
 Z-Axis Vector: [ 0, 0, 1 ]

POINT INFORMATION:

Point Name	C_SYS	Position (m)
Moment_Point	_Wheelbase_Center_CS	0, 0, 0

AXIS INFORMATION:

Axis Name	C_SYS	Position (m)	Direction
_Front_Wheel_Axis	_Base_Vehicle_Angle_	-0.3025, 0, 0.07559	0, -1, 0
_Rear_Wheel_Axis	_Base_Vehicle_Angle_	0.3025, 0, 0.07559	0, -1, 0